

# University of Salerno



## Department of Chemistry and Biology

Ph.D. in Chemistry-XXX course

Thesis on

# Calixarene Based Catalytic Systems

**Candidate**

Nicola Alessandro De Simone

**Supervisors**

Prof. Placido Neri

Prof. Annunziata Soriente

Prof. Franz H. Kohnke

**Ph. D. Coordinator**

Prof. Gaetano Guerra

*Academic Year 2016/2017*



*to Chiara*

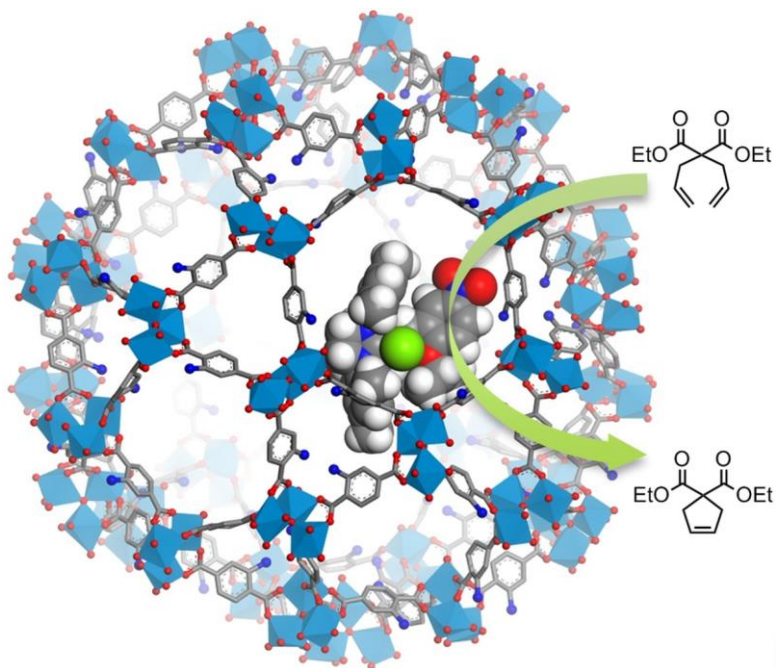


# Table of Contents

<b>1. Chapter 1-Introduction at Supramolecular Catalysis .....</b>	<b>7</b>
1.1. General Overview.....	9
1.2. Calixarenes as Supramolecular Catalysts .....	12
<b>2. Chapter 2-Goals and Outline of This Thesis.....</b>	<b>23</b>
<b>3. Chapter 3-Phase-Transfer Catalysis.....</b>	<b>27</b>
3.1. General Overview.....	29
3.2. Synthesis of new PTC Catalysts Calixarene-Based.....	33
3.3. Asymmetric PTC Catalysis .....	37
3.4. Recognition Abilities of Calix[4]arene-Amides toward Na <sup>+</sup> cation .....	44
<b>4. Chapter 4-Asymmetric Organocatalysis .....</b>	<b>55</b>
4.1. General Overview.....	57
4.2. Synthesis of new Bifunctional Organocatalysts .....	62
4.3. Asymmetric Conjugate Addition.....	64
<b>5. Chapter 5-Dinuclear Zirconium Complex Bearing 1,5-     Bridged-Calix[8]arene Ligand as Effective Catalyst for the     Synthesis of Macrolactones.....</b>	<b>73</b>
5.1. General Overview.....	75
5.2. Synthesis of the Dinuclear Zirconium Complex Bearing 1,5- Bridged Calix[8]arene Ligand .....	83
5.3. Ring Opening Polymerization of <i>rac</i> -LA, $\epsilon$ -CL and $\beta$ -BL.....	90
<b>6. Chapter 6-Experimental Section.....</b>	<b>99</b>
6.1. General Information .....	101
6.2. Synthesis of Catalysts.....	104

6.2.1.	Synthesis of Derivative <b>11</b> .....	104
6.2.2.	Synthesis of Derivative <b>12</b> .....	110
6.2.3.	Synthesis of Derivative <b>13</b> .....	117
6.2.4.	Synthesis of Derivative <b>14</b> .....	125
6.2.5.	Synthesis of Derivative <b>15</b> .....	131
6.2.6.	Synthesis of Derivative <b>18</b> .....	138
6.2.7.	Synthesis of Derivative <b>19</b> .....	143
6.2.8.	Synthesis of Derivative <b>35</b> .....	147
6.2.9.	Synthesis of Derivative <b>16</b> .....	153
6.2.10.	Synthesis of Derivative <b>31a</b> .....	159
6.3.	Preparation of Complexes and $K_a$ Determination.....	163
6.3.1.	General Procedure for the Preparation of $\text{Na}^+\text{C}X$ ( $X =$ <b>9, 12, 13</b> and <b>15</b> ) Complexes .....	163
6.3.2.	Determination of $\text{Na}^+\text{C}X$ ( $X =$ <b>9</b> and <b>15</b> ) $K_a$ Value ...	164
6.3.3.	Determination of $\text{Na}^+\text{C}12$ $K_a$ Value .....	164
6.3.4.	Synthesis of the Complex <b>17</b> (Zr-O- <i>t</i> Bu) <sub>2</sub> .....	178
6.4.	Catalytic Conditions .....	184
6.4.1.	General Procedure for the Phase-Transfer Alkylation of N-(Diphenylmethylene)glycine <i>tert</i> -Butyl Ester ( <b>14</b> ) Catalyzed by Chiral Calixarene-Amide <b>12</b> .....	184
6.4.2.	General Procedure for Catalytic Enantioselective Michael Reaction of Isobutyraldehyde with Maleimide in Water .....	185
6.4.3.	General Procedure for Solvent-free Catalytic Enantioselective Michael Reaction of Isobutyraldehyde with Maleimide.....	185
6.4.4.	Catalytic Asymmetric Solvent-free Michael Addition of Isobutyraldehyde to Nitroolefins .....	186
6.4.5.	Catalytic Enantioselective Solvent-free Addition of Dimethyl Malonate to Benzylideneacetone.....	186

## *Supramolecular Catalysis*





# *Chapter 1*

## *Introduction at Supramolecular Catalysis*

### *1.1. General Overview*

This chapter is intended to describe recent developments in the field of supramolecular catalysis, which has grown exponentially in the last few decades as indicated by the large number of articles present in the chemical literature.<sup>1</sup> In particular, chemical transformations require making and breaking of chemical bonds, which not always is an easy task, considering that reactions require sometimes prohibitive energy barriers to be overcome. In these situations catalysis is a powerful tool because it provides the concepts necessary to increase reaction rate and selectivity, so it is the keystone of the transformation of simple chemicals into everyday life commodities.

Although divided into heterogeneous catalysis and homogeneous catalysis, (the latter also divided into transition metal catalysis and organocatalysis), catalysis still remains a

multidisciplinary field linked with others such as supramolecular chemistry. The area at the intersection is called supramolecular catalysis.<sup>2</sup>

According to this definition, catalysis is seen as a supramolecular phenomenon in the meaning that the catalyst “recognizes” the substrate, “organizes” the transition state and “assembles” the product. In order to create a distinction, the term supramolecular catalysis is referred to those reactions in which non covalent interactions do not take part in the rate determining step, but play a crucial role in determining the reaction path. In fact secondary interactions such as H-bond, cation-dipole, dipole-dipole, cation- $\pi$ ,  $\pi$ - $\pi$  stacking and even Van der Waals and hydrophobic interactions can favor the formation of one enantiomer above the other in enantioselective reactions.

Supramolecular chemists have always been inspired by nature’s ability of harnessing secondary interactions to achieve complex tasks, so it is no surprise that in the field of catalysis they looked at enzymes as model.<sup>3</sup>

The conventional route, consisting in replicating the enzyme active site (model enzyme), sometimes proved to be difficult because of the structural complexity yielded by millions of years of evolution and natural selection. Another valuable

choice is to replicate enzyme functions without duplicating its structure (enzyme model or mimics)<sup>4</sup>.

In particular properties to borrow from enzymatic catalysis are substrate recognition, transition state stabilization and absence of product inhibition (although the last is not properly an enzyme characteristic). The key features necessary to get these properties are complementarity (of both shape and interactions) between catalyst and substrates, environmental confinement of the reactants and easy release of the products.

The design of catalysts with the above mentioned features takes advantage of theories that explain how biomolecules work, such as lock/key and induced fit. Not only are these two concepts fundamental to explain how receptors specifically recognize substrates, but also are inspiring principles in supramolecular chemistry as they contributed to the development of host-guest chemistry. Supramolecular catalysis takes enormous advantage of host-guest chemistry as the idea that drove the synthesis of the first enzyme inspired catalysts<sup>5</sup>.

Since then different strategies have been elaborated. One consists in synthesizing an artificial receptor (the host) bearing a catalytic moiety, in order to bring substrates (the guests) and

reactive centers in close proximity, thus increasing reaction rates.

Macrocyclic compounds have proven to be excellent supramolecular hosts, so it is quite obvious that many supramolecular catalysts were based on cyclodextrines,<sup>6</sup> cucurbiturils,<sup>7</sup> crown ethers,<sup>8</sup> cavitands<sup>9</sup> and calixarenes,<sup>10</sup> which from now on will be the main topic.

## ***1.2. Calixarenes as Supramolecular Catalysts***

Calix[*n*]arenes<sup>11</sup> are a well-known class of macrocyclic compounds which have been largely exploited in the last decades due to their peculiar three-dimensional shape and ease of functionalization.<sup>12</sup> The synthetic versatility of calixarene macrocycles makes them suitable for a wide range of applications including molecular recognition and sensing,<sup>13</sup> synthesis of interpenetrated architectures,<sup>14</sup> biomolecular recognition,<sup>15</sup> and catalysis.<sup>16</sup>

For example, de Mendoza and coworkers reported<sup>17</sup> the synthesis of two calix[6]arene based artificial receptors (Figure 1) able to coordinate dioctanoyl-L- $\alpha$ -phosphatidylcholine

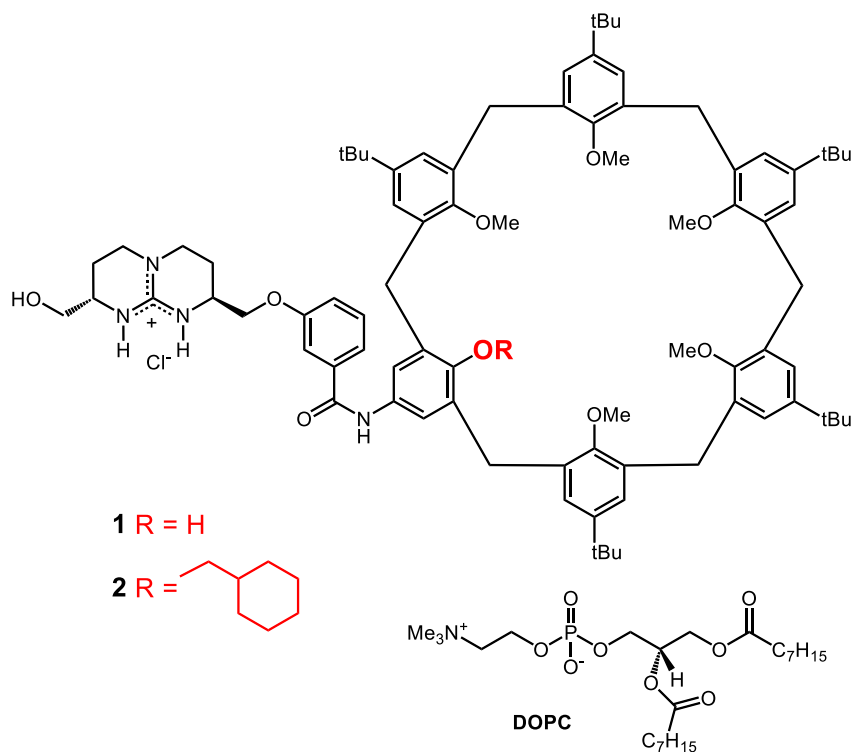


**Figure 1.** Structure of artificial receptors **1** and **2**.

(DOPC) thanks to the complementarity with both the quaternary ammonium and phosphate portion of the choline. The study outlined cation- $\pi$  interactions between the quaternary

ammonium and the aromatic walls of the calixarene macrocycle, and the presence of three H-bonds between the phosphate and both the amide and guanidinium protons.

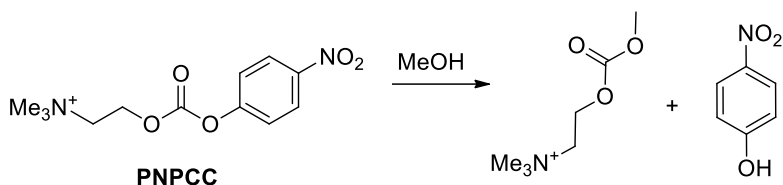


**Figure 2.** Methanolysis of PNPCC

Interactions through multiple binding sites are also responsible of the transition state stabilization during the methanolysis of *p*-nitrophenylcholine carbonate (PNPCC). Derivatives **1** and **2** catalyze the cleavage of PNPCC respectively 600 and 1000 times better than an equimolar mixture of the disconnected subunits (calixarene macrocycle and guanidinium alone), thus revealing the existence of a synergistic effect. In particular, the calixarene moiety, although not showing catalytic activity, contributes to stabilizing the transition state by interacting with the non-reactive portion of the substrate.

Another interesting example of artificial enzyme has been provided by Reinhoudt and coworkers.<sup>18</sup>

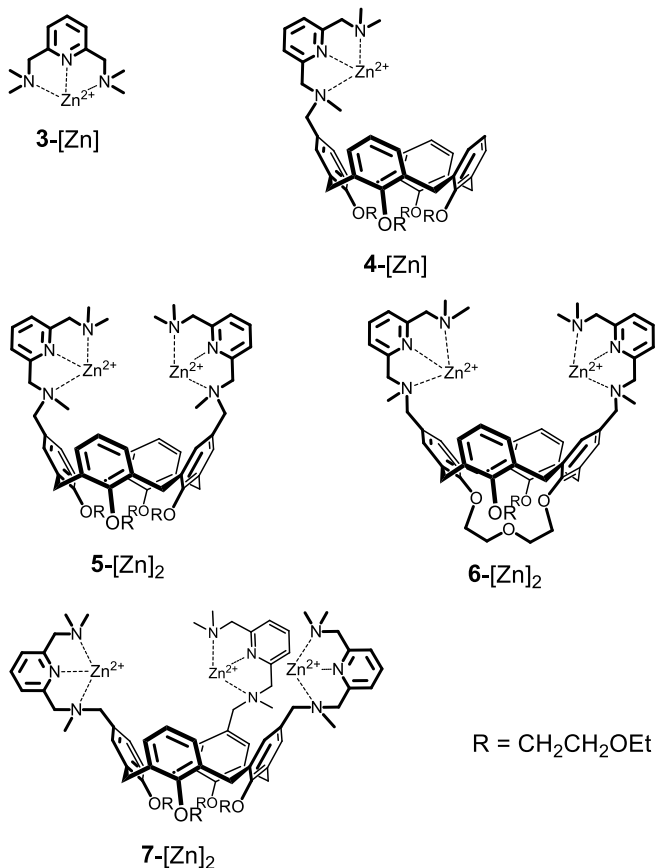


**Figure 3.** Mono-, di- and trinuclear (ZnII) artificial phosphatases.

In this case, a calix[4]arene derivative has been used as a scaffold to attach one, two or three  $\alpha,\alpha'$ -aminomethylpyridine

moieties obtaining ligands **4**, **5**, **6** and **7** (Figure 3). After addition of  $\text{Zn}(\text{ClO}_4)_2$  the resulting complexes behaved as artificial, phosphatases in the catalytic cleavage of RNA model substrate 2-hydroxypropyl-*p*-nitrophenylphosphate (HPNP). Complex **4**-[Zn] catalyzed the reaction 6 folds better than the reference compound **3**-[Zn] thus revealing that hydrophobic effects played a role in the catalytic process. Dinuclear complex **5**-[Zn]<sub>2</sub> yielded a 23000 fold rate enhancement with respect to the uncatalyzed reaction. This enormous result could be explained assuming a synergistic action of the two Zn(II) centers. Interestingly dinuclear complex **6**-[Zn]<sub>2</sub> was 8 times less active than the more flexible analogue **5**-[Zn]<sub>2</sub>, showing that an increase in rigidity determines a decrease in the cooperativity between the metal ions. From this study emerged that the most effective catalyst is the trinuclear complex **7**-[Zn]<sub>3</sub>, as a rate acceleration of 32000 times was observed. Compared with the dinuclear complex **5**-[Zn]<sub>2</sub> the additional Zn(II) center in **7**-[Zn]<sub>3</sub> is responsible of a 40% higher rate enhancement in HPNP cleavage. A possible mechanism explaining these outstanding activity considers double Lewis acid activation of the phosphate by two adjacent Zn(II) centers, whereas the third metal center helps deprotonating the substrate by the action of a coordinated

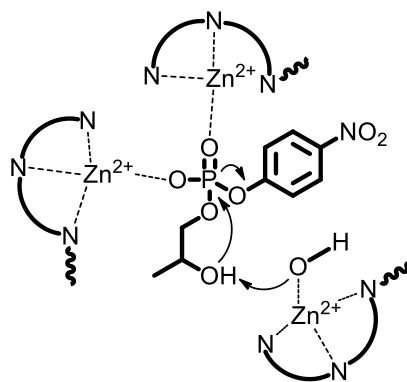
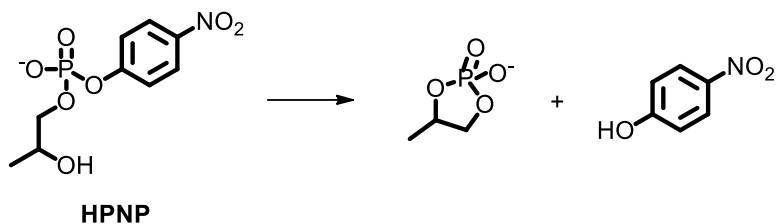


**Figure 4.** Proposed mechanism for HPNP cleavage by trinuclear phosphatase model

hydroxide (Figure 4). Apart from these examples dealing with a binding cavity linked to a catalytic site, another approach to the design of supramolecular catalysts consists in a cavity able to bind two or more different substrates at the same time. If sufficient transition state stabilization (or ground state destabilization) is provided, then the reaction occurs even without catalytic moiety. Furthermore, the cavity could organize

the reactants in such a way that the resulting product is different, in terms of regio- and stereoselectivity, from that commonly obtained.

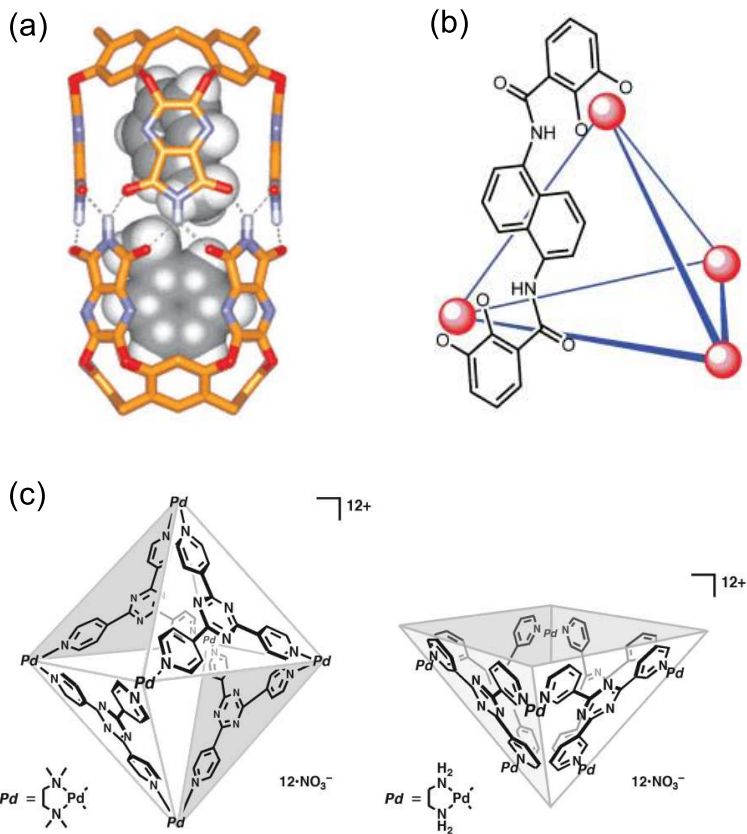


**Figure 5.** (a) Energy-minimized structure of the complex of the Rebek capsule and two toluene molecules. (b) Schematic representation of the Raymond tetrahedral cage. (c) Fujita square (left) and open-square hollow complex (right).

Pioneering studies by Rebek,<sup>19</sup> Fujita<sup>20</sup> and Raymond<sup>21</sup> demonstrated that self-assembled hosts could be very useful in this kind of catalysis (Figure 5). For example Rebek non-covalent capsule catalyzed dipolar addition, while Fujita square and open-square hollow containers favored Diels Alder reaction. Raymond reported tetrahedral metal-ligand cage able to catalyze acid hydrolysis of orthoformate even in basic media.

Calixarenes also proved to be suitable scaffolds for the synthesis of container molecules to harvest several trademark features of enzymatic catalysis. Wang and coworkers<sup>22</sup> reported the formation of container **8** after reaction of *p*-*tert*-butylsulfonylcalix[4]arene, Co(II) or Ni(II) and a linker such as

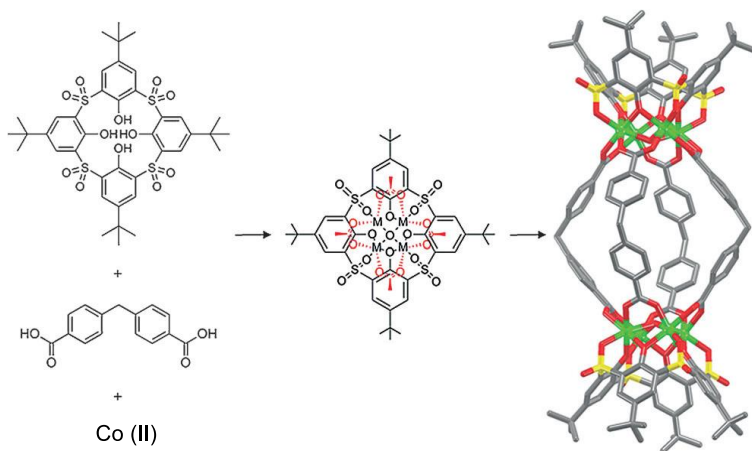


**Figure 6.** Assembly of supercontainer **8**.

4,4'-methylenedibenzoic acid (Figure 6). Screening of the catalytic activity of **8** for the Knoevenagel condensation involving the nucleophilic addition of malononitrile to aromatic aldehydes highlighted an interesting feature. Among all the substrate tested the only fair yield (67%) was obtained with sterically demanding 1-pyrenecarboxaldehyde. According to the authors this outstanding reactivity can be rationalized on the basis of a lock-and-key type match between **8** and 1-

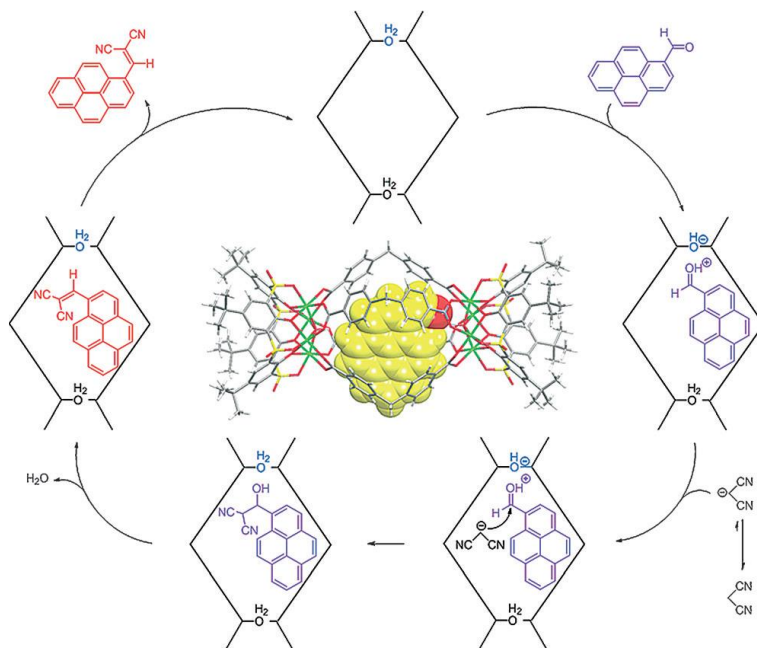


**Figure 7.** Proposed mechanism for the Knoevenagel condensation catalyzed by **8**.

pyrenecarboxaldehyde. The relatively weak Brønsted acidity of the  $\mu_4$ -H<sub>2</sub>O means that **8** does not readily protonate and activate an aldehyde unless the substrate possesses a suitable molecular size and shape to fit inside the cavity and allows its aldehyde moiety to be preorganized within the close proximity of the active site. Moreover, the final alkenyl product is easily released from the cavity because of its bulkiness, thus avoiding product inhibition (Figure 7).

All these examples so far discussed show the versatility of calixarene macrocycles in the design of supramolecular catalysts. In fact they could be used both as scaffolds to attach catalytic moieties (as artificial receptors **1** and **2**, and ligands **4-7**) and as building blocks in the self-assembly of supramolecular cages (as supercontainer **8**). Another important feature is the variety of reactions calixarene derivatives can catalyze. They could act as enzyme mimics in the strict sense, behaving as hydrolases and phosphatases acting on their substrate (like PNPCC and HPNP), but the resemblance with enzymes could also be interpreted in a more general way, as in the last example, where the concept of enzyme mimics is applied to a common organic reaction like the Knoevenagel condensation.



## *Goals and Outline of This Thesis*





## *Chapter 2*

### *Goals and Outline of This Thesis*

Given examples described above, our aim was to explore the role that calixarene cavities could play in determining the outcome of common chemical reactions. In order to do that, we synthesized new calix[4]arene derivatives **9-16** (Figure 8a-b), functionalized at their lower or upper rim with chiral catalytic moieties, and calix[8]arene zirconium complex **17**(Zr-O-*t*Bu)<sub>2</sub> (Figure 8c). Compounds **9-15** proved to be good Na<sup>+</sup> complexing agents, thanks to the amide pendants, so they have been tested in asymmetric phase transfer alkylation reactions thanks to a collaboration with the group of Dr. Della Sala (see Chapter 3).<sup>23</sup> Derivative **16**, bearing a thiourea and a primary amine, has the typical design of bifunctional catalysts, therefore has been tested in Michael type reactions between carbonyl nucleophiles and activated alkenes, in collaboration with the group of Prof. Lattanzi (see Chapter 4).<sup>24</sup> Since our interests did not confine to organocatalysis, we decided to start a collaboration with Prof. Grassi research group, involving the

synthesis and characterization of complex **17** ( $\text{Zr-O-}^t\text{Bu}$ )<sub>2</sub> and the evaluation of its activity in the ring opening polymerization of cyclic esters (see Chapter 5).<sup>25</sup>

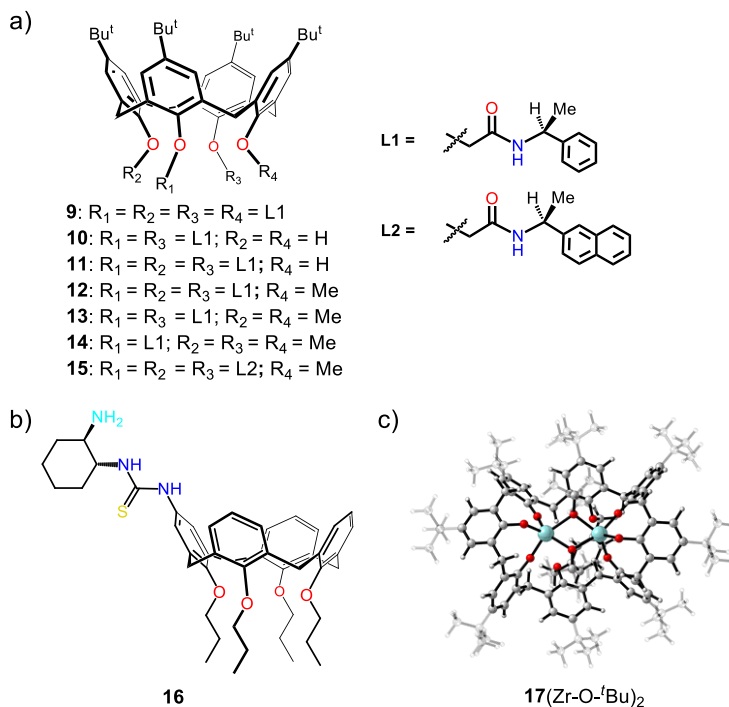
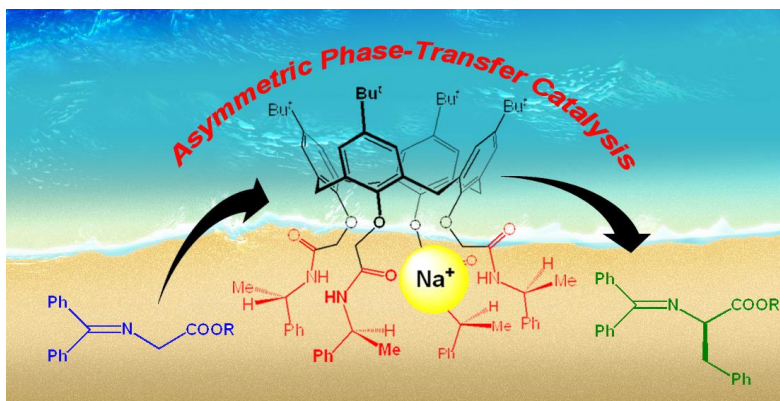


**Figure 8.** (a) Phase Transfer Catalysts **9–15**. (b) Bifunctional Catalyst **16**. (c) Complex **17**(Zr-O-<sup>t</sup>Bu)<sub>2</sub>.

## *Phase-Transfer Catalysis*





## *Chapter 3*

### *Phase-Transfer Catalysis (PTC)*

#### *3.1. General Overview*

During last decades phase-transfer catalysis,<sup>26</sup> requiring simple procedures, mild reaction conditions and providing large scale synthesis, has emerged as a powerful protocol in those fields where green chemistry standards are required, such as food or pharmaceutical industry.

The reaction between the species situated in two distinct and immiscible phases (generally an organic and an aqueous, or solid, one) occurs thanks to compounds with a good affinity for both media, such as quaternary ammonium ions, able to operate the transfer of the reactants from a phase to another (phase-transfer catalyst, PTC).

Thanks to their aromatic cavity and to the *tert*-butyl groups, calixarenes show hydrophobic character, but it is possible to enhance hydrophilicity by functionalization with ionic moieties, so that amphyphylic calixarene based PTC have been

developed.<sup>27</sup> In these cases the macrocycle acts as a scaffold bearing quaternary ammonium groups as the actual phase-transfer catalysts, thus ignoring calixarenes properties as supramolecular hosts.

It has long been known the high affinity that calix[4]arene-

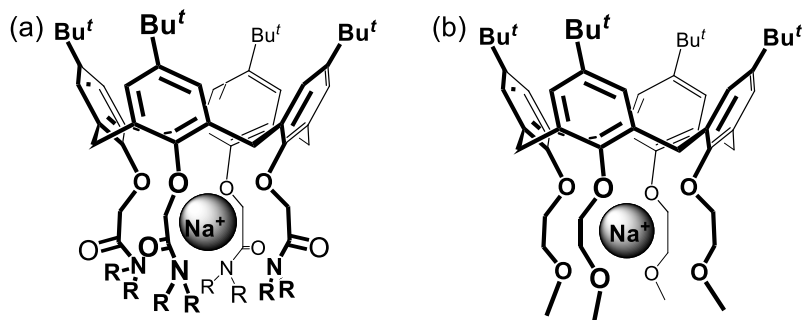


**Figure 9.** (a) Complexation of Na<sup>+</sup> with calix[4]arene-tetramide hosts. (b) The first example of calix[4]arene-based PTC.

amide hosts display towards alkali metal cations. The studies conducted by Arnaud-Neu and coworkers<sup>28</sup> showed that Na<sup>+</sup> was the best extracted cation, among the alkali metal cations series (Figure 9a).<sup>29</sup>

These cation-recognition abilities of calixarene-amides have been particularly exploited in sensing devices<sup>29a,c-e</sup> for the detection of metal ions and for the extraction of alkali picrates,<sup>28</sup>

whereas their employment in phase transfer catalysis has surprisingly remained elusive.

Shinkai<sup>30</sup> (Figure 9b) and Taniguchi<sup>31</sup> reported about thirty years ago some examples of PTC exploiting the cation-

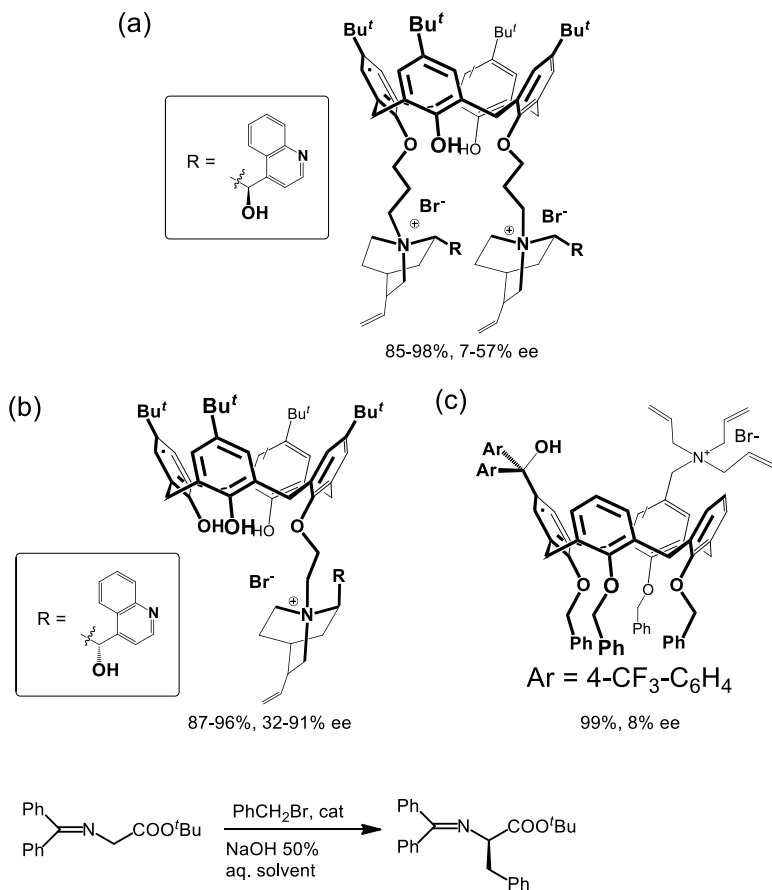


**Figure 10.** Calixarene based PTC proposed by (a) Sirit, (b) Su, (c) Shimizu.

recognition abilities of calixarene-ether derivatives. Since then, however, this strategy has been completely disregarded.<sup>32</sup> Although calix[4]arene-tetraamides are better hosts for alkali-metal cations than calixarene-ethers, their employment in the field of phase-transfer catalysis has been inexplicably uninvestigated. The development of enantioselective reactions using a PTC protocol is a task of great importance because of the possibility to obtain optically active molecules of biological and pharmaceutical interest.<sup>33</sup> In this regard, the synthesis of optically active  $\alpha$ -amino acids via phase transfer alkylation of prochiral protected glycine derivatives with chiral calixarene-ammonium catalysts has been studied in the last decade. Thus, Sirit<sup>34</sup> and co-workers designed a chiral calix[4]arene, bearing at the lower rim two ammonium pendant groups derived from cinchona alkaloid, as a phase-transfer catalyst for the enantioselective synthesis of  $\alpha$ -amino acids. Analogously, Su<sup>35</sup> and Shimizu<sup>36</sup> reported calix[4]arene-based phase-transfer catalysts, bearing cationic pendant groups at the lower and the upper rim respectively, for the enantioselective  $\alpha$ -functionalization of glycine. Surprisingly, no examples of asymmetric phase-transfer catalysis exploiting the cation-

recognition abilities of chiral calixarene-amide hosts have been reported to date.

Prompted by these considerations we designed chiral calix[4]arene-amides **9-15** (Figure 11) and we wish to report here on their abilities as phase-transfer catalysts in the asymmetric alkylation of *N*-(diphenylmethylene)-glycine esters.

### 3.2. Synthesis of new PTC Calixarene-Based Catalysts.

Calixarene-amide derivatives **9** and **10** were synthesized according to the procedures reported by Stibor and coworkers.<sup>37</sup>

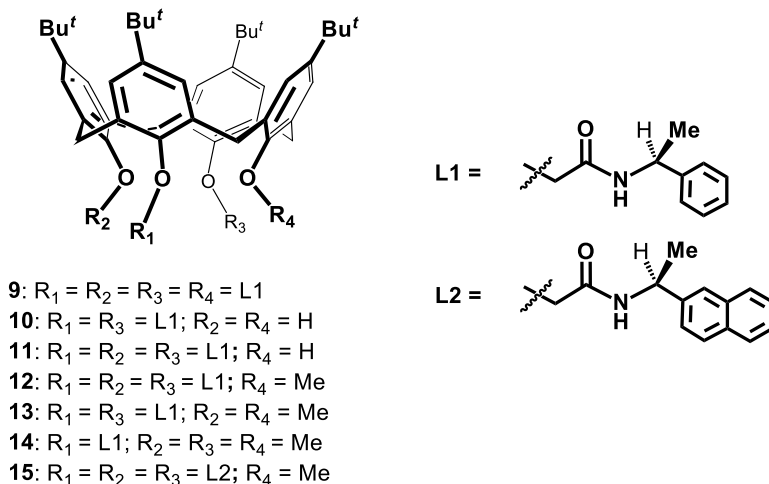


**Figure 11.** Calix[4]arene amides **9-15**.

Calixarene-monohydroxy-triamide **11** was obtained following the procedure reported in figure 12a. In details, the known calix[4]arene-tri-carboxylic acid **17**<sup>38</sup> was converted into the corresponding acyl chloride and then coupled with (S)- $\alpha$ -methylbenzylamine to give **11** in 20 % yield, which was characterized by HR ESI(+)-MS, <sup>1</sup>H and <sup>13</sup>C NMR spectroscopy (see experimental section).

Calixarene-monomethoxy-triamide **12** was obtained following a synthetic route similar to **11** (Figure 12a). The methylation of the free OH group of **16** in the presence of potassium carbonate afforded 25-methoxy-26,27,28-tris-((ethoxycarbonyl)methoxy)-5,11,17,23-tetra-tert-butyl-calix[4]arene **18**<sup>39</sup> in 70 % yield. Derivative **18** was suspended in a mixture of EtOH/H<sub>2</sub>O and hydrolyzed in the presence of NaOH to give triacid **19** in 96 % yield, which was first converted into the corresponding acyl chloride, then coupled with (S)- $\alpha$ -methylbenzylamine to give **12** in 57 % yield.

The synthesis of calix-dimethoxy-diamide **13** is outlined in Figure 12b. The known diacid derivative **20**<sup>40</sup> was converted into the corresponding diacyl chloride and then directly coupled with (S)- $\alpha$ -methylbenzylamine to give **13** in 80 % yield, which was characterized by HR ESI(+)-MS, <sup>1</sup>H and <sup>13</sup>C NMR

spectroscopy.(see experimental section) Calix-trimethoxy-monoamide **14** was easily obtained (Figure 12c) transforming the known monoacid derivative **21**<sup>41</sup> into the corresponding acyl chloride by treatment with oxalyl chloride, and subsequent coupling with (S)- $\alpha$ -methylbenzylamine to give **14** in 60 % yield. Finally, calix-monomethoxy-naphthyl-triamide **15** was obtained in 76 % yield, by coupling the acyl chloride of **19** (Figure 12a) with (S)-1-(2-naphthyl)ethylamine.

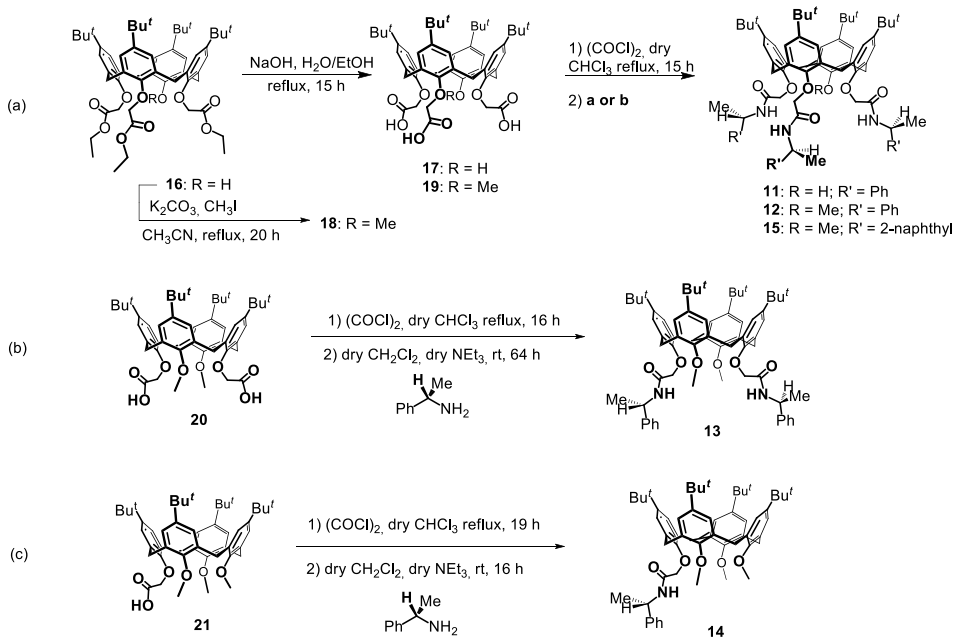


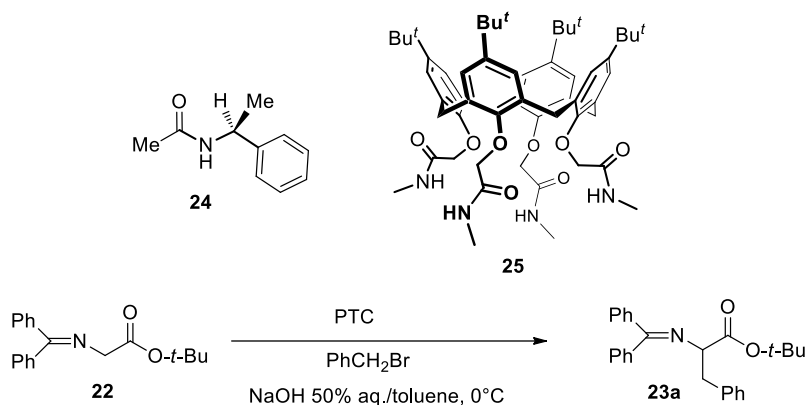
**Figure 12.** Synthesis of derivatives **11-15**. Conditions a): dry  $\text{CH}_2\text{Cl}_2$ , dry  $\text{NEt}_3$ , (*S*)- $\alpha$ -methylbenzylamine, 15 h, room temperature. Conditions b): dry  $\text{CH}_2\text{Cl}_2$ , dry  $\text{NEt}_3$ , (*S*)-1-(2-naphthyl)ethylamine, 3 d (63 h), room temperature.

### 3.3. *Asymmetric PTC Catalysis.*

Thanks to a collaboration with Prof. I. Izzo, Dr. G. Della Sala and Dr. R. Schettini, calix[4]arene-amides **9-15** were tested in the phase-transfer alkylation of N-(diphenylmethylene)-glycine *tert*-butyl ester **22** with benzyl bromide in a liquid-liquid system NaOH 50%/toluene at 0 °C, with a catalyst loading of 5 mol % (Table 1, entries 1-7). The alkylation catalyzed by tetramide **9** led to the (R)-benzylated product **23a** with a good yield but with disappointing enantioselectivity (Table 1, entry 1). Comparable yields and faster reactions were obtained with amides **10** and **11**, but the resulting enantioselectivities were even lower (Table 1, entries 2 and 3), probably due to the undesired alkylation of the hydroxyl of **10** and **11**.

To avoid the side reaction, we focused on calix-methoxy-amides **12-14**. A significant improvement of both yield and enantioselectivity was achieved with triamide **12** (Table 1, entry 4). The enantioselectivity decreased when reducing the number of chiral amide moieties (entries 5 and 6), as monoamide **14**, led to racemic product and incomplete conversion even after 20 h. A possible explanation is that in this case, the presence of only one chiral amide group results in reduced cation-complexing

abilities, while synergistic action of two or three amide pendants increases stereodifferentiating abilities. Using compound **15**, functionalized with (*S*)- $\alpha$ -methylnaphthylamine pendants, in place of (*S*)- $\alpha$ -methylbenzylamine, slowed down the reaction



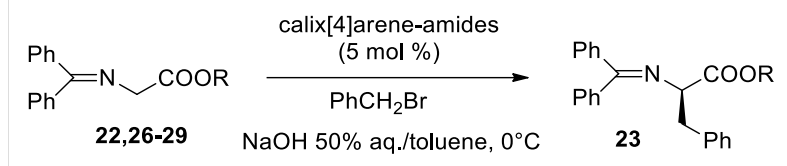
- (a): uncatalyzed, 8 % yield, racemate.  
 (b): cat. **24** (20 mol %), 9 % yield, racemate.  
 (c): cat. **25** (5 mol %), 40 % yield.

**Figure 13.** Phase-transfer benzylation of *N*-(diphenylmethylene)-glycine *t*-butyl ester **22** catalyzed by amide **24** and calixarene-tetramide **25**.

and led to lower ee value (Table 1, entry 7), due to excessive steric hindrance, that probably results in reduced access to the catalytic site. A comparison of the yields obtained in the presence of calixarene-amides **9-15** with the low conversion

observed in the uncatalyzed reaction (8% yield after 24 h, Figure 13a) confirmed the catalytic activity of these macrocycles.

**Table 1.** Phase-transfer benzylation of *N*-(diphenylmethylene)-glycine esters promoted by calix[4]arene-amides **9-15**.<sup>[a]</sup>



Entry	Catalyst	Substrate	Time [h]	Yield <sup>[b]</sup> [%]	ee <sup>[c,d]</sup> [%]
1	<b>9</b>	<i>t</i> -Bu- ( <b>22</b> )	20	77	13
2	<b>10</b>	<i>t</i> -Bu- ( <b>22</b> )	4	71	7
3	<b>11</b>	<i>t</i> -Bu- ( <b>22</b> )	4	83	5
4	<b>12</b>	<i>t</i> -Bu- ( <b>22</b> )	5	92	28
5	<b>13</b>	<i>t</i> -Bu- ( <b>22</b> )	4	92	13
6	<b>14</b>	<i>t</i> -Bu- ( <b>22</b> )	20	48	rac
7	<b>15</b>	<i>t</i> -Bu- ( <b>22</b> )	20	97	9
8	<b>12</b>	Et- ( <b>26</b> )	3	77	4
9	<b>12</b>	Bn- ( <b>27</b> )	7	80	rac
10	<b>12</b>	Ph(Me) <sub>2</sub> C- ( <b>28</b> )	6	84	24
11	<b>12</b>	Ph <sub>2</sub> CH- ( <b>29</b> )	5	74	6 (S)

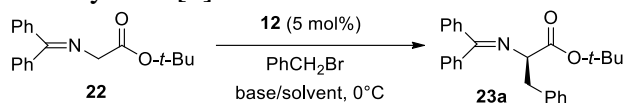
[a] All reactions were performed in a liquid-liquid system with 0.08 mmol of substrate **22,26-29**, benzyl bromide (1.2 equiv.), and catalyst (5 mol %) in toluene (0.8 mL) and NaOH 50% aq (0.5 mL). [b] Isolated yields. [c] Determined by HPLC using a Chiralcel OD-H chiral stationary phase. [d] The absolute configuration of the products were determined by comparison of the HPLC retention times and optical rotations with literature values.<sup>34,42</sup>

In order to prove the effect of calixarene scaffold on catalytic activity and enantioselectivity, we conducted the reaction in the presence of chiral monoamide **24** (0.20 equiv., Figure 13b). Racemic benzylated product **23a** was obtained in 9% yield, presumably as a result of the background reaction. The achiral tetramide **25**, although less active than its chiral analogue **9**, also showed a moderate catalytic activity (5 mol% cat., 40 % yield, Figure 13c). We assumed that the calixarene scaffold plays an essential role in phase-transfer catalysis activity by preorganizing and orienting properly the amide groups in such a way as to favor the complexation of Na<sup>+</sup> cation.

Successively, we evaluated the effect of the ester group in the substrate, using the best catalyst **12**. As expected,<sup>42</sup> the presence of less hindered ester groups, such as ethyl and benzyl, reduced the stereoselectivity of alkylation (Table 1, entries 8 and 9). Cumyl ester **28** afforded lower ee (Table 1, entry 10). A disappointing result was also observed with the benzhydryl ester **29**, with an unexpected inversion of enantioselectivity (Table 1, entry 11).

After screening of the catalysts and the ester groups of the substrates, we directed our attention towards examining the

**Table 2.** Optimization of phase-transfer benzylation of **22** promoted by calix[4]arene-triamide **12**.<sup>[a]</sup>



Entry	Solvent	Base	Time [h]	Yield <sup>[b]</sup> [%]	ee <sup>[c,d]</sup> [%]
1	toluene	NaOH 50% aq.	5	92	28
2	Et <sub>2</sub> O	NaOH 50% aq.	5	87	4
3	CH <sub>2</sub> Cl <sub>2</sub>	NaOH 50% aq.	7	83	6
4	CHCl <sub>3</sub>	NaOH 50% aq.	30	78	5
5	chlorobenzene	NaOH 50% aq.	5	90	rac
6	<i>m</i> -xylene	NaOH 50% aq.	20	82	3
7	<i>p</i> -xylene	NaOH 50% aq.	7	84	rac
8	<i>o</i> -xylene	NaOH 50% aq.	5	88	17
9	mesitylene	NaOH 50% aq.	7	86	35
10	mesitylene/ CH <sub>2</sub> Cl <sub>2</sub> 9:1	NaOH 50% aq.	6	89	26
11	mesitylene	NaOH (s)	92	75	4 (S)
12	mesitylene	KOH 50% aq.	92	76	10 (S)
13	mesitylene	KOH (s)	44	79	15 (S)
14	mesitylene	CsOH (s)	44	72	11 (S)
15 <sup>[e]</sup>	mesitylene	NaOH 50% aq.	92	12	14
16 <sup>[f]</sup>	mesitylene	NaOH 50% aq.	7	73	28
17 <sup>[g]</sup>	mesitylene	NaOH 50% aq.	20	73	13

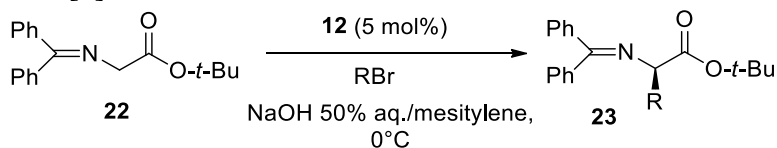
[a] Reactions were performed in a liquid-liquid system with 0.08 mmol of **22**, benzyl bromide (1.2 equiv.), and catalyst (5 mol %) in toluene (0.8 mL) and NaOH 50% aq. (0.5 mL), except where otherwise noted. [b] Isolated yields. [c] Determined by HPLC using a Chiralcel OD-H chiral stationary phase. [d] The absolute configuration of the product was determined by comparison of the HPLC retention time and optical rotation with literature values.<sup>42</sup> [e] Reaction performed at -20°C. [f] 10 mol % of catalyst loading was used. [g] 2.5 mol % of catalyst loading was used.

effect of other parameters, such as solvent, base, catalyst loading, and temperature, on the benzylation of t-butyl ester **22** promoted by **12**. Good yields but poor enantioselectivities were obtained in different reaction media such as chlorinated solvents, ether, chlorobenzene, and xylenes (Table 2, entries 2-8). On the other hand, a significant improvement, up to 35% ee, was obtained in mesitylene (Table 2, entry 9), while adding a 10% amount of CH<sub>2</sub>Cl<sub>2</sub> in mesitylene resulted in lower ee (Table 2, entry 10). The use of inorganic bases other than aqueous NaOH 50% resulted in low values and a startling inversion of the enantioselectivity (Table 2, entries 11-14). Replacement of sodium with the larger potassium or cesium cation, determines a change in the host-guest interactions that lead to a different tridimensional structure. This may affect the mode of association with the carbanion and hence enantioselectivity. At -20°C the reaction proceeded slowly, resulting in low conversion and enantioselectivity, even after prolonged reaction time (Table 2, entry 15). Lower enantioselectivities were also obtained with smaller or higher catalyst loadings (Table 2, entries 16 and 17). While examples of reduced enantioselectivity with increasing amount of catalyst has been frequently described,<sup>43</sup> much less common is the

opposite effect.<sup>44</sup> Presumably, at higher concentrations, aggregation of the host-guest complex is responsible of the low enantioselectivity.

Finally, we carried out this calix[4]arene-amide catalyzed reaction with other alkylating agents, under optimized conditions (NaOH 50% aq., 5 mol. % of triamide **12**, in mesitylene, Table 3). Good yields of alkylated products were obtained in all cases. Higher enantioselectivities were achieved

**Table 3.** Phase-transfer alkylation of **22** promoted by calix[4]arene-triamide **12**.<sup>[a]</sup>



Entry	R	Product	Time [h]	Yield <sup>[b]</sup> [%]	ee <sup>[c,d]</sup> [%]
1	benzyl	<b>23a</b>	7	86	35
2	4-methylbenzyl	<b>23b</b>	7	85	47
3	4-( <i>t</i> -butyl)benzyl	<b>23c</b>	20	79	44
4	2-methylbenzyl	<b>23d</b>	7	75	15
5 <sup>[e]</sup>	allyl	<b>23e</b>	20	75	15

[a] All reactions were performed in a liquid-liquid system with 0.08 mmol of **22**, benzyl bromide (1.2 equiv.), and catalyst (5 mol %) in toluene (0.8 mL) and NaOH 50% aq (0.5 mL). [b] Isolated yields. [c] Determined by HPLC using a Chiralcel OD-H chiral stationary phase. [d] The absolute configuration of the product was determined by comparison of the HPLC retention time and optical rotation with literature values.<sup>42</sup> [e] 1.5 equiv. of allyl bromide were used.

with p-alkyl substituted benzyl substrates (Table 3, entries 2 and 3), whereas with a ortho-substituted substrate and with allyl bromide a 15% ee resulted (Table 3, entries 4 and 5).

### ***3.4. Recognition Abilities of Calix[4]arene-Amides toward Na<sup>+</sup> Cation.***

The complexation of Na<sup>+</sup> by calix[4]arene-amide catalyst is the fundamental step in the phase-transfer alkylation of glycine ester **22** with benzyl bromide (Tables 1-3), so we decided to investigate the recognition abilities of the most active calix[4]arene-amides catalysts **9**, **12**, **13**, **15** toward Na<sup>+</sup> guest. <sup>1</sup>H NMR titration experiments<sup>45</sup> of a CDCl<sub>3</sub> solution of host with NaTFPB [tetrakis[3,5-bis(trifluoromethyl)phenyl]borate]<sup>46</sup> were performed. The choice of this particular sodium salt resides in the fact that hydrophobic TFPB<sup>-</sup>, that is known to be a weakly coordinating anion,<sup>47</sup> confers relatively good solubility to its sodium salt in organic solvents,<sup>48</sup> thus allowing to determinate the apparent association constant of the complex by direct integration of its <sup>1</sup>H NMR signals with respect to those of the free host.



after addition of NaTFPB. The addition of 0.5 equiv of NaTFPB results in the appearance of new signals (Figure 14b). In details, it is possible to individuate a new AX system (4.25 and 3.26 ppm,  $J = 12.0$  Hz) in the  $^1\text{H}$  NMR spectrum (in red in figure 14b), attributable to the  $\text{ArCH}_2\text{Ar}$  groups of the  $\text{Na}^+\text{C}\mathbf{9}$  complex in slow exchange with those of the free host **9** on the NMR time scale. The  $\text{OCH}_2$  protons of the free host **9**, resonating at 4.33 ppm (AB system), form a new AX system (4.52 and 3.89 ppm,  $J = 13.2$  Hz) after complexation with  $\text{Na}^+$  (in magenta in figure 14b). After a further addition of 0.5 equiv of NaTFPB the system was equilibrated for 3 days at 25 °C and a 74% yield of the  $\text{Na}^+\text{C}\mathbf{9}$  complex was calculated by  $^1\text{H}$  NMR signal integration of both complexed and free host **9** (Figure 14c). From the percentage of formation of the  $\text{Na}^+\text{C}\mathbf{9}$  complex an apparent association constant ( $K_a$ ) of  $1.22 \pm 0.04 \times 10^4 \text{ M}^{-1}$  was calculated.

Successively, we studied the binding affinity of calixarene-monomethoxy-triamide **12** toward NaTFPB in  $\text{CDCl}_3$  (Figure 15). Structure elucidation of free **12** was made by 1D and 2D NMR spectroscopy.  $^1\text{H}$  NMR spectrum ( $\text{CDCl}_3$ , 298 K) of compound **12** (Figure 15a) displays four AX systems at 4.49/3.24, 4.31/2.94, 4.11/3.24, and 4.08/3.24 ppm (COSY spectrum, see experimental section) which correlate in the

HSQC spectrum with CH<sub>2</sub> carbon signals at 31.6, 31.5, and 31.8 (x2) ppm, respectively. By the known Gutsche's and de Mendoza's rules,<sup>49</sup> these data were only compatible with a cone

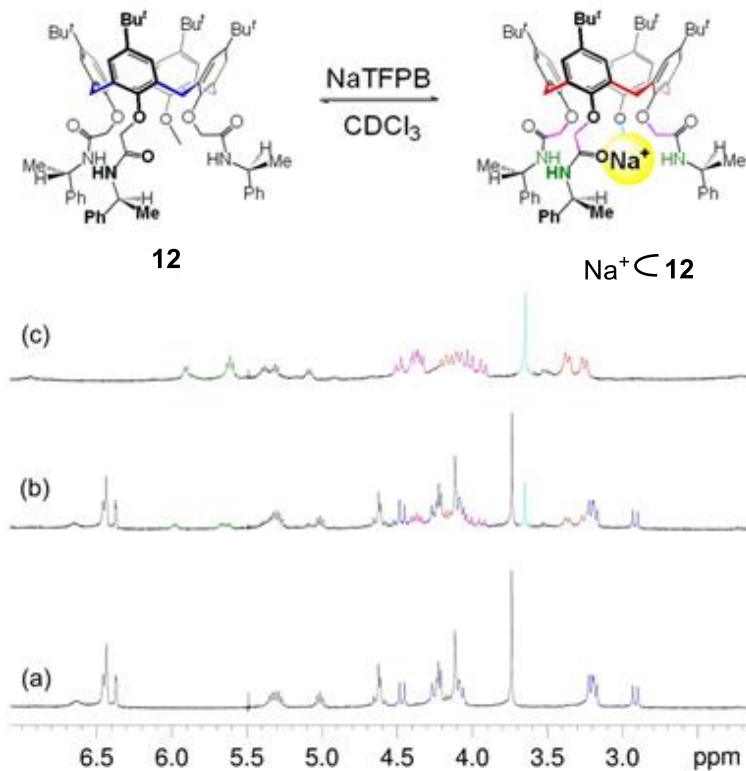


**Figure 15.** <sup>1</sup>H NMR spectra (400 MHz, CDCl<sub>3</sub>, 298 K) of: (a) triamide **12** (1.9 mM) (b) an equimolar solution (1.9 mM) of **12** and NaTFPB after mixing; (c) an equimolar solution (1.9 mM) of **12** and NaTFPB after equilibration for 3 d (72 h) at 298 K.

conformation of **12**. An important information about the peculiarity of the cone conformation adopted by **12**, is given by the presence in the  $^1\text{H}$  NMR spectrum of shielded aromatic signals in the 6.40-6.47 ppm region (integrating for 4 H). This is an evidence of the fact that the calixarene skeleton of **12** adopts a pinched conformation. The pinched-cone conformation adopted by **12** in solution was studied by DFT calculations at the B3LYP/6-31G(d,p) level of theory, highlighting the presence of two stabilizing intramolecular H-bonding interactions between amide groups at the lower rim.

The addition of 0.5 equiv. of NaTFPB salt to a  $\text{CDCl}_3$  solution of **12** resulted in the appearance of a new set of signals in the  $^1\text{H}$  NMR spectrum attributable to the formation of the  $\text{Na}^+\text{C}\text{12}$  complex, which was in slow exchange with free **12** on the NMR time scale (Figure 15b). Further addition of 0.5 equivalents of NaTFPB salt and equilibration for 3 days at  $25^\circ\text{C}$  quantitatively afforded  $\text{Na}^+\text{C}\text{12}$  (Figure 15c).

After determining the 1:1 stoichiometry of the  $\text{Na}^+\text{C}\text{12}$  complex by spectral integration (with respect to the  $\text{TFPB}^-\text{ArH}$  signal), structure elucidation was made by means of 1D and 2D NMR studies (2D HSQC and COSY spectra; 600 MHz,  $\text{CDCl}_3$ ; see experimental section). In details, the disappearance in the  $^1\text{H}$

NMR spectrum of the signals of **12** between 6.40-6.47 ppm, which are attributable to the aromatic rings of the pinched-cone inwardly oriented with respect to the calix-cavity, reveals that Na<sup>+</sup> complexation determines a conformational change of **12** from the pinched-cone to a “classic” cone conformation, in which the above mentioned aromatic protons resonate between 7.01 and 7.39 ppm. This conformational shift is probably due to the fact that Na<sup>+</sup> complexation occurs thanks to cation dipole interactions with the oxygens at the lower rim, determining the encapsulation of the cation and disrupting hydrogen bonds between amide groups that stabilized the pinched-cone conformation. Thus, the <sup>1</sup>H NMR signals attributable to the OCH<sub>2</sub> groups at the lower rim of **12** are downfield shifted in the Na<sup>+</sup>⊂**12** as a consequence of the cation proximity. On the other hand, the singlet at 3.74 ppm attributable to the OCH<sub>3</sub> group of **12** is upfield shifted at 3.65 ppm. This quite surprising result can be explained by a close inspection of the DFT-optimized structure of the Na<sup>+</sup>⊂**12** complex at the B3LYP/6-31G(d,p) theory level, that indicates that the OCH<sub>3</sub> group is in close proximity to a phenyl ring, thus establish a C-H⋯π interaction, with a C-H⋯π centroid distance of 2.81 Å (Figure 16\*). This result fully elucidate the different trend observed for OMe signal

with respect to OCH<sub>2</sub> groups at the lower rim of **12** after Na<sup>+</sup> complexation.

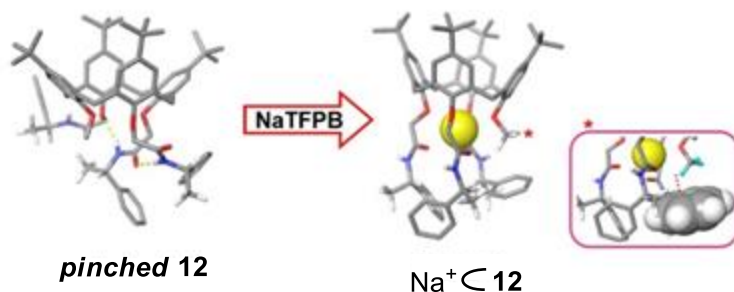


**Figure 16.** DFT-optimized structures of free **12**, in the pinched-cone conformation, and Na<sup>+</sup>⊂**12** complex at the B3LYP/6-31G(d,p) theory level (some H atoms have been omitted for clarity). Dotted lines in yellow indicate intramolecular H-bonds stabilizing the pinched conformation (average N-H···O=C distance 2.87 Å). Inset (\*): particular of the C-H···π interaction between methyl group and phenyl ring in the Na<sup>+</sup>⊂**12** complex.

In a similar way, addition of 0.5 equiv. of NaTFPB to a CDCl<sub>3</sub> solution of naphthyl-triamide **15**, resulted in the appearance of a new set of signals. In particular, four new AX systems are displayed (4.04 and 3.19 ppm, J = 11.8 Hz; 4.14 and 3.30 ppm, J = 11.8 Hz; 4.17 and 3.37 ppm, J = 12.4 Hz; 4.21 and 3.22 ppm, J = 12.0 Hz) which were attributable to ArCH<sub>2</sub>Ar

groups of Na<sup>+</sup>⊂**15** complex in slow exchange on the NMR time scale. In addition, three AX systems were individuated (4.33 and 3.85 ppm, J = 14.8 Hz; 4.37 and 4.05 ppm, J = 11.6 Hz and 4.60 and 4.44 ppm, J = 13.6 Hz) due to the OCH<sub>2</sub> groups of Na<sup>+</sup>⊂**15** complex. Finally, the OCH<sub>3</sub> group was present as a singlet at 3.60 ppm. Upon a further addition of 0.5 equivalents of NaTFPB salt, the formation of the Na<sup>+</sup>⊂**15** complex was complete after equilibration for 3 days at 25 °C. A percentage of formation of 78 % was calculated by integration of the OCH<sub>3</sub> singlets for free and complexed **15**, which gave an apparent association constant (*K<sub>a</sub>*) of 9.16±0.04×10<sup>3</sup> M<sup>-1</sup> (see experimental section).

Direct signal integration wasn't suitable for determining the apparent association constant of the Na<sup>+</sup>⊂**12** complex because the intensities of the <sup>1</sup>H NMR signals (Figure 15c) of the free host **12** were below the reliable 10 % limit. Therefore, *K<sub>a</sub>* was calculated by means of a competition experiment<sup>45</sup> between hosts **12** and **15**. A 1:1:1 mixture of **12**, **15** and NaTFPB equilibrated for 3 days at 25 °C, afforded Na<sup>+</sup>⊂**12** and Na<sup>+</sup>⊂**15** complexes with a percentage of formation of 56 and 44%, respectively, from which, an apparent association constant of 1.26±0.09×10<sup>4</sup> M<sup>-1</sup> was calculated for the formation of Na<sup>+</sup>⊂**12** complex (see experimental section).

Finally, we investigated the binding abilities of host **13**. In order to elucidate the structure of free **13** we recurred to VT  $^1\text{H}$  NMR studies. In fact,  $^1\text{H}$  NMR spectrum of calix-dimethoxy-diamide **13** recorded at  $-40\text{ }^\circ\text{C}$  shows an AX system at 4.12 and 3.20 ppm, due to the resonance of the  $\text{ArCH}_2\text{Ar}$  groups, which correlates in the 2D HSQC spectrum with a signal at 31.2 ppm. From the known Gutsche's and de Mendoza's rules,<sup>49</sup> these data were only compatible with a cone conformation of **13**.  $\text{Na}^+\subset\mathbf{13}$  complex formed after adding 1 equiv. of NaTFPB to a  $\text{CDCl}_3$  solution of **13** at  $25\text{ }^\circ\text{C}$ , as proved by the emerging, in the  $^1\text{H}$  NMR spectrum, of new set of slowly exchanging signals. In depth study of the NaTFPB/**13** mixture by mean of 1D and 2D NMR spectra revealed that calix[4]arene-diamide **13** can bind  $\text{Na}^+$  adopting two different conformations (Figure 17). In details, four doublets were present at 4.06, 3.95, 3.33, and 3.31 ppm which correlated with carbon resonances at 29.8 and 30.0 ppm, attributable to  $\text{ArCH}_2\text{Ar}$  groups between *syn* oriented Ar-rings, and compatible with a calixarene in a cone conformation ( $\text{Na}^+\subset\mathbf{13}^{\text{cone}}$ ). Moreover, the corresponding  $\text{OCH}_2$  resonate at 4.52 and 4.40 ppm, while the  $\text{OCH}_3$  singlet was present at 3.52 ppm. Besides, 1D and 2D NMR spectra allowed to individuate and characterize a  $\text{Na}^+\subset\mathbf{13}$  complex in which the calixarene

adopts a partial-cone conformation ( $\text{Na}^+\text{C13}^{\text{paco}}$ ). In fact, two AB systems at 3.76 and 3.82 ppm, which correlated in the HSQC spectrum with carbon atoms resonating at 37.5 and 37.9 ppm, were characteristic of methylene groups between anti oriented Ar-rings. In addition, two AB systems attributable to  $\text{OCH}_2$  groups were detected at 4.51/4.26 and 4.60/4.28 ppm. Finally, two singlets, attributable to the lower rim and inverted  $\text{OCH}_3$

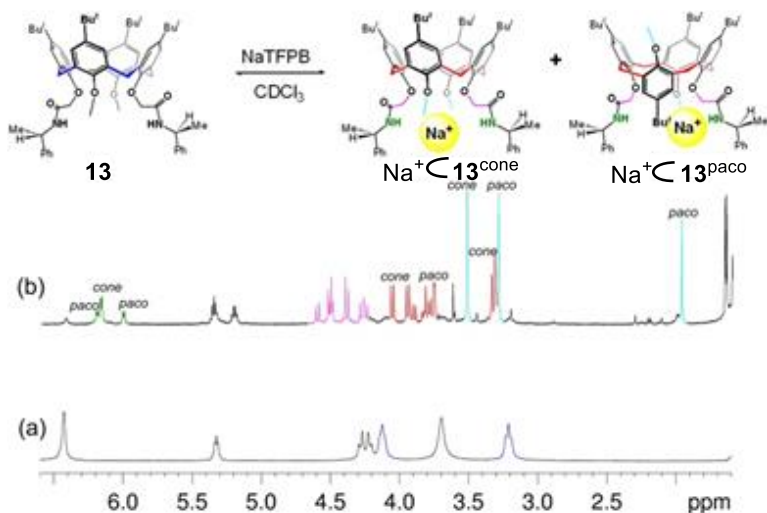


**Figure 17.** Expansion of the  $^1\text{H}$  NMR spectra (400 MHz,  $\text{CDCl}_3$ , 298 K) of: (a) derivative **13** (1.9 mM) (b) an equimolar solution (1.9 mM) of **13** and **NaTFPB** after equilibration for 3 d at 298 K.

group of the  $\text{Na}^+\text{C13}^{\text{paco}}$  complex resonated at 3.30 and 1.97 ppm, respectively.

Calix[4]arene-amides **9**, **12**, and **15** showed good complexing ability toward  $\text{Na}^+$  cation, thus explicating their activity as PTC. A possible mechanism for the asymmetric phase-transfer alkylation of **22** consider the interfacial formation of a tight ion pair between  $\text{Na}^+$ ⊂calixarene-amide complex and the enolate anion generated after deprotonation of **22**. The chiral lipophilic ion pair can diffuse into the organic layer and undergo enantioselective alkylation.

This study constitutes a valuable application of host-guest chemistry to catalysis, as, for the first time, calix[4]arene-amides **9-15** turned out to be active in the phase-transfer alkylation of N-(diphenylmethylene)glycine esters, thanks to their complexing properties. In depth investigation of the cation binding abilities of compounds **9**, **12**, **13** and **15** was performed, in order to elucidate their catalytic activity. Apparent association constants determined for catalysts **9**, **12**, **15** using NaTPB guest confirmed the importance of efficient  $\text{Na}^+$  complexation in order to reach high performances. Our hope is that these results could focus the attention on calixarenes modified with complexing moieties as PTC catalysts.

## *Asymmetric Organocatalysis*





# Chapter 4

## Asymmetric Organocatalysis

### 4.1. General Overview

Asymmetric organocatalysis consists in the use of small optically pure organic molecules in order to favor the formation of an enantiomer above the other during a reaction.

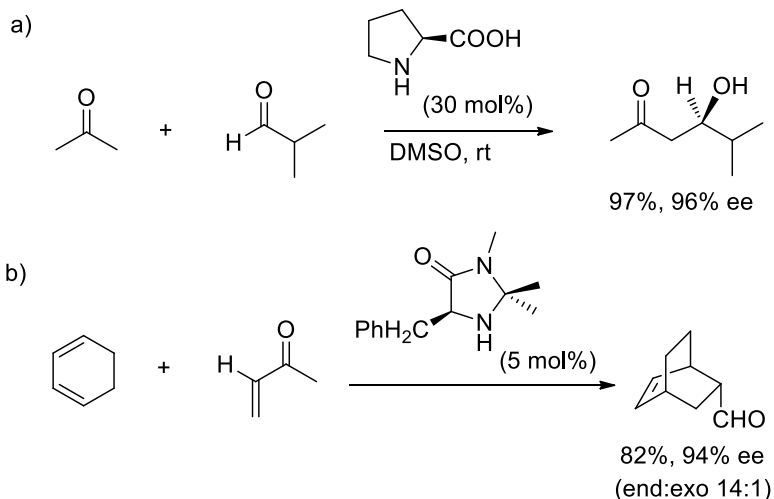


**Figure 18.** (a) Aldol reaction catalyzed by L-proline. (b) Diels-Alder reaction promoted by MacMillan catalyst.

This discipline aroused in the early 2000 when List and Barbas discovered that the aldol reaction of acetone and a series of aldehydes in presence of L-proline yielded  $\beta$ -hydroxyl-ketones with high enantioselectivities (Figure 18a),<sup>50</sup> and MacMillan reported a phenylalanine derived imidazolidinone promoting enantioselective Diels-Alder reactions (Figure 18b).<sup>51</sup>

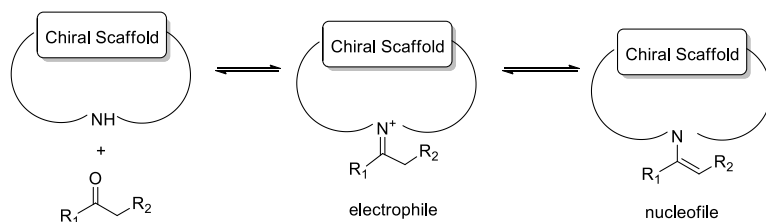


**Figure 19.** Substrate activation via covalent bond formation.

These pioneering works paved the way to the flourishing of aminocatalysis,<sup>52</sup> a branch of organocatalysis characterized by the fact that reactions are promoted by primary or secondary amines, which activate the reactants by means of covalent bond formation (Figure 19). According to this mechanism, an aminocatalyst could activate a carbonyl compound either by enhancing its electrophilic or nucleophilic character via formation of an iminium or enamine intermediate, respectively.

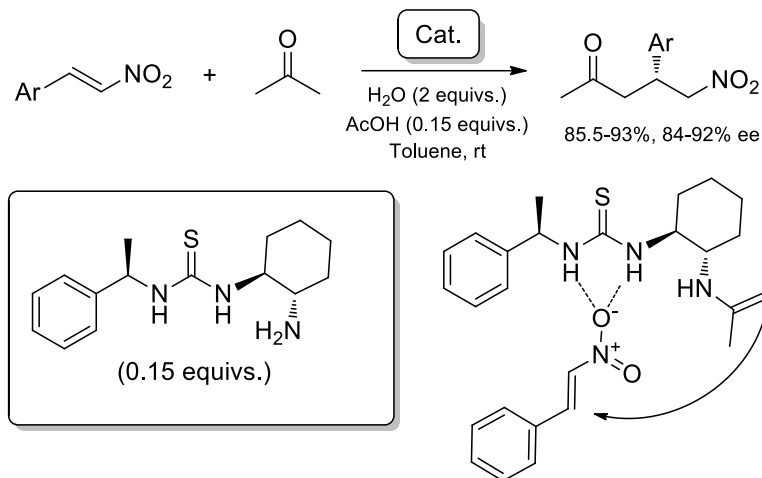


**Figure 20.** Asymmetric Michael addition of acetone to aromatic nitroolefins promoted by a primary amine thiourea bifunctional organocatalyst.

In more recent years a novel class of organocatalysts have been proposed, called bifunctional organocatalysts.<sup>53</sup> Their feature is the presence of a Brønsted acidic moiety in addition to an amine function, attached to a chiral scaffold. This trait allows simultaneous activation of both nucleophile and electrophile via general acid-base catalysis. If the catalyst combine a primary amine and a urea or thiourea as the acidic moiety, then is possible to combine nucleophile activation via enamine formation and electrophile activation via hydrogen bond: the generation of a rigid transition state is responsible of the high selectivities obtained (Figure 20).<sup>54</sup>

An interesting perspective consists in combining a bifunctional catalyst and a calixarene macrocycle in order to

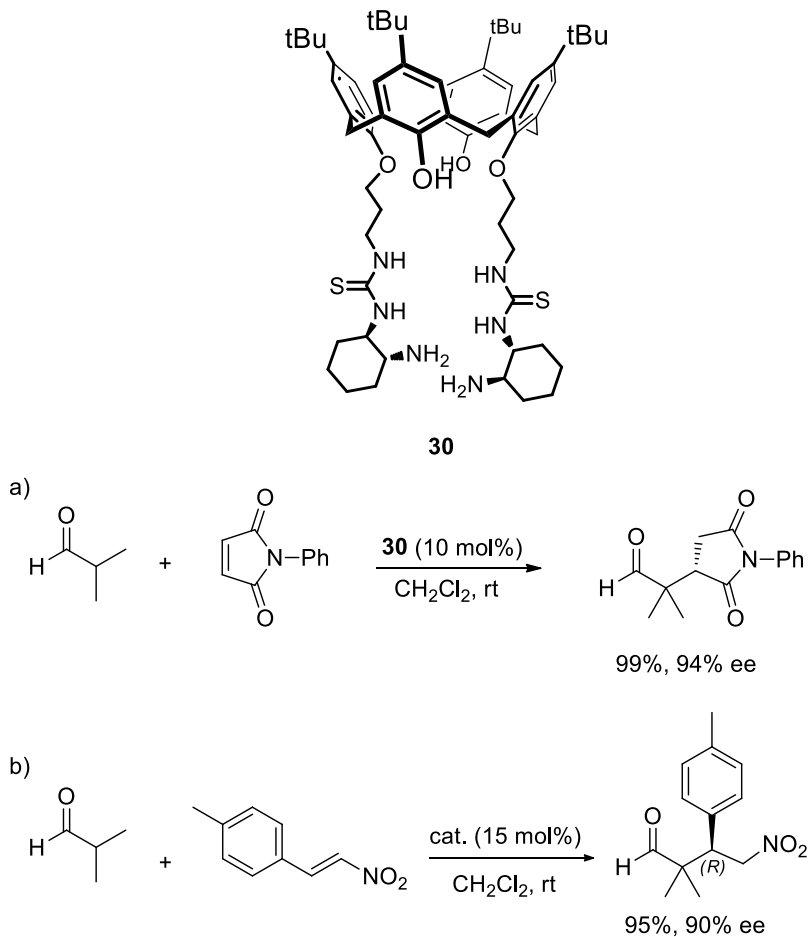


**Figure 21.** Catalytic addition of isobutyraldehyde to (a) N-phenylmaleimide and (b) *p*-methyl-*trans*- $\beta$ -nitrostyrene.

have an additional site for substrate recognition not involved in the catalytic process.

To the best of our knowledge the only example of such a compound has been reported by Sirit and Durmaz in the asymmetric Michael reactions of  $\alpha,\alpha$ -disubstituted aldehydes with maleimides (Figure 21a) and nitroolefins<sup>55</sup> (Figure 21b). The study outlined that compound **30** promotes the conjugate addition of a series of branched aldehydes to maleimide or nitroolefins in  $\text{CH}_2\text{Cl}_2$  at room temperature with high yield and enantiomeric excesses. Anyway the *trans*-1,2-diaminocyclohexane moiety is known to be itself an excellent bifunctional catalyst and its distance from the calixarene macrocycle raise doubts about the cavity involvement in the

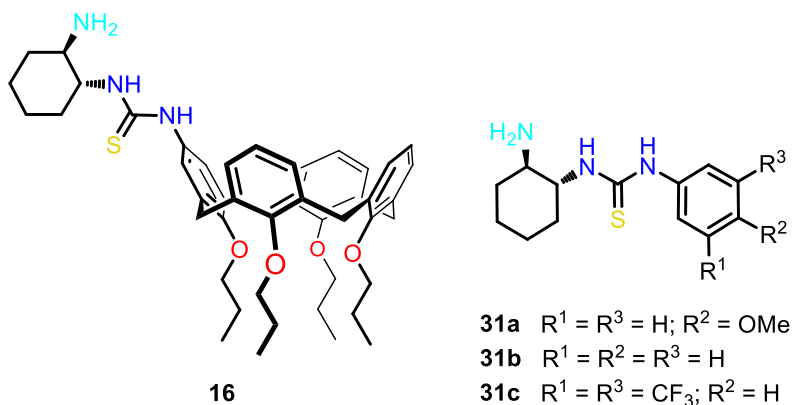


**Figure 22.** Bifunctional organocatalysts **16** and **31**.

transition state. Moreover catalysis by compound **30** is not a green process for two reasons: one is the solvent used ( $\text{CH}_2\text{Cl}_2$ ), the other is the fact that to a certain catalyst loading actually corresponds a double amount of chiral amine.

Prompted by these considerations we designed calix[4]arene **16** bearing the chiral primary amine, thiourea moiety at the upper rim, in close proximity to the cavity (Figure 22). Derivative **16** has then been tested in the conjugate addition of carbonyl nucleophiles (isobutyraldehyde and dimethyl malonate) to activated alkenes (N-phenylmaleimide, *trans*- $\beta$ -nitroolefins and benzylideneacetone), exploiting enamine and iminium activation strategies. In order to prove the effect of the calixarene cavity the catalytic activity of compound **16** has been compared to that of non-macrocyclic compound **31**<sup>56</sup> (Figure 22).

#### ***4.2. Synthesis of new Bifunctional Organocatalysts***

Derivatives **16** and **31a** have been synthesized as outlined in Figure 23. Compound **16** has been prepared treating known mono amino derivative **32**<sup>57</sup> with thiophosgene in refluxing toluene for two hours. Resulting isothiocyanate **33**<sup>57</sup> is used

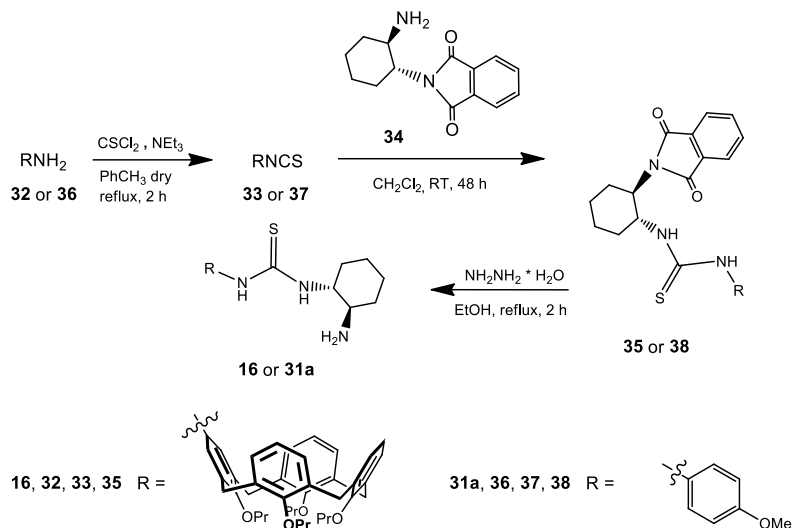


**Figure 23.** Synthetic Scheme of compounds **16** and **31a**.

without purification in the coupling reaction with the known mono protected *trans*-(*R,R*)-1,2-diaminocyclohexane derivative **34**<sup>58</sup> in dry  $\text{CH}_2\text{Cl}_2$  at room temperature, obtaining compound **35** in 60% yield after column chromatography. Compound **35** has been characterized by HR ESI(+)-MS,  $^1\text{H}$  and  $^{13}\text{C}$  NMR spectroscopy. Compound **35** has then been heated in refluxing ethanol in presence of  $\text{NH}_2\text{NH}_2$  thus obtaining compound **16** after precipitation from  $\text{CH}_3\text{CN}$  in 52% yield. Compound **16** has been characterized by HR ESI(+)-MS,  $^1\text{H}$  and  $^{13}\text{C}$  NMR spectroscopy (see experimental section).

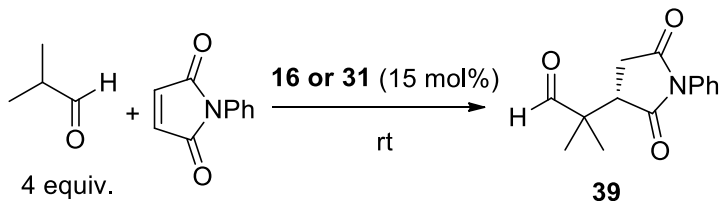
Similarly compound **31a** has been prepared starting from 4-methoxyaniline **36**, which was converted into the corresponding isothiocyanate **37** and then reacted with compound **34** to give thiourea derivative **38**. Deprotection of **38** with  $\text{NH}_2\text{NH}_2$  in refluxing ethanol gave **31a** in 76% yield. Compound **31a** has been characterized by HR ESI(+)-MS,  $^1\text{H}$  and  $^{13}\text{C}$  NMR spectroscopy.

### 4.3. Asymmetric Conjugate Addition

A collaboration with Prof. A. Lattanzi and Dr. S. Meninno highlighted the catalytic properties of derivative **16**.

Initially derivative **16** has been tested in the Michael addition of isobutyraldehyde (2 equiv.) to N-phenylmaleimide in a  $\text{CHCl}_3/\text{H}_2\text{O}$  system using a catalyst loading of 15 mol%, and compared to the literature data<sup>54c</sup> (Table 4, entries 1, 2, 3). Under these conditions, (*R*)-2-(2,5-dioxo-1-phenylpyrrolidin-3-yl)-2-methylpropanal<sup>59</sup> **39** was obtained in 50% yield and 94% enantiomeric excess after 50 minutes at room temperature (Table 4, entry 1). Although less active than **31b** and **31c**, **16** performed comparable enantioselectivity. This promising result

**Table 4.** Catalytic enantioselective Michael reaction of isobutyraldehyde with maleimide.



Entry	Catalyst	Solvent	Time [min]	Yield <sup>[b]</sup> [%]	ee <sup>[c,d]</sup> [%]
1 <sup>[a]</sup>	<b>16</b>	CHCl <sub>3</sub> H <sub>2</sub> O (15 mol%)	50	50	94
2	<b>31b</b>	CHCl <sub>3</sub> H <sub>2</sub> O (15 mol%)	40	93	97
3	<b>31c</b>	CHCl <sub>3</sub> H <sub>2</sub> O (15 mol%)	40	96	94
4	<b>16</b>	H <sub>2</sub> O	80	98	77
5	<b>16</b>	-	30	98	88
6	<b>31a</b>	-	30	98	72

[a] reaction performed using 2 equiv. of isobutyraldehyde. [b] Isolated yields.

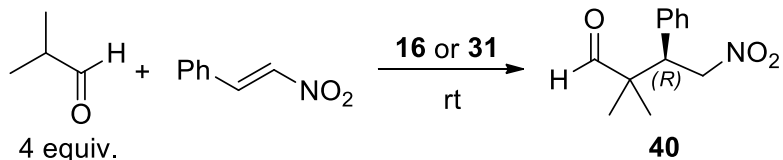
[c] Determined by HPLC using a Chiralcel OD-H chiral stationary phase. [d] The absolute configuration of the products were determined by comparison of the HPLC retention times and optical rotations with literature values.<sup>54c,59</sup>

prompted us to investigate different reaction media. Instead of a screening of different solvents, we preferred greener alternatives such as “on water”<sup>60</sup> and solvent free conditions (Table 1, entries 4, 5). Using water as the reaction media led to highly increased product yield, but enantioselectivity decreased. A possible explanation is that hydrophobic interactions forces the reactants

in close proximity thus enhancing hydrogen bond between the thiourea moiety of **16** and N-phenylmaleimide, making the substrate more electrophilic.<sup>61</sup> On the other hand water hinders formation of the enamine intermediate between the primary amine of **16** and isobutyraldehyde, which is responsible of the tight transition state and the resulting enantioselectivity. Consequently, an alternative non covalent pathway via enolate would occur, likely proceeding with lower enantiocontrol. Solvent free conditions (Table 4, entry 5) combine excellent reactivity (98% yield after 30 minutes), due to reactants aggregation, and good enantioselectivity (88% ee), due to efficient formation of enamine intermediate. To evaluate the role of the calixarene scaffold on catalytic activity and enantioselectivity a solvent free reaction of isobutyraldehyde and N-phenylmaleimide in presence of derivative **31a** was performed (Table 4, entry 6). Compound **39** was obtained after 30 minutes in 98% yield and 72% ee, thus demonstrating that, although not playing any role in activating the substrates, the macrocycle contributes in organizing the transition state.

Encouraged by results shown in table 4, we decided to extend the scope of possible Michael acceptors to *trans*- $\beta$ -nitroolefins. The optimized reactions conditions (4 equiv. of

**Table 5.** Catalytic enantioselective Michael reaction of isobutyraldehyde with *trans*- $\beta$ -nitrostyrene.



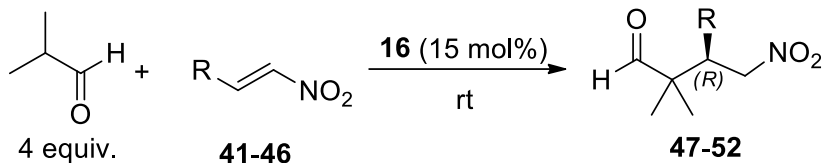
Entry	Catalyst (mol%)	Solvent	Time [h]	Yield <sup>[a]</sup> [%]	ee <sup>[c,d]</sup> [%]
1	<b>16</b> (15)	-	16	98	90
2	<b>31a</b> (15)	-	42.5	41	92
3	<b>16</b> (10)	-	22	29	92
4	<b>16</b> (5)	-	38	16 <sup>[b]</sup>	-
5	<b>16</b> (5)	CH <sub>2</sub> Cl <sub>2</sub>	48	7.5 <sup>[b]</sup>	-
6	<b>16</b> (5)	toluene	48	6.9 <sup>[b]</sup>	-
7	<b>16</b> (10)	toluene	60	29	90
8	<b>16</b> (15)	H <sub>2</sub> O	8	77	87

[a] Isolated yields. [b] NMR conversion. [c] Determined by HPLC using a Chiralpak AD-H chiral stationary phase. [d] The absolute configuration of the products were determined by comparison of the HPLC retention times and optical rotations with literature values.<sup>62</sup>

aldehyde, solvent free, catalyst loading 15 mol%) were employed, using *trans*- $\beta$ -nitrostyrene as substrate (Table 5, entry 1). (*R*)-2,2-dimethyl-4-nitro-3-phenylbutanal<sup>62</sup> **40** was obtained after 16 hours in 98 % yield and 90% ee using compound **30**, while compound **31a** led to comparable enantioselectivity (92% ee), but displayed lower activity (41% yield after 42.5 hours).

While in the case of N-phenylmaleimide the role of the calixarene scaffold was to enhance the enantioselectivity (Table 4, entries 5 vs. 6), in the case of *trans*- $\beta$ -nitrostyrene the macrocycle plays a different role, being responsible of a consistent increase in the catalytic activity (Table 5, entries 1 vs. 2). Further studies were devoted to decrease the catalyst loading to 10% and 5% (Table 5, entries 3 and 4, respectively). Unfortunately, activity definitely decreased, although enantioselectivity was still good (Table 5, entry 3). Changing from solvent free conditions to CH<sub>2</sub>Cl<sub>2</sub>, toluene or “on water” conditions (Table 5, entries 5-8) did not bring any improvement. The substrate scope using isobutyraldehyde with a variety of aromatic nitroalkenes **41-46** was then investigated under optimized conditions: **16** (15 mol%), solvent free (Table 6). Compounds **47-52** were obtained in yields ranging from 52 to 91% and ees from 89 to 93%. Substrate substitution on the phenyl ring little affected the enantioselectivity, which remained fairly good. On the other hand, catalytic activity is highly substrate-dependent. Electronic effects of substituents do not easily justify the observed activity as the *p*-OMe substituted derivative (Table 6, entry 1) afforded better yield than *o*-Chloro

**Table 6.** Catalytic enantioselective Michael reaction of isobutyraldehyde with *trans*- $\beta$ -nitroolefins.



Entry	R	Time [h]	Yield <sup>[a]</sup> [%]	ee <sup>[b, c]</sup> [%]
1	<i>p</i> -MeOC <sub>6</sub> H <sub>4</sub>	52	78	90
2	<i>o</i> -ClC <sub>6</sub> H <sub>4</sub>	75	57	93
3	<i>p</i> -FC <sub>6</sub> H <sub>4</sub>	24	91	91
4	<i>m</i> -BrC <sub>6</sub> H <sub>4</sub>	51	53	90 <sup>[d]</sup>
5	Furan-2-yl	16	53	90
6	<i>p</i> -BrC <sub>6</sub> H <sub>4</sub>	53	52	89

[a] Isolated yields. [b] Determined by HPLC using a Chiralpak AD-H chiral stationary phase. [c] The absolute configuration of the products were determined by comparison of the HPLC retention times and optical rotations with literature values.<sup>62</sup> [d] Determined by HPLC using a Chiralcel OD-H chiral stationary phase.

and *m*-Bromo substituted ones (Table 6, entries 2, 4). Steric and solubility effects might play a role. Additionally the sterically demanding calixarene scaffold might prevent effective coordination of differently substituted nitroolefins by the adjacent thiourea.

A stereochemical model for the reaction between isobutyraldehyde and *trans*- $\beta$ -nitrostyrene catalyzed by **16** has been proposed using molecular dynamics calculations (Figure

24). This structure, although not predicted by quantum mechanics methods, might represent the real transition state with

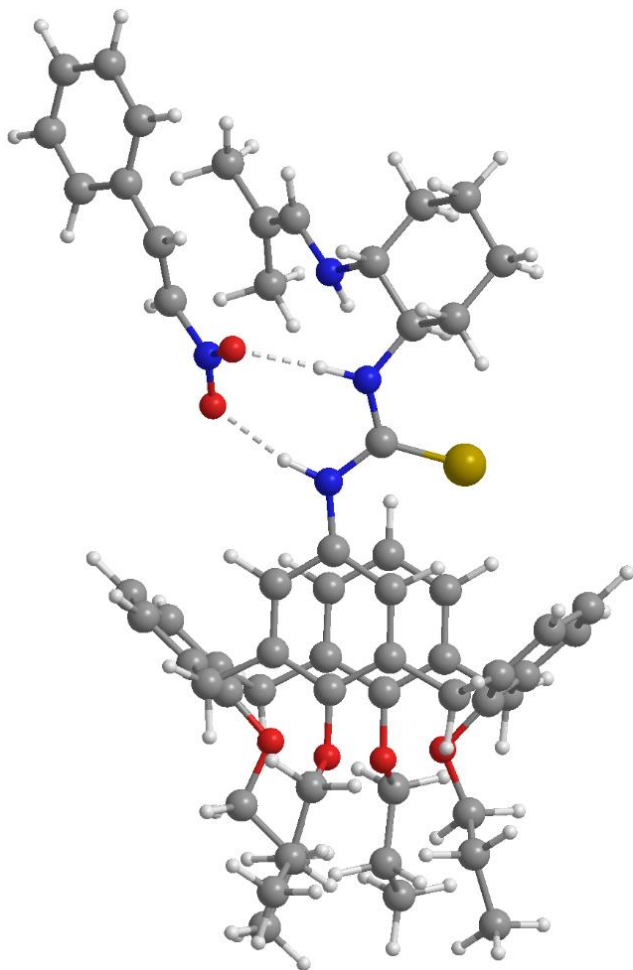


**Figure 24.** Proposed stereochemical model for the reaction of isobutyraldehyde with *trans*- $\beta$ -nitrostyrene catalyzed by **16**.

good approximation. In particular the reactants are at a certain distance from the calixarene cavity so they only interact with the amine-thiourea moiety during the step controlling the

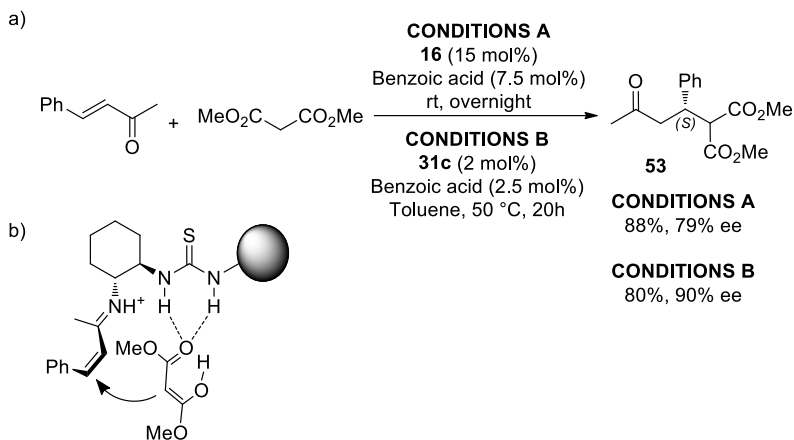


**Figure 25.** (a) Michael reaction of dimethyl malonate with benzylideneacetone catalyzed by **16** and **31c**. (b) Proposed stereochemical model.

enantioselectivity, in accord with the experimental data.

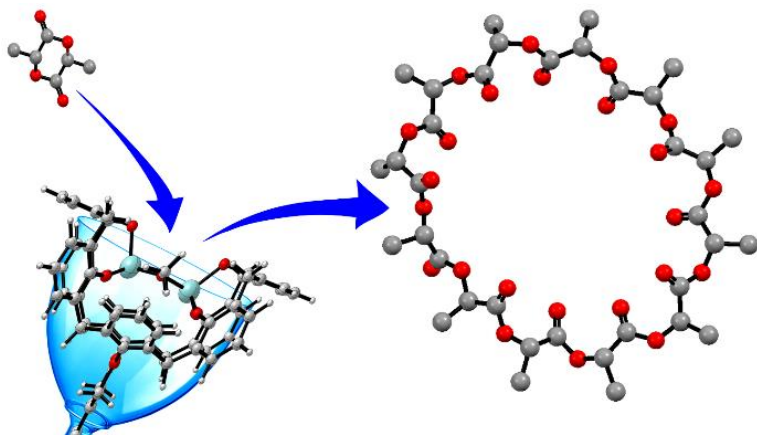
Finally, compound **16** has been tested in the catalytic enantioselective solvent-free addition of dimethyl malonate to benzylideneacetone and compared with the literature data for compound **31c**<sup>63</sup> (Figure 25a). A catalyst loading of 15 mol%, of **16** in presence of benzoic acid (7.5 mol%) as a co-catalyst, promoted the formation of compound **53** in 88% yield and 79% enantiomeric excess (conditions a). On the other hand using

compound **31c** (2 mol%), combined with benzoic acid (2.5 mol%) in toluene at 50° C resulted in comparable yield (80%) and slightly higher enantiomeric excess (90%). Also in this case the use of calixarene based catalyst **16** under solvent free conditions resulted in enhanced activity with respect to similar linear bifunctional catalysts

Unlike addition of isobutyraldehyde to maleimides and nitroolefins, which are examples of enamine catalysis, Michael addition of malonates to enones catalyzed by primary amine-thioureas is supposed to proceed via activation of the electrophile by formation of an iminium ion and simultaneous stabilization of the enol tautomer of the nucleophile (Figure 25b).

In conclusion, we reported here the synthesis of the novel calix[4]arene based primary amine-thiourea bifunctional catalyst **16**. Screening of the catalytic ability of compound **16** in Michael type additions highlighted high efficiency and versatility, thus paving the way to further research directed to the design of more active and selective calixarene based organocatalysts.

*Dinuclear Zirconium Complex Bearing 1,5-Bridged-Calix[8]arene Ligand as Effective Catalyst for the Synthesis of Macrolactones*





## *Chapter 5*

# *Dinuclear Zirconium Complex Bearing 1,5-Bridged-Calix[8]arene Ligand as Effective Catalyst for the Synthesis of Macrolactones*

### *5.1. General Overview*

In the last decades, more and more attention has been paid to reducing the production of petrochemically derived plastics, due to economic and environmental concerns. This situation has risen growing interest toward the green and degradable alternatives to polyolefins.<sup>64</sup> On the cutting edge of research in this field are aliphatic polyesters, such as polylactide, polyhydroxybutyrate, polyglycolide, and polycaprolactone. Polylactide (PLA), obtained from lactide (LA), the cyclic dimer of lactic acid (produced by fermentation of glucose from corn or sugar beet), is a biocompatible and biodegradable polyester, its use has increased from the 1990s due to higher and higher demand for sustainable plastics, and reduction of monomer's

cost. PLA has already found use as commodity polymer for short-time applications (e.g., packaging, fibers) and as engineering material in biomedical and pharmaceutical fields for the production of resorbable surgical sutures and stents, controlled drug release systems, and scaffolds for tissue engineering.<sup>65</sup>

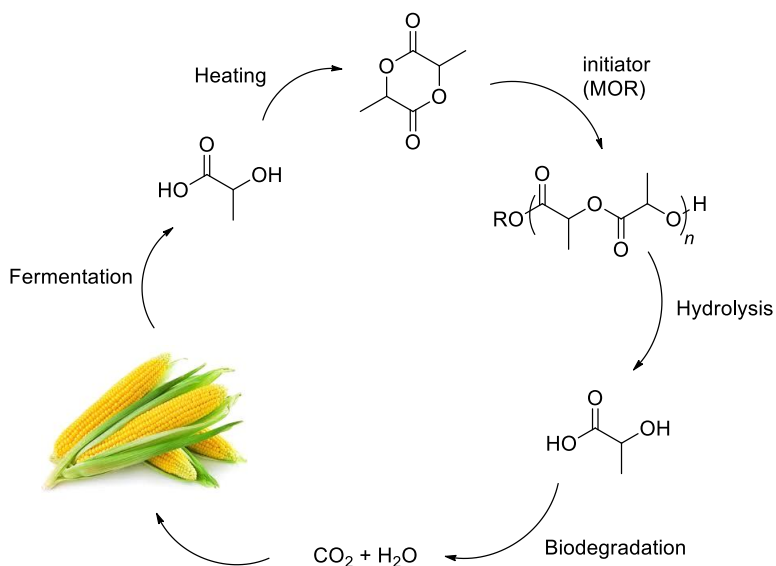


**Figure 26.** The lifecycle of polylactide (PLA).

The properties of the material highly depend on the chain structure so macromolecules with non-linear architectures are getting more and more attention. Cyclic aliphatic polyesters<sup>66</sup>

for example display very interesting features, like the fact that the glass transition temperature doesn't significantly change with dimensions, or the retarded degradation profile with respect to linear analogues.<sup>67</sup> Another substantial difference between linear and cyclic aliphatic polyesters regards the biological properties. Not only does cyclic topology increase the blood circulation time<sup>68</sup> and tumor uptake,<sup>69</sup> but it also might lead to enhanced supramolecular properties. The sum of these qualities makes cyclic aliphatic polyesters suitable scaffolds for biomedical applications. Unfortunately this very interesting

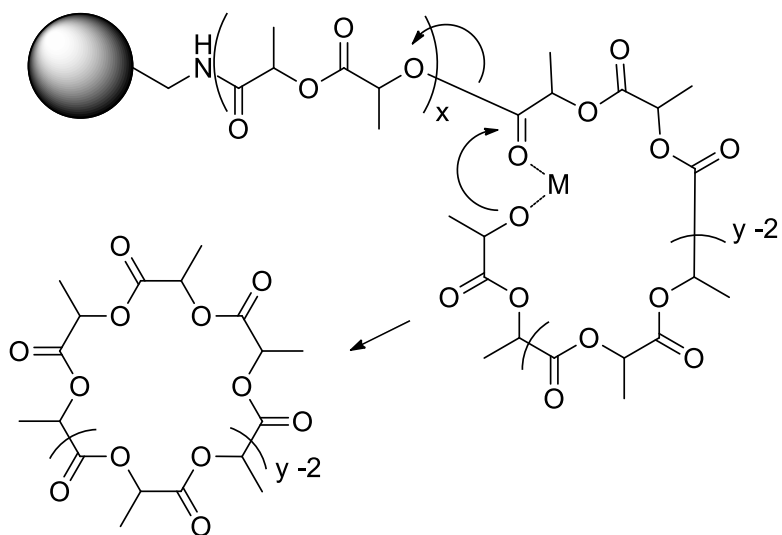


**Figure 27.** Solid phase synthesis of cyclic PLA

class of polymers have received little attention because of the difficulties in both preparation and purification.<sup>70</sup> A possible synthetic strategy consists in growing a polyester chain on a solid support, than the statistical intramolecular transesterification releases cyclic polymers in solution.<sup>71</sup> (Figure 27). Another approach is the cyclization using high dilution conditions of  $\alpha,\omega$ -functionalized linear chains. A final important technique is the so called ring expansion polymerization. The main feature of this approach is the absence of linear polyesters as intermediate, since the macromolecules are generated by addition of monomers into a labile bond of a cyclic initiator. The bond can be either a metal oxygen bond (generally Sn-O) of an organometallic complex,<sup>72</sup> or the connection between an alkoxide and an imidazolium ion pair generated by the addition of *N*-heterocyclic carbenes to a monomer unit.<sup>73</sup> Waymouth et al. reported an example of such a strategy in the synthesis of PLA. The first step is the nucleophile attack of 1,3-dimesitylimidazol-2-ylidene to a LA molecule, thus generating the cyclic zwitterionic initiator. The alkoxide moiety then attacks other LA units in the propagation step. Finally, the backbiting transesterification releases the cyclic PLA (Figure 28).

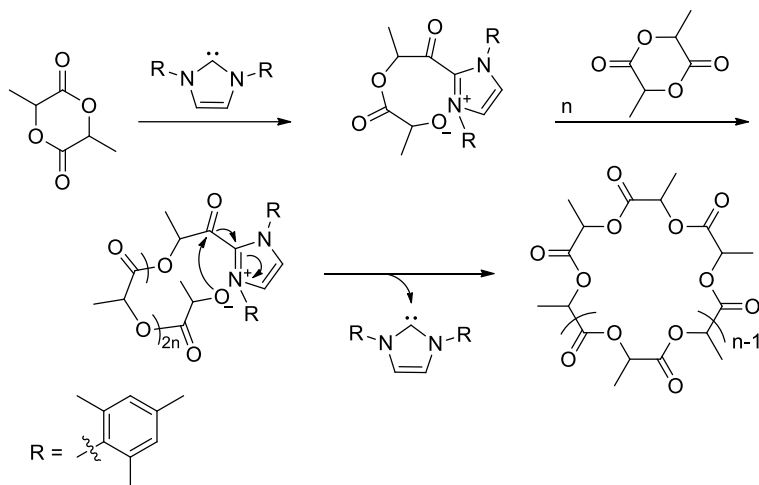


**Figure 28.** Zwitterionic N-heterocyclic carbene catalyzed ring expansion cyclopolymerization of lactide.

At the best of our knowledge, synthesis of cyclic polyesters using the well-established procedure, consisting in the ring-opening polymerization (ROP) of LA catalyzed by metal complexes,<sup>74</sup> has not been so far reported. In order to develop a catalytic ROP system able to selectively yield cyclic polymers a fine tuning of both metal and ligand is needed.

For example one of the most relevant metal complexes, especially from an industrial point of view, is  $\text{Sn}(\text{Oct})_2$ , which is toxic, hence tin employment in biomedical applications should be avoided, preferring biocompatible metals like zinc or titanium.

Recently bimetallic complexes are gaining more attention as a promising class of catalysts.<sup>75</sup> Tolman and coworkers showed<sup>76</sup> that a binuclear zinc metal alkoxide was a highly active catalyst for the preparation of PLA. In addition, a study by Williams and coworkers, comparing the performances of di- and monozinc catalysts, showed that synergistic effect between two metal centers enhances the activity of binuclear catalysts with respect to mononuclear analogues.

Group 4 metal complexes have been widely studied in the ROP of cyclic esters because of their low toxicity and good control over polymerization process.<sup>77</sup> Surprisingly, at the best of our knowledge, only few dinuclear group 4 catalysts have found use in the ROP of LA.<sup>78</sup>

Beyond the choice of the metal, the other issue in order to lead the polymerization process to the formation of cyclic polyesters, is the choice of a suitable rigid, bulky ligand. Calix[n]arenes, being composed of phenol units connected by methylene bridges, constitute an ideal platform for the synthesis of metal complexes: the calixarene moiety behaves as an oxo surface protecting one side of the complex, thus conferring significant stability. Some titanium complexes bearing tiny, rigid, preorganized calix[4]arenes have already been reported

and used in the polymerization of cyclic esters.<sup>79</sup> However, larger, flexible and less preorganized calixarenes are the ideal framework for designing bimetallic catalysts, because they are able to coordinate more than one metal simultaneously in close proximity, as in the titanium *p-tert*-butylcalix[8]arene complex  $[\text{Ti}_4(p\text{-tert-butylcalix[8]arene})(\text{O}^n\text{Pr})_8(\text{THF})_2]$  reported by McIntosh and coworkers.<sup>80</sup> This complex has two main features. One is the conformation adopted by the calixarene ligand, usually referred to as double cone, because it resembles two reversed calix[4]arene in the cone conformation. The other is that each calix[4]arene-like unit coordinates two titanium centers connected by two bridging propoxides. The complex Catalyzed the ROP of LA, even though no data have been reported (Figure 29.)

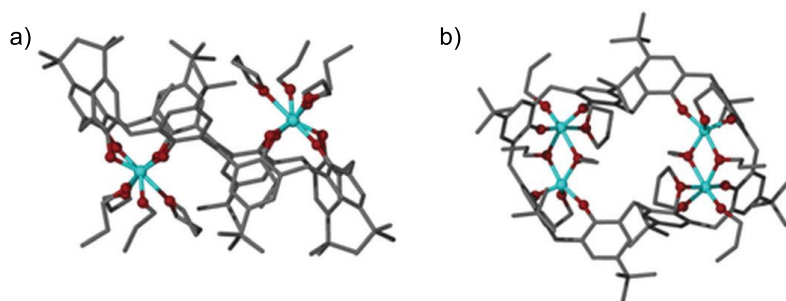


**Figure 29.** (a) Complex  $\text{Ti}_4(p\text{-tert-butylcalix[8]arene})(\text{O}^n\text{Pr})_8(\text{THF})_2$ . (b) The orthogonal view.

Unlike calix[4]arene scaffold, which undergoes little changing during coordination to metal centers, calix[8]arene flexibility allows substantial structure modification with the ligand adapting its shape to the metals, thus obtaining peculiar architectures with interesting properties. On the other hand, too much flexibility could result in many possible conformers, thus complicating the study of such systems.

In fact in the anionic  $[\text{Ti}_2(p\text{-tert-butylcalix[8]arene})(\text{O}^i\text{Pr})_2]^-$  species, the calix[8]arene ligand adopts a so called ‘tennis-ball’ conformation, with four phenolic oxygens coordinated to each Ti(IV),<sup>81</sup> different from the double cone described previously.

Working with Prof. A. Grassi, Dr. S. Milione, Dr. A. Buonerba, and Dr. R. Lapenta, complex **17**(Zr-O-*t*Bu)<sub>2</sub> has been prepared, featuring a calix[8]arene ligand bridged between the first and fifth phenolic group with a *m*-xylene-diyl functionality. The choice was made in order to reduce the number of conformers the ligand can adopt, thus balancing flexibility and preorganization. Moreover, we focused on zirconium complexes because of their higher activity with respect to titanium analogues.<sup>77</sup> Using such a ligand has also the purpose of locating the metal atoms in an open catalytic pocket thus creating an enzyme-like environment conferring to complex **17**(Zr-O-*t*Bu)<sub>2</sub>

peculiar properties in the ring opening polymerization of *rac*-lactide (LA),  $\epsilon$ -caprolactone ( $\epsilon$ -CL) and  $\beta$ -butyrolactone ( $\beta$ -BL).

### 5.2. Synthesis of the Dinuclear Zirconium Complex Bearing 1,5-Bridged-Calix[8]arene Ligand

The calix[8]arene, 1,5-bridged with a *m*-xylene-diyl functionality **17H<sub>6</sub>** (Figure 32) was synthesized according to the procedure reported in literature.<sup>82</sup> The protonolysis of **17H<sub>6</sub>** with two equivalents of Zirconium(IV) *tert*-butoxide, in toluene (or THF) at room temperature, yielded complex **17(Zr-O-*t*Bu)<sub>2</sub>**

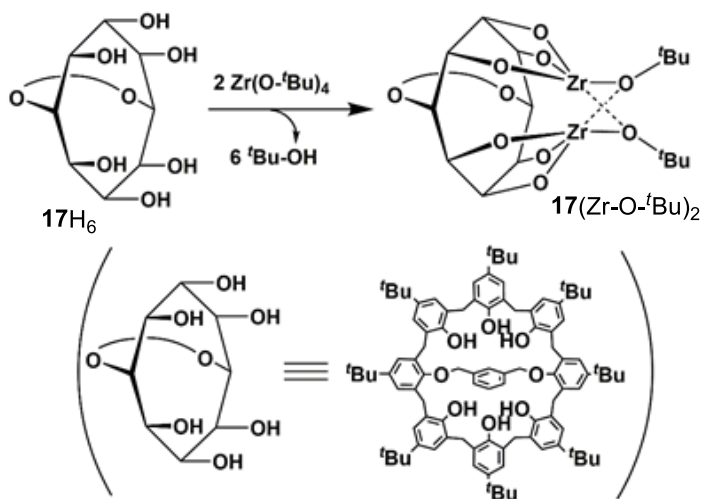


**Figure 30.** Synthesis of **17(Zr-O-*t*Bu)<sub>2</sub>**.

(Figure 30), which was recovered after crystallization in toluene. Unfortunately, the needle-shaped crystals obtained were unsuitable for single x-ray diffraction, so structure elucidation of complex **17**(Zr-O-*t*Bu)<sub>2</sub> was made combining mono- (<sup>1</sup>H, <sup>13</sup>C NMR, DEPT135) and two-dimensional (2D COSY, 2D HSQC, 2D NOESY) NMR techniques with high resolution mass spectrometry (see experimental section).

As expected <sup>1</sup>H NMR spectra of ligand **17**H<sub>6</sub> recorded at 25 °C features only sharp singlets (Figure 32), suggesting fast rotation of the phenol units around the methylene bridges. On the other hand, the <sup>1</sup>H NMR spectra of **17**(Zr-O-*t*Bu)<sub>2</sub> acquired in a polar coordinating solvent (pyridine-*d*<sub>5</sub>) showed sharp signals even at high temperature (Figure 31). Noteworthy, the methylene protons on the calixarene ring resonate as two AX spin systems ( $\delta = 3.22$  and 4.82 ppm with  $J$  of 14.5 Hz;  $\delta = 3.03$  and 4.30 ppm with  $J$  of 12.4 Hz), clearly indicating a blocked conformation, on the NMR time scale. Moreover, a singlet signal was found for the methylenes of the di-ether bridge of the macrocycle (5.12 ppm, Figure 31), suggesting that the calix bridge is crossed by a plane of symmetry. The presence of two, instead of three AX systems can be explained by the presence of a further plane of symmetry perpendicular to that containing the

bridge, through which passes a  $C_2$  axis; whole indicating a  $C_{2v}$  symmetry for the complex. This conclusion is confirmed by the presence of four types of aromatic protons. The integration ratio between the signals due to the *tert*-butoxide groups bounded to the zirconium atoms and the *tert*-butyl on the calixarene macrocycle is coherent with the presence of two *tert*-butoxide groups per molecule of ligand.

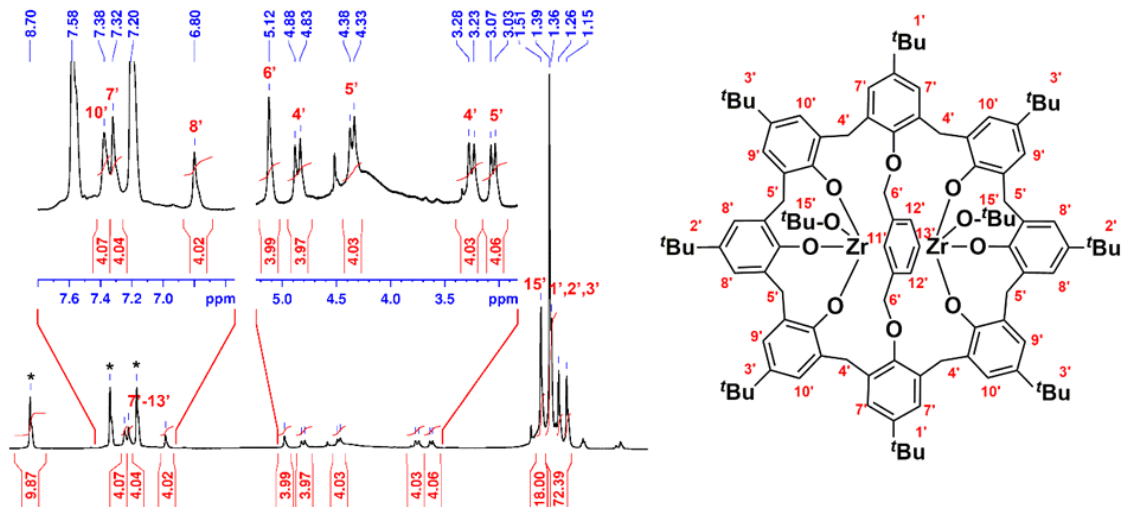


**Figure 31.**  $^1\text{H}$  NMR spectra, with the diagnostic signals labelled, of complex **17** ( $\text{Zr-O-}^t\text{Bu}$ ) $_2$  (600 MHz, pyridine- $d_5$ , 90°C).

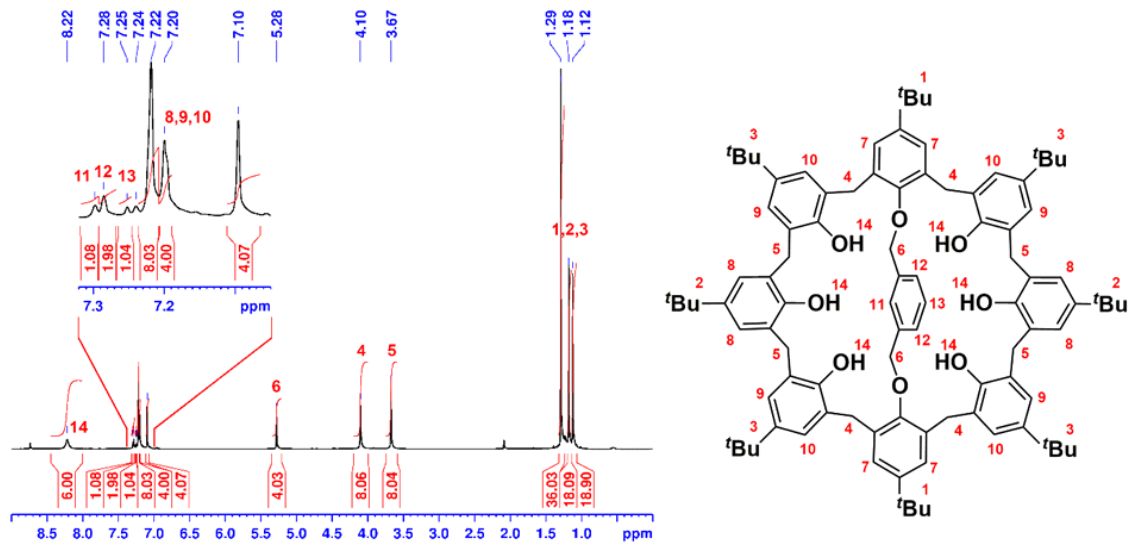


**Figure 32.**  $^1\text{H}$  NMR spectra, with the diagnostic signals labelled, of ligand **17H<sub>6</sub>** (600 MHz,  $\text{CDCl}_3$ , 25°C).

The structure proposed for  $17(\text{Zr-O-}^t\text{Bu})_2$  after NMR investigation, was optimized by DFT calculations and depicted in Figure 33.

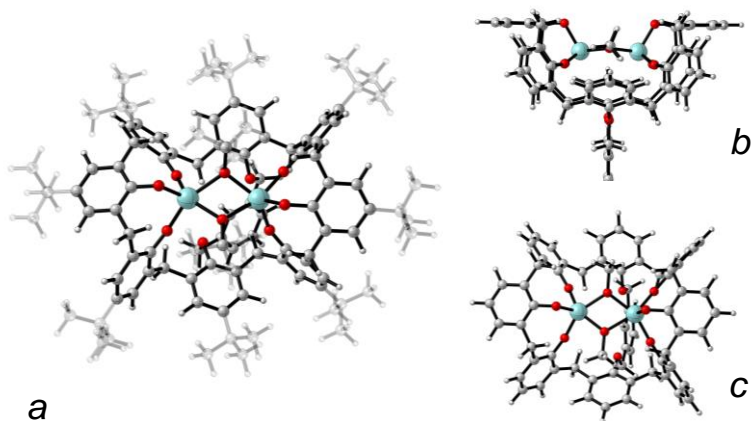


**Figure 33.** (a) Minimum-energy structure for  $17(\text{Zr-O-}^t\text{Bu})_2$ . (b) Top and (c) front views of the minimum-energy structure for the model complex of  $17(\text{Zr-O-}^t\text{Bu})_2$ .

In this structure, the calixarene adopts a double-cone conformation with the two calix[4]arene subunits in a “syn-cones” orientation. Each substructure bounds a Zirconium atom. The ligand is folded in such a way to direct the two substructures toward one another locating the two-Zirconium atoms in close proximity and enabling the formation of a four-membered alkoxy-bridged Zr–O–Zr–O ring. The bridging and terminal alkoxy groups bind to the Zirconium atoms with typical bond

lengths of 2.18–2.27 and 1.98–2.01 Å, respectively. In this structure, each Zirconium atom is in a pentacoordinated environment, the saturation of the coordination sphere can occur with the binding of a pyridine molecule for each metal center. DFT calculation on a model complex (the complex lacking of tert-butyl groups) predicted the coordination of two pyridines to be exothermic by 17.9 kcal/mol. That assumption has been confirmed by NMR analysis of the complex synthesized in toluene and in solution treated with pyridine.

### 5.3. Ring Opening Polymerization of *rac*-LA, $\epsilon$ -CL and $\beta$ -BL

Complex **17**(Zr-O<sup>*t*</sup>Bu)<sub>2</sub> has been tested in the ROP of LA. Initially, activity screening was performed varying temperature at monomer/catalyst ratio of 100 (Table 7, entries 1-4). Increasing temperature resulted in increasing activity, given that 97% conversion is reached in 30 minutes at 100 °C and a turnover frequency of 194 h<sup>-1</sup> (Table 7, entry 4). Polymers obtained had all narrow molecular weight distributions (PDI = 1.10-1.30), anyway measured molecular weights were far lower than the calculated ones, thus indicating transesterification reactions occurring during the ROP.

**Table 7.** Ring opening polymerization of *rac*-LA,  $\epsilon$ -CL and  $\beta$ -BL promoted by **17**(Zr-O-*t*Bu)<sub>2</sub>.

Entry <sup>a)</sup>	Monomer	Monomer/Cat. (molar ratio)	T (°C)	t (min)	Conversion <sup>b)</sup> (%)	TON <sup>c)</sup>	TOF <sup>d)</sup> (h <sup>-1</sup> )	$M_{n(\text{exp})}$ <sup>e)</sup> (DA)	$M_{n(\text{th})}$ <sup>f)</sup> (DA)	PDI <sup>g)</sup>
1 <sup>g)</sup>	<i>rac</i> -LA	100	25	1440	50	50	2	629	3603	1.10
2	<i>rac</i> -LA	100	50	660	90	90	8	686	6486	1.14
3	<i>rac</i> -LA	100	80	108	93	93	52	629	6702	1.28
4	<i>rac</i> -LA	100	100	30	97	97	194	705	6990	1.23

<sup>a)</sup> Reaction conditions: Complex **17**(Zr-O-*t*Bu)<sub>2</sub> (4.6  $\mu$ mol, 7.8 mg) and toluene (2.4 mL). <sup>b)</sup> Determined by <sup>1</sup>H NMR spectroscopy (CDCl<sub>3</sub> as solvent, 25 °C). <sup>c)</sup> Turnover number (*mol* of polymerized *rac*-Lactide per *mol* of catalyst). <sup>d)</sup> Turnover frequency (TON per reaction time). <sup>e)</sup> Experimental molecular weight ( $M_{n(\text{exp})}$ ) and polydispersity index (PDI,  $M_w/M_n$ ) determined by GPC in THF using polystyrene standards and corrected using a factor of 0.58. <sup>f)</sup> Calculated molecular weight using:  $M_{n(\text{th})}$  (kg mol<sup>-1</sup>) = 144.13 × ([*rac*-LA]<sub>0</sub>/[C])/2 × (*rac*-LA conversion). <sup>g)</sup> Dichloromethane as solvent.

**Table 8.** Ring opening polymerization of *rac*-LA,  $\epsilon$ -CL and  $\beta$ -BL promoted by **17**(Zr-O-*t*Bu)<sub>2</sub>.

Entry <sup>a)</sup>	Monomer	Monomer/Cat. (molar ratio)	T (°C)	t (min)	Conversion <sup>b)</sup> (%)	TON <sup>c)</sup>	TOF <sup>d)</sup> (h <sup>-1</sup> )	$M_{n(\text{exp})}$ <sup>e)</sup> (DA)	$M_{n(\text{th})}$ <sup>f)</sup> (DA)	PDI <sup>e)</sup>
1	<i>rac</i> -LA	250	100	40	93	233	349	3209	16755	1.28
2	<i>rac</i> -LA	500	100	60	96	480	480	8579	34591	1.27
3	<i>rac</i> -LA	750	100	80	98	735	551	15760	52968	1.30
4	<i>rac</i> -LA	1000	100	100	98	980	588	26619	70624	1.47
5	$\epsilon$ -CL	100	100	3	97	97	3233	621	5536	1.23
6	$\beta$ -BL	100	100	840	90	90	6.4	599	3874	1.25

<sup>a)</sup> Reaction conditions: Complex **17**(Zr-O-*t*Bu)<sub>2</sub> (4.6  $\mu$ mol, 7.8 mg) and toluene (2.4 mL). <sup>b)</sup> Determined by <sup>1</sup>H NMR spectroscopy (CDCl<sub>3</sub> as solvent, 25 °C). <sup>c)</sup> Turnover number (*mol* of polymerized *rac*-Lactide per *mol* of catalyst). <sup>d)</sup> Turnover frequency (TON per reaction time). <sup>e)</sup> Experimental molecular weight ( $M_{n(\text{exp})}$ ) and polydispersity index (PDI,  $M_w/M_n$ ) determined by GPC in THF using polystyrene standards and corrected using a factor of 0.58. <sup>f)</sup> Calculated molecular weight using:  $M_{n(\text{th})}$  (kg mol<sup>-1</sup>) = 144.13 ×  $\frac{[rac\text{-LA}]_0}{[C]} \times \frac{1}{2} \times (rac\text{-LA conversion})$ .

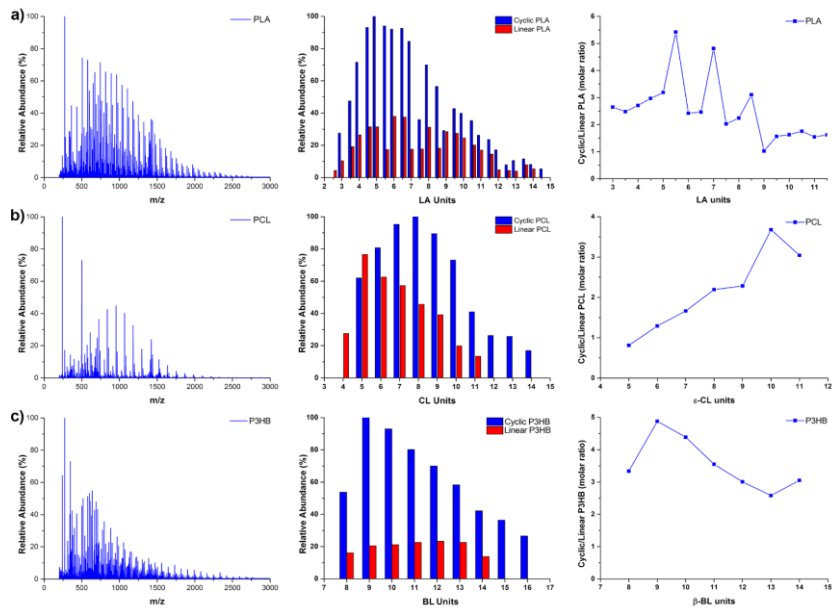


**Figure 34.** MALDI-TOF-MS spectra (on the left), the corresponding molecular weight distribution profiles with assignments for the cyclic and the linear polymer chains (in the middle) and the cyclic/linear molar ratio for the polymer chains as a function of the number of molecules inserted (on the right) for: (a) PLA, (b) PCL and (c) P3HB.

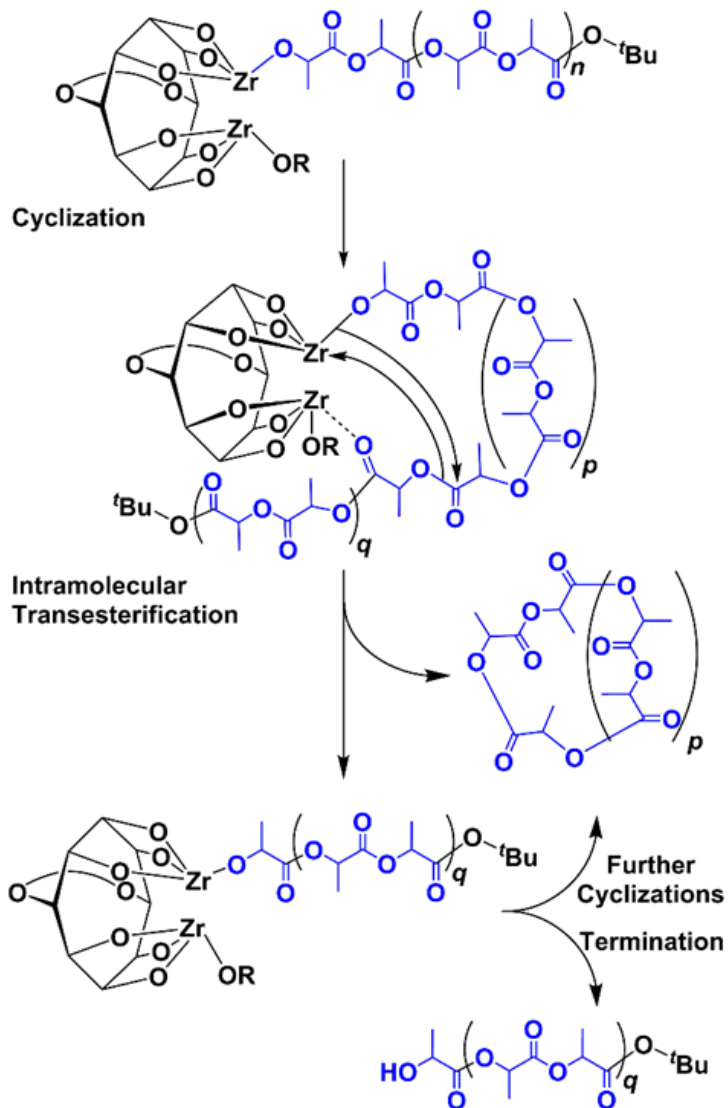


**Figure 35.** Proposed mechanism for the intramolecular transesterification reaction.

In order to highlight the phenomenon, matrix assisted laser desorption ionization time of flight mass spectrometry (MALDI-TOF-MS) analysis of the polymer were performed (Figure 34). The mass spectrum for PLA (Figure 34a) shows signals undoubtedly ascribable to cyclic polyesters adduct with  $\text{Na}^+$  and  $\text{K}^+$ , thus confirming that intramolecular transesterification reaction occur during polymerization. Linear PLA chains including *tert*-butyl moiety were also found as minority products. Cyclic/linear PLA ratio reaches maximum level at three different values of monomer units, thus suggesting that only certain conformations of the growing chain favor the cyclization reaction. The process probably occurs when the growing chain fold in order to bring one of the carbonyl groups in close proximity to the metal center. Non-covalent interactions between the growing chain and the two zirconium atoms activate the carbonyl facilitating the cyclization reaction (Figure 35).

Following screening of the catalytic activity was made increasing the monomer/catalyst ratio in order to determine the relevance of the transesterification reaction with respect to the monomer coordination/insertion (Table 8, entries 1-4). Surprisingly **17**(Zr-O-*t*Bu)<sub>2</sub> is still active even at high monomer loading, as quantitative conversion of 1000 equiv. of LA at 100

°C required 100 minutes (Table 8, entry 4). As the monomer/catalyst ratio increased, molecular weights also increased. Even the difference between measured and calculated molecular weights increased, thus highlighting that high monomer concentrations favor the transesterification reaction with respect to the propagation.

Complex **17**(Zr-O-*t*Bu)<sub>2</sub> was also screened in the polymerization of  $\epsilon$ -CL and  $\beta$ -BL (Table 8, entries 5 and 6). Conversion of  $\epsilon$ -CL was total after 3 minutes, while  $\beta$ -BL required 14 hours to afford the corresponding polymer P3HB in high yield. As PLA, molecular weights were narrowly distributed, although measured values were lower than calculated ones. Also in this case, transesterification reaction prevails over propagation. MALDI-TOF-MS analysis of the polymers (Figure 34b and c) highlighted the formation of cyclic oligomers as main product. Analysis of cyclic/linear polymer ratio in function of the number of monomer units reveals the absence of specific chain lengths favoring the cyclization reaction, as a result of higher flexibility of PCL and P3HB with respect to PLA, in particular the maximum ratio for PCL reaches up to ten monomer units of  $\epsilon$ -CL.

In conclusion, the protonolysis of ligand **17**H<sub>6</sub> with Zr(IV) *tert*-butoxide afforded complex **17**(Zr-O-*t*Bu)<sub>2</sub>, whose structure, determined by NMR analysis, showed C<sub>2v</sub> symmetry. Complex **17**(Zr-O-*t*Bu)<sub>2</sub> proved to be an active catalyst in the ring opening polymerization of LA, ε-CL and β-BL, thus promoting a general method for the synthesis of cyclic polyesters. Since synthesis and purification of such compounds generally is a hard task, we hope that our work could help developing new easy strategies for the preparation of cyclic polyesters.



## *Experimental Section*





## *Chapter 6*

### *Experimental Section*

#### *6.1 General Information.*

HR MALDI mass spectra were acquired on a FT-ICR mass spectrometer equipped with a 7T magnet. All chemicals were reagent grade and were used without further purification. Compounds **24**<sup>83</sup> and **25**<sup>84</sup> were prepared as reported in the literature. Anhydrous solvents were used as purchased from the supplier. When necessary compounds were dried *in vacuo* over CaCl<sub>2</sub> or P<sub>2</sub>O<sub>5</sub>. Reaction temperatures were measured externally. Reactions were monitored by TLC silica gel plates (0.25 mm) and visualized by UV light, or by spraying with H<sub>2</sub>SO<sub>4</sub>-Ce(SO<sub>4</sub>)<sub>2</sub>, ninhydrin or anisaldehyde. Flash chromatography was performed on silica gel 60 (particle size: 0.040–0.063 mm) and the solvents employed were of analytical grade. Enantiomeric excesses of products **23a-e**, **39**, **40**, **47-52** were determined by chiral HPLC using Chiralcel or Daicel columns with an UV detector set at 260 nm. Optical rotation values were measured at

$\lambda = 589$  nm, corresponding to the sodium D line, at the temperatures indicated. NMR spectra were recorded on a 600 [600 ( $^1\text{H}$ ) and 150 MHz ( $^{13}\text{C}$ )], 400 MHz spectrometer [400 ( $^1\text{H}$ ) and 100 MHz ( $^{13}\text{C}$ )] or 300 MHz spectrometer [300 ( $^1\text{H}$ ) and 75 MHz ( $^{13}\text{C}$ )]. Chemical shifts are reported relative to the residual solvent peak ( $\text{CHCl}_3$ :  $\delta$  7.26,  $\text{CDCl}_3$ :  $\delta$  77.23; TCDE:  $\delta$  6.0, TCDE:  $\delta$  74.0). Standard pulse programs, provided by the manufacturer, were used for 2D COSY and 2D HSQC experiments. One-dimensional  $^1\text{H}$  and  $^{13}\text{C}$  spectra, and two-dimensional COSY-45 and heteronuclear single quantum correlation (HSQC) were used for NMR peak assignment. COSY-45 spectra were taken using a relaxation delay of 2 s with 30 scans and 170 increments of 2048 points each. HSQC spectra were performed with gradient selection, sensitivity enhancement, and phase-sensitive mode using Echo/Antiecho-TPPI procedure. A typical experiment comprised 20 scans with 113 increments of 2048 points each. Glassware and vials used in the polymerization were dried in an oven at 120 °C overnight and exposed three times to vacuum–nitrogen cycles. All solvents and reagents used were dried and purified before use. Toluene (Sigma-Aldrich, 99.5%) and hexane (Sigma-Aldrich, 99%) were preliminarily dried over Calcium chloride, while

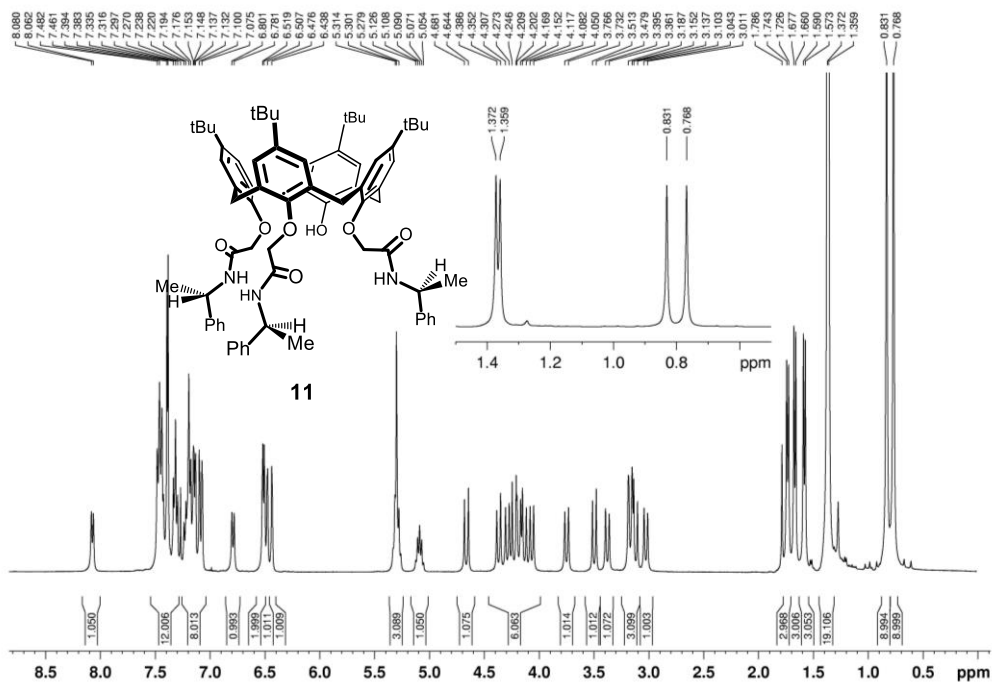
THF (Sigma-Aldrich, 99%) was preliminarily treated with potassium hydroxide. Then, all solvents were purified by distillation from sodium under a nitrogen atmosphere.

## 6.2. Synthesis of Catalysts

### 6.2.1. Synthesis of Derivative 11.

Oxalyl chloride (0.88 mL, 10 mmol) was slowly added to a stirred solution of **17**<sup>37</sup> (0.22 g, 0.27 mmol) in 10 mL of dry CHCl<sub>3</sub> at 0 °C. The reaction mixture was refluxed under nitrogen atmosphere for 15 h, then was cooled at room temperature and the solvent was removed under reduced pressure to give a dark solid. The crude product was dissolved in 5 mL of dry CHCl<sub>3</sub> and added dropwise to a stirred solution of (S)- $\alpha$ -methylbenzylamine (0.10 mL, 0.80 mmol) and dry Et<sub>3</sub>N (0.11 mL, 0.80 mmol) in 10 mL of dry CHCl<sub>3</sub> at 0 °C. The reaction mixture was stirred for 15 h at room temperature under nitrogen atmosphere, then was washed with a 1N aqueous solution of HCl (2  $\times$  5 mL). The aqueous phase was extracted with CHCl<sub>3</sub> (3  $\times$  5 mL). The collected organic layers were washed with H<sub>2</sub>O (10 mL), dried over Na<sub>2</sub>SO<sub>4</sub> and evaporated under reduced pressure. The crude product was purified by column chromatography (SiO<sub>2</sub>, CHCl<sub>3</sub>) to give the compound **11** as a white solid (0.060 g, 20 % yield): mp 126–128 °C;  $[\alpha]_{\text{D}}^{20} = -38.5 \pm 0.7$  ( $c = 0.100$ , CHCl<sub>3</sub>); <sup>1</sup>H NMR (400 MHz, CDCl<sub>3</sub>, 298 K):  $\delta$  8.06 (d,  $J = 8.2$  Hz, NH, 1H), 7.48 – 7.07 (overlapped ArH + NH, 21H), 6.79 (d,

$J = 8.2$  Hz,  $NH$ , 1H), 6.52 (s,  $ArH$ , 1H), 6.51 (s,  $ArH$ , 1H), 6.48 (s,  $ArH$ , 1H), 6.44 (s,  $ArH$ , 1H), 5.31 – 5.28 (overlapped,  $CHPhCH_3 + OH$ , 3H), 5.09 (m,  $CHPhCH_3$ , 1H), 4.66 (d,  $J = 14.6$  Hz,  $OCH_2CO$ , 1H), 4.37 (d,  $J = 13.8$  Hz,  $OCH_2CO$ , 1H), 4.29 (d,  $J = 13.3$  Hz,  $ArCH_2Ar$ , 1H), 4.23 (d,  $J = 14.6$  Hz,  $OCH_2CO$ , 1H), 4.19 (d,  $J = 13.1$  Hz,  $ArCH_2Ar$ , 1H), 4.14 (d,  $J = 13.8$  Hz,  $OCH_2CO$ , 1H), 4.07 (d,  $J = 12.9$  Hz,  $ArCH_2Ar$ , 1H), 3.75 (d,  $J = 13.1$  Hz,  $ArCH_2Ar$ , 1H), 3.50 (d,  $J = 13.7$  Hz,  $OCH_2CO$ , 1H), 3.38 (d,  $J = 13.3$  Hz,  $ArCH_2Ar$ , 1H), 3.17 (d,  $J = 13.1$  Hz,  $ArCH_2Ar$ , 2H), 3.12 (d,  $J = 13.7$  Hz,  $OCH_2CO$ , 1H) 3.03, (d,  $J = 12.9$  Hz,  $ArCH_2Ar$ , 1H), 1.74 (d,  $J = 7.0$  Hz,  $CHPhCH_3$ , 3H), 1.67 (d,  $J = 7.0$  Hz,  $CHPhCH_3$ , 3H), 1.58 (d,  $J = 6.9$  Hz,  $CHPhCH_3$ , 3H), 1.37 (s,  $C(CH_3)_3$ , 9H), 1.36 (s,  $C(CH_3)_3$ , 9H), 0.83 (s,  $C(CH_3)_3$ , 9H), 0.77 (s,  $C(CH_3)_3$ , 9H).  $^{13}C$  NMR (100 MHz,  $CDCl_3$ , 298 K):  $\delta$  168.9, 167.9, 167.5, 151.9, 151.6, 151.5, 149.8, 147.6, 146.7, 146.5, 143.3, 143.0, 142.8, 142.7, 135.4, 135.2, 131.6, 131.1, 130.8, 130.4, 128.9, 128.8, 128.7, 128.4, 128.3, 128.0, 127.8, 127.6, 126.9, 126.7, 126.6, 125.8, 125.7, 125.5, 125.5, 125.3, 75.8, 75.7, 74.0, 49.5, 49.0, 48.9, 34.4, 34.2, 33.9, 33.8, 32.1, 31.9, 31.8, 31.5, 31.3, 31.1, 21.9, 21.3, 20.1. HRMS (ESI+)  $m/z$   $[M]^+$  calcd for  $C_{74}H_{90}N_3O_7$ , 1132.6773; found 1132.6778.



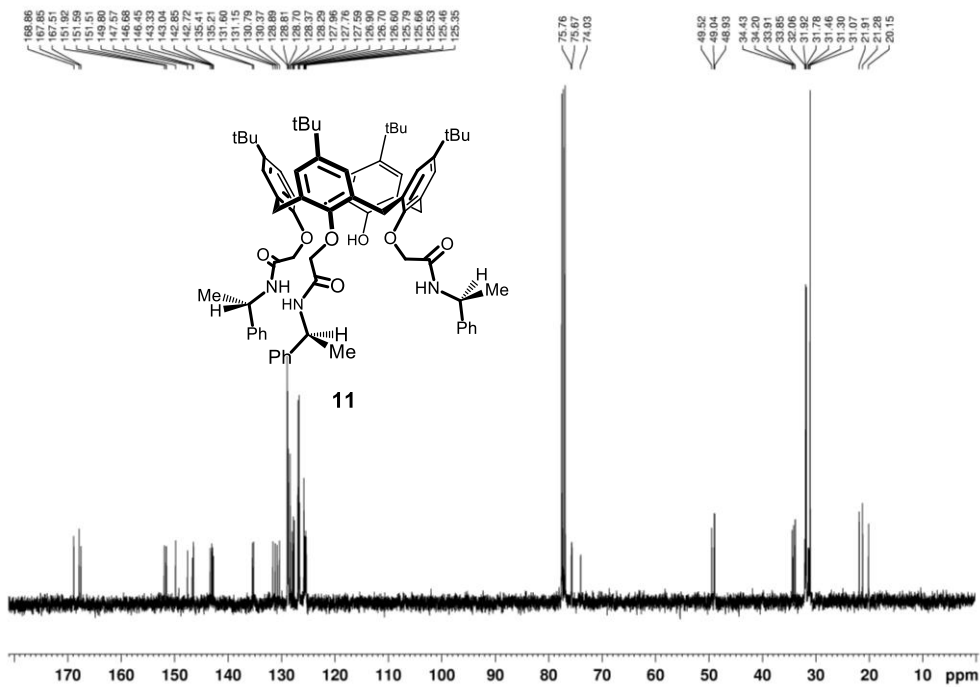


**Figure 37.**  $^{13}\text{C}$  NMR spectrum of derivative **11** (100 MHz,  $\text{CDCl}_3$ , 298 K).



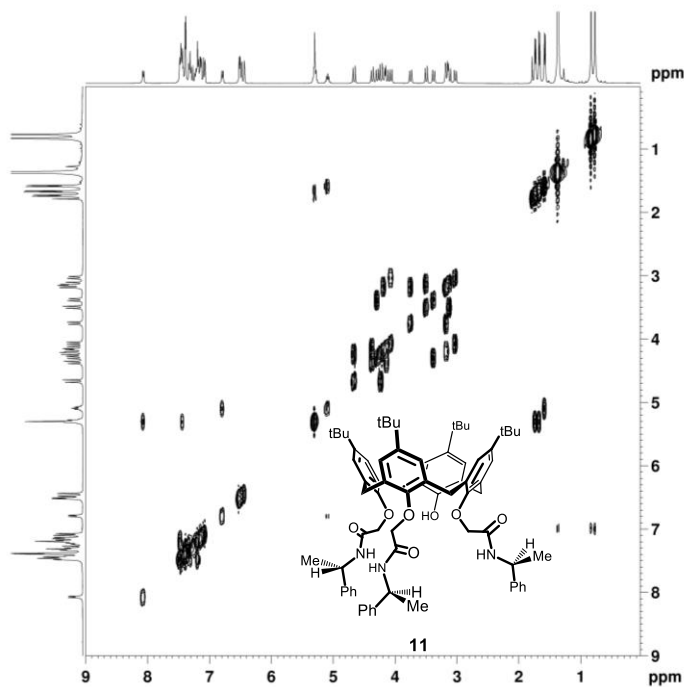


**Figure 39.** 2D COSY-45 spectrum (400 MHz,  $\text{CDCl}_3$ , 298 K) of **11**.

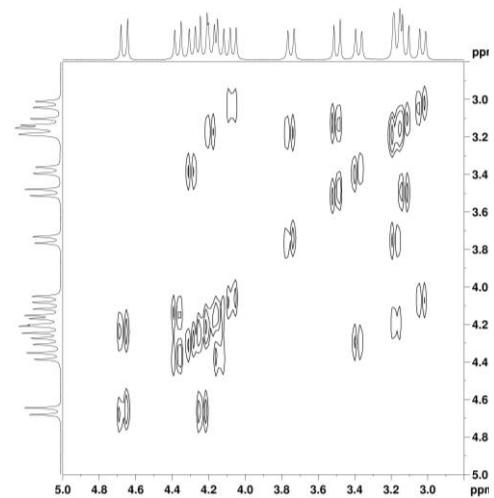


**Figure 40.** Section of 2D COSY-45 spectrum (400 MHz,  $\text{CDCl}_3$ , 298 K) of **11**.

### 6.2.2. *Synthesis of Derivative 12.*

Oxalyl chloride (1.5 mL, 18 mmol) was slowly added to a stirred solution of **19** (0.38 g, 0.46 mmol) in 20 mL of dry CHCl<sub>3</sub> at 0 °C. The reaction mixture was refluxed under nitrogen atmosphere for 13 h, then was cooled at room temperature and the solvent was removed under reduced pressure to give a dark solid. The crude product was dissolved in 13 mL of dry CHCl<sub>3</sub> and added dropwise to a stirred solution of (S)- $\alpha$ -methylbenzylamine (0.18 mL, 1.4 mmol) and dry Et<sub>3</sub>N (0.19 mL, 1.4 mmol) in 23 mL of dry CHCl<sub>3</sub> at 0 °C. The reaction mixture was stirred for 22 h at room temperature under nitrogen atmosphere, then was washed with a 1N aqueous solution of HCl (2  $\times$  15 mL). The aqueous phase was extracted with CHCl<sub>3</sub> (3  $\times$  10 mL). The collected organic layers were washed with H<sub>2</sub>O (20 mL), dried over Na<sub>2</sub>SO<sub>4</sub> and evaporated. The crude product was purified by column chromatography (SiO<sub>2</sub>, CHCl<sub>3</sub>/hexane from 6/4 to 9/1 (v/v)) to give the derivative **12** as a white solid (0.22 g, 57 %): mp 140–143 °C;  $[\alpha]_{\text{D}}^{20} = -26.4 \pm 0.4$  ( $c = 1.00$ , CHCl<sub>3</sub>); **<sup>1</sup>H NMR** (400 MHz, CDCl<sub>3</sub>, 298 K):  $\delta$  7.73 (broad, NH, 1H), 7.70 (d,  $J = 8.4$  Hz, NH, 1H), 7.46 (d,  $J = 7.2$  Hz, ArH, 2H), 7.40 (d,  $J = 7.2$  Hz, ArH, 2H), 7.28–7.02 (overlapped, ArH, 15H), 6.78 (broad, NH, 1H), 6.47–6.45 (overlapped, ArH, 3H),

6.40 (s, ArH, 1H), 5.35 – 5.27 (m, NCHPhCH<sub>3</sub>, 2H), 5.04 – 5.00 (m, NCHPhCH<sub>3</sub>, 1H), 4.69 – 4.60 (overlapped, OCH<sub>2</sub>CO, 2H), 4.49 (d, *J* = 13.2 Hz, ArCH<sub>2</sub>Ar, 1H), 4.30 (d, *J* = 13.2 Hz, ArCH<sub>2</sub>Ar, 1H), 4.22 (s, OCH<sub>2</sub>CO, 2H), 4.13 (s, OCH<sub>2</sub>CO, 2H), 4.11 (d, *J* = 12.4 Hz, ArCH<sub>2</sub>Ar, 1H), 4.08 (d, *J* = 12.4 Hz, ArCH<sub>2</sub>Ar, 1H), 3.74 (s, OCH<sub>3</sub>, 3H), 3.24 (overlapped, ArCH<sub>2</sub>Ar, 3H), 2.94 (d, *J* = 13.2 Hz, ArCH<sub>2</sub>Ar, 1H), 1.65 (d, *J* = 6.8 Hz, CHPhCH<sub>3</sub>, 3H), 1.58 (d, *J* = 7.2 Hz, CHPhCH<sub>3</sub>, 3H), 1.41 (d, *J* = 6.8 Hz, CHPhCH<sub>3</sub>, 3H), 1.34 (s, C(CH<sub>3</sub>)<sub>3</sub>, 9H), 1.33 (s, C(CH<sub>3</sub>)<sub>3</sub>, 9H), 0.86 (s, C(CH<sub>3</sub>)<sub>3</sub>, 9H), 0.85 (s, C(CH<sub>3</sub>)<sub>3</sub>, 9H). <sup>13</sup>C NMR (100 MHz, CDCl<sub>3</sub>, 298 K): δ 168.33, 168.28, 168.1, 154.9, 153.1, 152.0, 145.8, 145.6, 145.2, 145.1, 143.3, 143.1, 142.8, 134.9, 134.7, 134.7, 131.3, 131.3, 130.8, 128.5, 128.4, 127.2, 126.5, 126.3, 126.2, 126.1, 125.8, 125.1, 124.7, 124.6, 74.7, 74.6, 60.2, 48.7, 48.5, 48.3, 34.1, 33.6, 31.6, 31.5, 31.2, 31.0, 21.8, 21.5, 21.2. HRMS (ESI+) *m/z* [M + Na]<sup>+</sup> calcd for C<sub>75</sub>H<sub>91</sub>N<sub>3</sub>NaO<sub>7</sub>, 1168.6749; found 1168.6756.

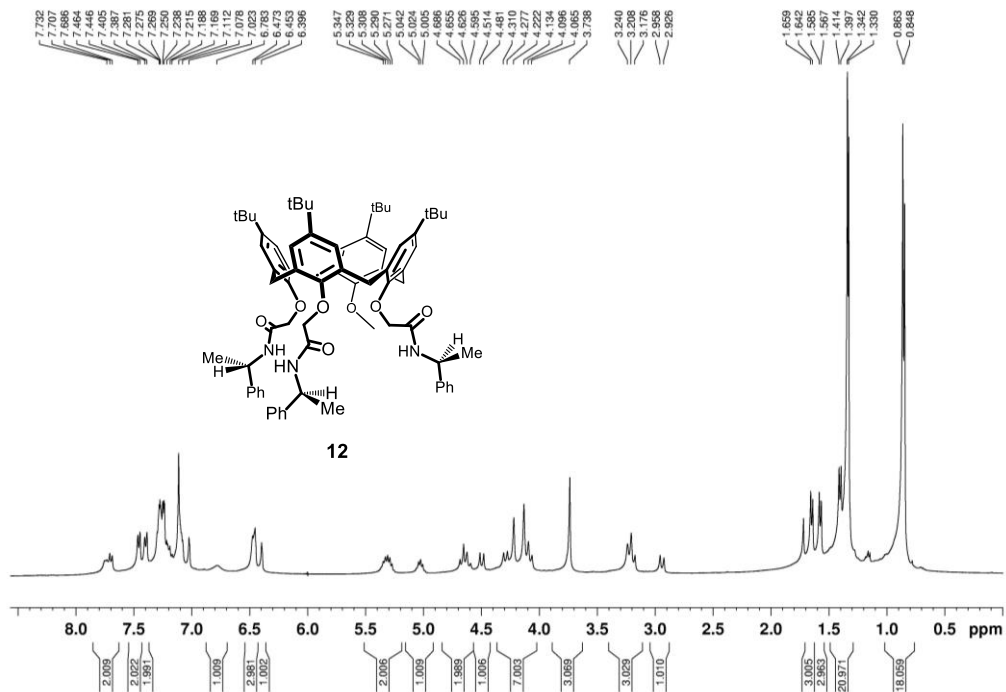


**Figure 41.**  $^1\text{H}$  NMR spectrum of derivative **12** (400 MHz,  $\text{CDCl}_3$ , 298 K).

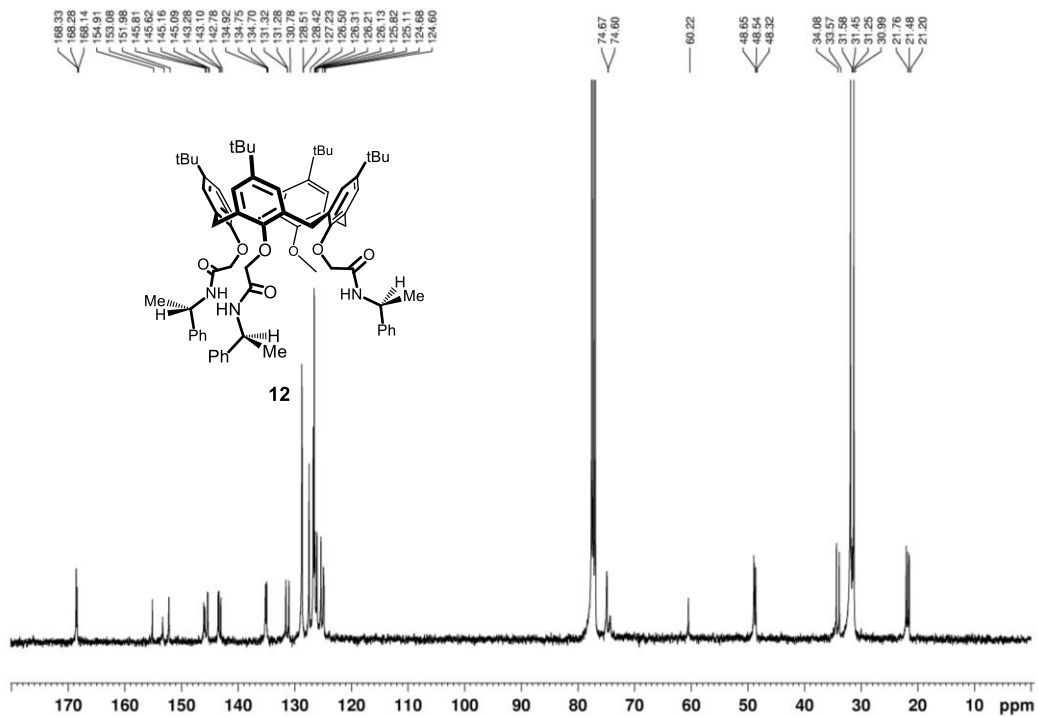


**Figure 42.**  $^{13}\text{C}$  NMR spectrum of derivative **12** (100 MHz,  $\text{CDCl}_3$ , 298 K).

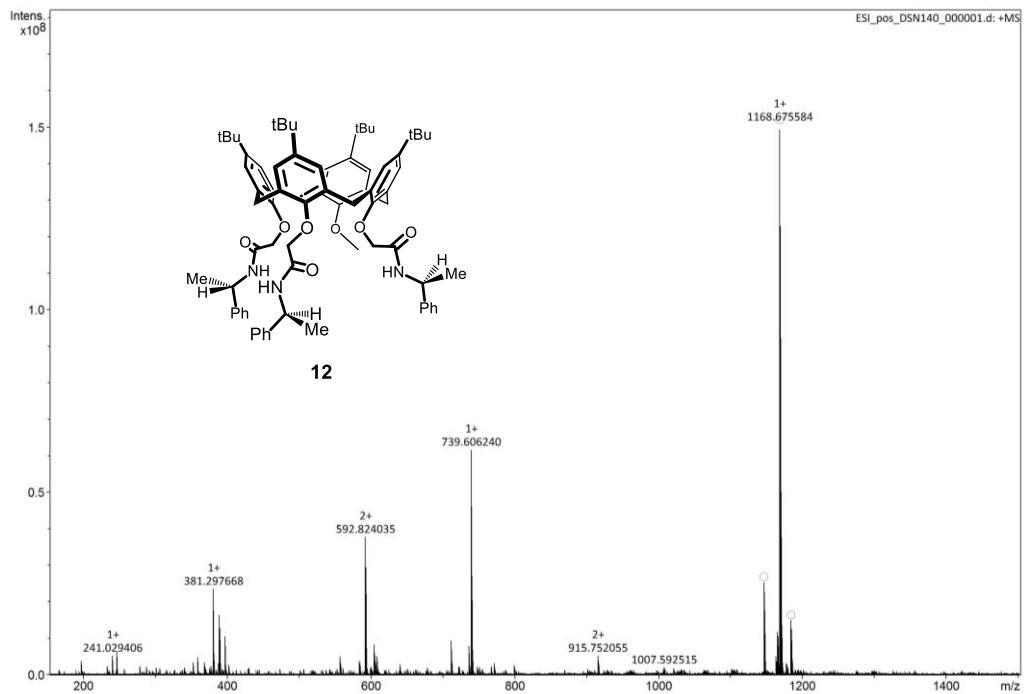


**Figure 43.** HR-ESI (+) MS spectrum of derivative **12**.

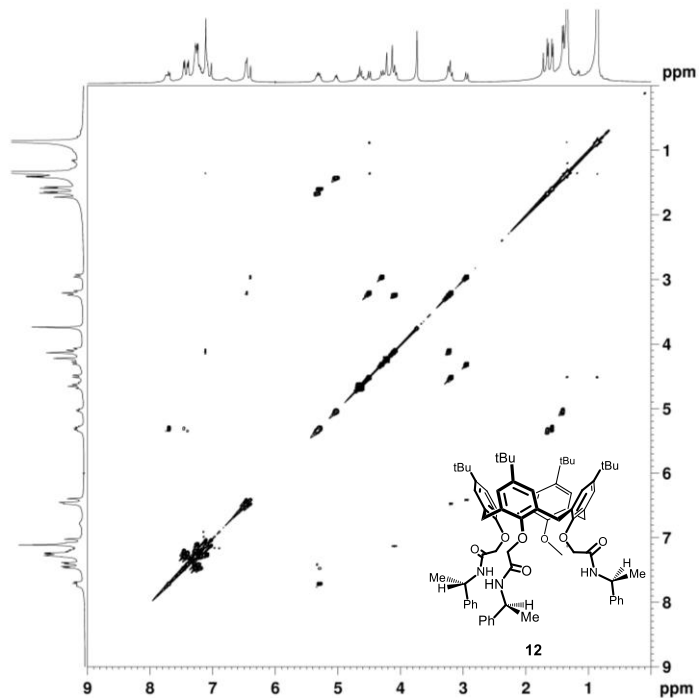


**Figure 44.** 2D COSY-45 spectrum (400 MHz, CDCl<sub>3</sub>, 298 K) of **12**.

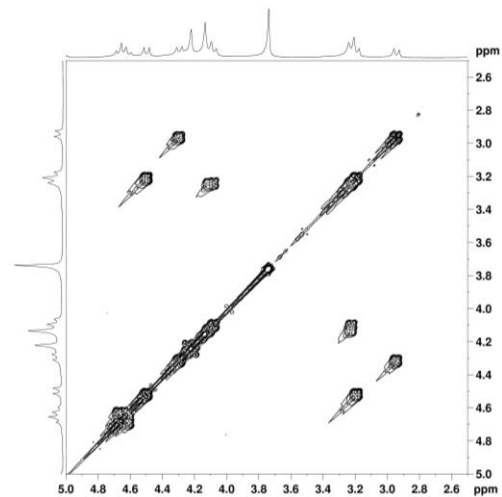


**Figure 45.** Section of 2D COSY-45 spectrum (400 MHz, CDCl<sub>3</sub>, 298 K) of **12**.

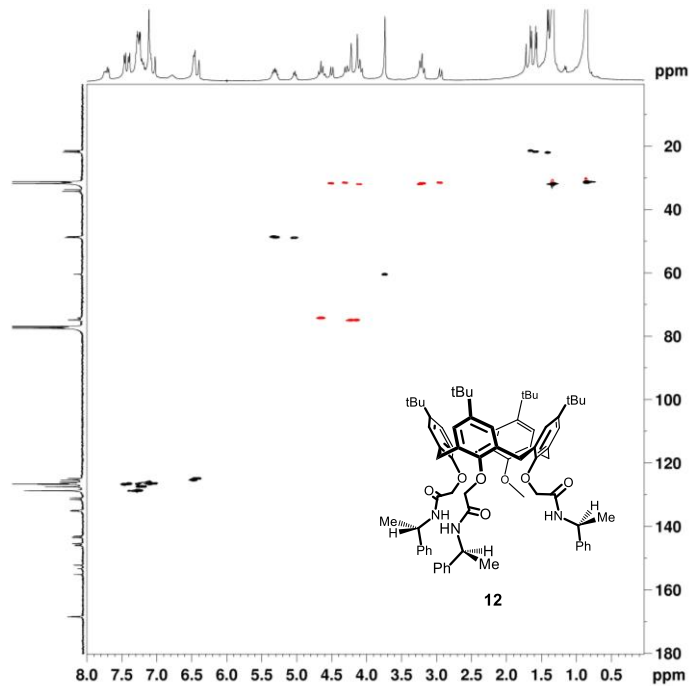


**Figure 46.** HSQC Spectrum (400 MHz,  $\text{CDCl}_3$ , 298 K) of **12**.

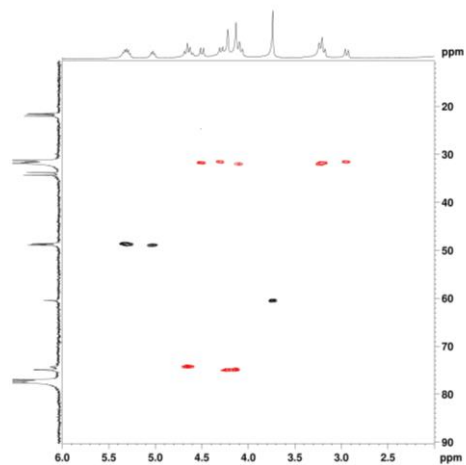


**Figure 47.** Section of HSQC spectrum (400 MHz,  $\text{CDCl}_3$ , 298 K) of **12**.

### 6.2.3. Synthesis of Derivative 13.

Oxalyl chloride (0.27 mL, 3.2 mmol) was slowly added to a stirred solution of **20** (0.097 g, 0.12 mmol) in 5 mL of dry  $\text{CHCl}_3$  at 0 °C. The reaction mixture was refluxed under nitrogen atmosphere for 16 h, then was cooled at room temperature and the solvent removed under reduced pressure to give a white solid. The crude product was dissolved in 1 mL of dry  $\text{CHCl}_3$  and added dropwise to a stirred solution of (S)- $\alpha$ -methylbenzylamine (0.03 mL, 0.2 mmol) and dry  $\text{Et}_3\text{N}$  (0.03 mL, 0.2 mmol) in 3 mL of dry  $\text{CHCl}_3$  at 0 °C. The reaction mixture was stirred for 64 h at room temperature under nitrogen atmosphere, then was washed with a 1N aqueous solution of HCl ( $2 \times 5$  mL). The aqueous phase was extracted with  $\text{CHCl}_3$  ( $3 \times 5$  mL). The collected organic layers were washed with  $\text{H}_2\text{O}$  (5 mL), dried over  $\text{Na}_2\text{SO}_4$  and evaporated. The crude product was purified by column chromatography ( $\text{SiO}_2$ ,  $\text{CHCl}_3$ ) to afford **13** as a white solid (0.096 g, 80 %): mp 237-239 °C;  $[\alpha]_{\text{D}}^{20} = -34.68 \pm 0.04$  ( $c = 0.997$ ,  $\text{CHCl}_3$ );  $^1\text{H NMR}$  (600 MHz,  $\text{CDCl}_3$ , 298 K):  $\delta$  7.30 – 7.20 (overlapped,  $\text{NH} + \text{ArH}$ , 12H), 7.12 (s,  $\text{ArH}$ , 4H), 6.42 (s,  $\text{ArH}$ , 4H), 5.31 (overlapped,  $\text{COCHPhCH}_3$ , 2H), 4.27-4.21 (overlapped,  $\text{OCH}_2\text{CO}$ , 4H), 4.11 (broad,  $\text{ArCH}_2\text{Ar}$ , 4H), 3.69 (s,  $\text{OCH}_3$ , 6H), 3.20 (broad,  $\text{ArCH}_2\text{Ar}$ , 4H),

1.49 (d,  $J = 6.6$  Hz,  $\text{CHPhCH}_3$ , 6H), 1.32 (s,  $\text{C}(\text{CH}_3)_3$ , 18H), 0.81 (s,  $\text{C}(\text{CH}_3)_3$ , 18H).  $^{13}\text{C}$  NMR (150 MHz,  $\text{CDCl}_3$ , 298 K):  $\delta$  168.4, 154.8, 146.3, 145.5, 142.6, 135.3, 131.1, 131.0, 128.9, 127.7, 126.1, 125.0, 74.3, 60.3, 48.0, 34.3, 33.7, 31.8, 31.1, 21.7. HRMS (ESI+)  $m/z$   $[\text{M}+\text{H}]^+$  calcd for  $\text{C}_{66}\text{H}_{83}\text{N}_2\text{O}_6$ , 999.6246; found 999.6260.

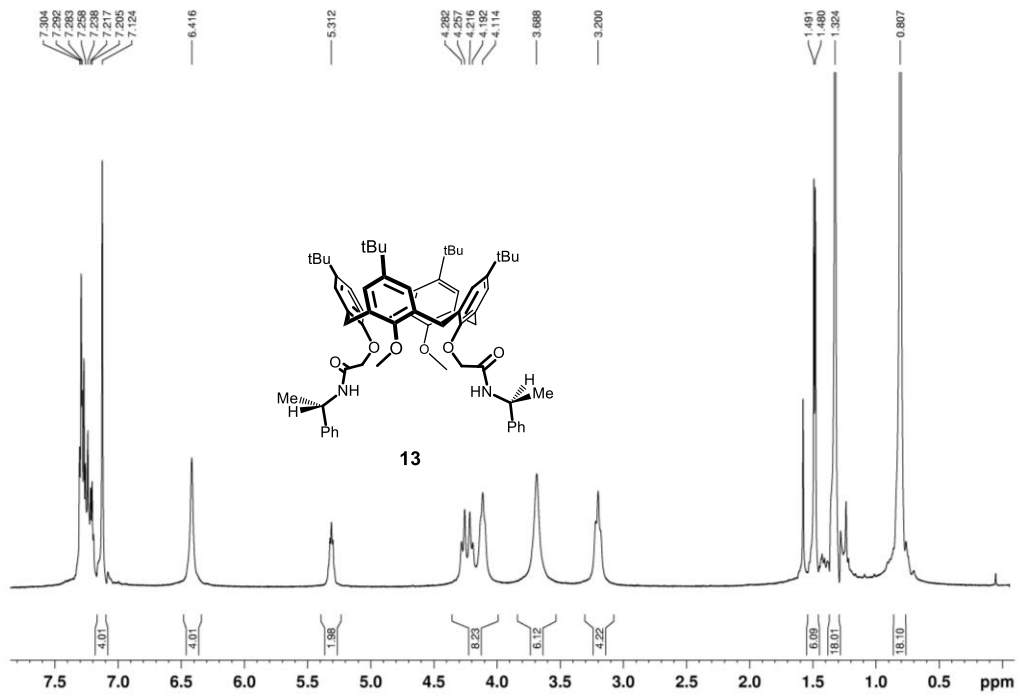


**Figure 48.**  $^1\text{H}$  NMR spectrum of derivative **13** (600 MHz,  $\text{CDCl}_3$ , 298 K).

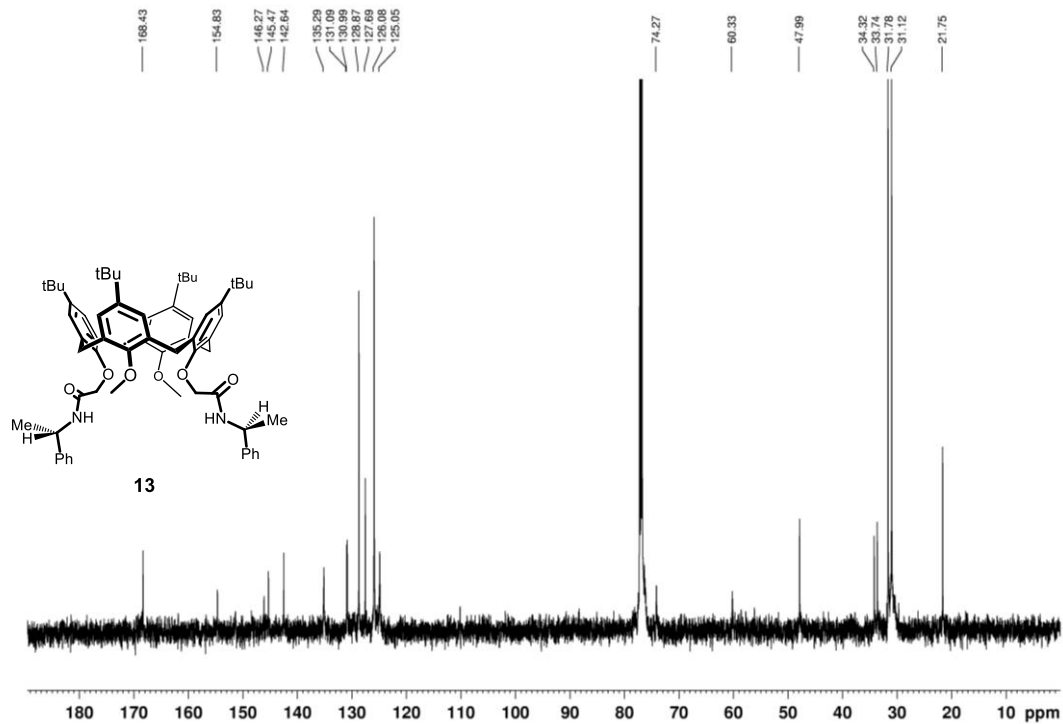


**Figure 49.** <sup>13</sup>C NMR spectrum of derivative **13** (150 MHz, CDCl<sub>3</sub>, 298 K).

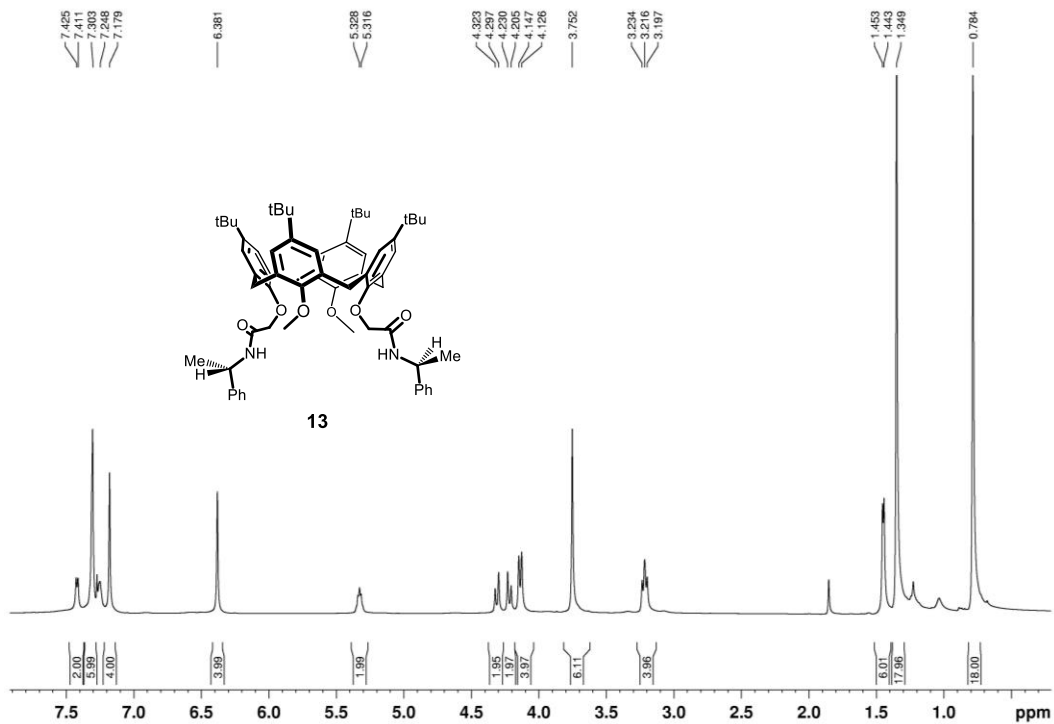


**Figure 50.**  $^1\text{H}$  NMR spectrum of derivative **13** (600 MHz,  $\text{CDCl}_3$ , 233 K).

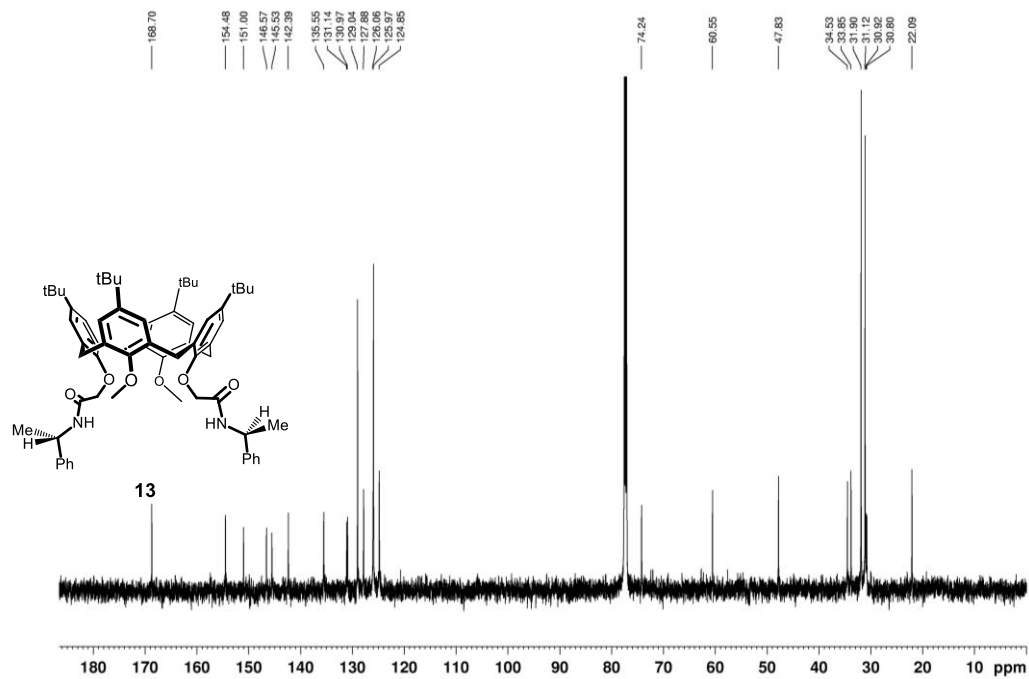


**Figure 51.**  $^{13}\text{C}$  NMR spectrum of derivative **13** (150 MHz,  $\text{CDCl}_3$ , 233 K).

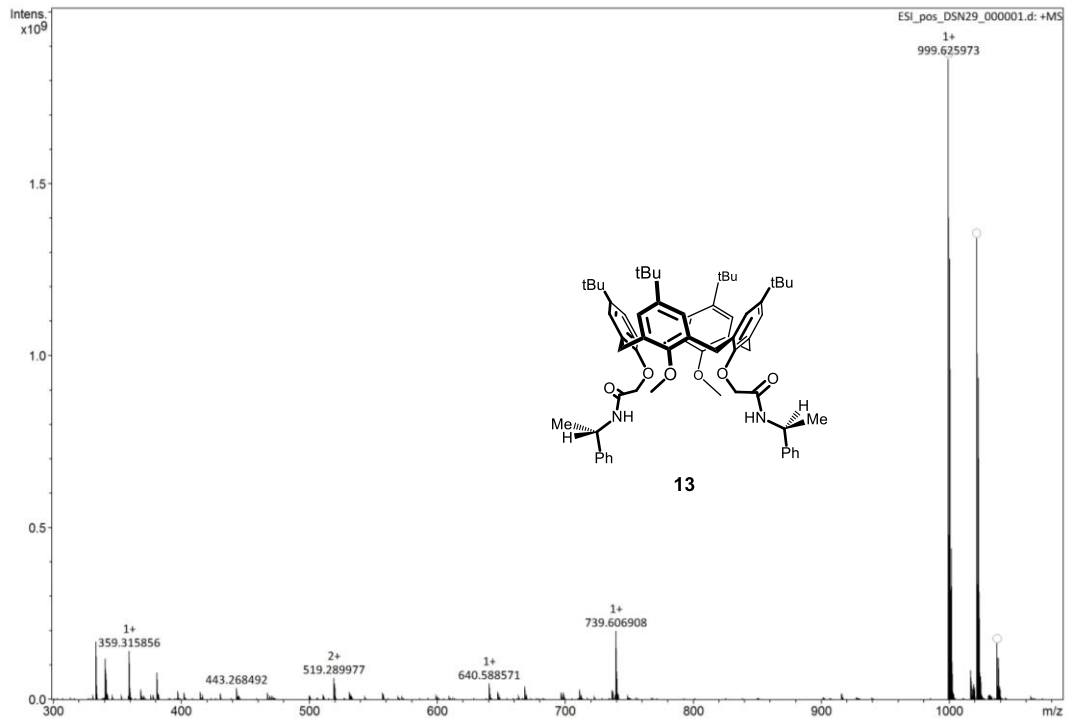


**Figure 52.** HR-ESI (+) MS spectrum of derivative **13**.

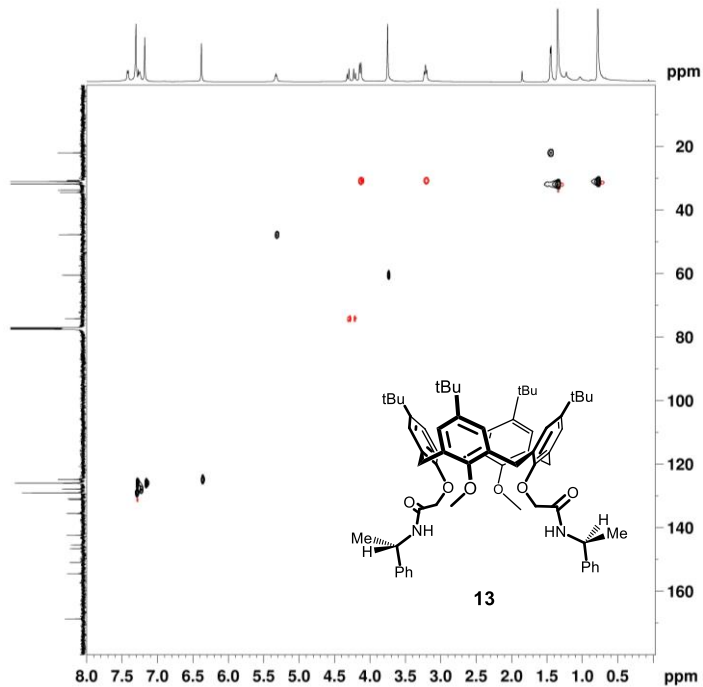


**Figure 53.** HSQC Spectrum (600 MHz,  $\text{CDCl}_3$ , 233 K) of **13**.

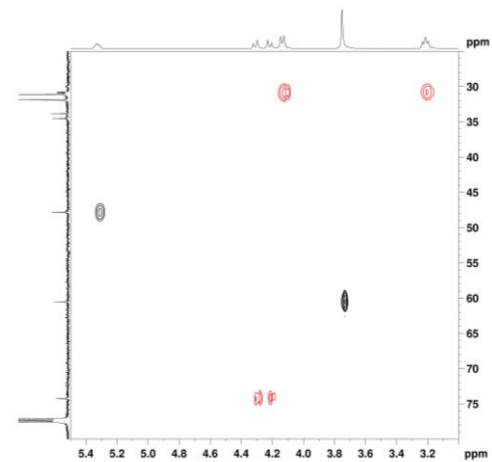


**Figure 54.** Section of HSQC spectrum (600 MHz,  $\text{CDCl}_3$ , 233 K) of **13**.

#### 6.2.4. Synthesis of Derivative 14.

Oxalyl chloride (0.26 mL, 3.1 mmol) was slowly added to a stirred solution of **21** (0.18 g, 0.24 mmol) in 10 mL of dry CHCl<sub>3</sub> at 0 °C. The reaction mixture was refluxed under nitrogen atmosphere for 19 h, then was cooled at room temperature and the solvent was removed under reduced pressure to give a white solid. The crude product was dissolved in 6 mL of dry CHCl<sub>3</sub> and added dropwise to a stirred solution of (S)- $\alpha$ -methylbenzylamine (0.03 mL, 0.2 mmol) and Et<sub>3</sub>N (0.03 mL, 0.2 mmol) in 3 mL of dry CHCl<sub>3</sub> at 0 °C. The reaction mixture was stirred for 16 h at room temperature under nitrogen atmosphere, then was washed with a 1N aqueous solution of HCl (2  $\times$  5 mL). The aqueous phase was extracted with CHCl<sub>3</sub> (3  $\times$  5 mL). The collected organic layers were washed with H<sub>2</sub>O (10 mL), dried over Na<sub>2</sub>SO<sub>4</sub> and evaporated. The crude product was purified by column chromatography (SiO<sub>2</sub>, CH<sub>2</sub>Cl<sub>2</sub>) to afford **14** as a white solid (0.12 g, 60 %): mp 106 –107 °C;  $[\alpha]_D^{20} = -15.4 \pm 0.8$  ( $c = 1.00$ , CHCl<sub>3</sub>); <sup>1</sup>H NMR (600 MHz, TCDE, 353 K):  $\delta$  7.22 (s, ArH, 5H), 7.13 (s, NH, 1H), 6.94 – 6.87 (overlapped, ArH, 4H), 6.65 (s, ArH, 2H), 6.51 (s, ArH, 2H), 5.16 (broad, COCHPhCH<sub>3</sub>, 1H), 4.15 (broad, OCH<sub>2</sub>CO, 2H), 4.00 (broad, ArCH<sub>2</sub>Ar, 2H), 3.88 (broad, ArCH<sub>2</sub>Ar, 4H), 3.33 (s, OCH<sub>3</sub>, 3H),

3.20 (s, OCH<sub>3</sub>, 6H), 3.14 (broad, ArCH<sub>2</sub>Ar, 2H), 1.45 (broad, CHPhCH<sub>3</sub>, 3H), 1.17 (s, C(CH<sub>3</sub>)<sub>3</sub>, 9H), 1.14 (s, C(CH<sub>3</sub>)<sub>3</sub>, 9H), 0.98 (s, C(CH<sub>3</sub>)<sub>3</sub>, 9H), 0.83 (s, C(CH<sub>3</sub>)<sub>3</sub>, 9H). <sup>13</sup>C NMR (150 MHz, TCDE, 353 K): δ 168.5, 155.1, 154.8, 152.0, 145.3, 144.3, 143.0, 134.6, 134.3, 132.7, 131.7, 128.7, 127.4, 126.2, 126.1, 125.5, 125.4, 125.3, 74.2, 60.4, 60.1, 49.6, 48.3, 34.0, 34.0, 33.7, 33.7, 31.7, 31.6, 31.4, 31.2, 29.7, 21.3. HRMS (ESI+) *m/z* [M + Na]<sup>+</sup> calcd for C<sub>57</sub>H<sub>73</sub>NNaO<sub>5</sub>, 874.5381; found 874.5391.

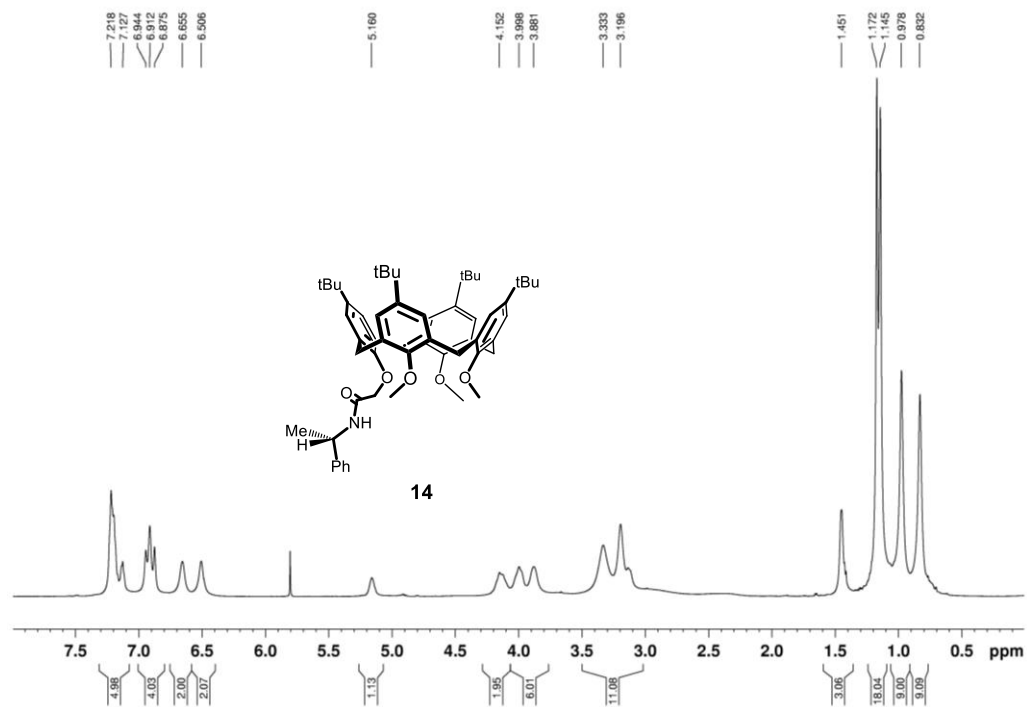


**Figure 55.**  $^1\text{H}$  NMR spectrum of derivative **14** (600 MHz, TCDE, 353 K).

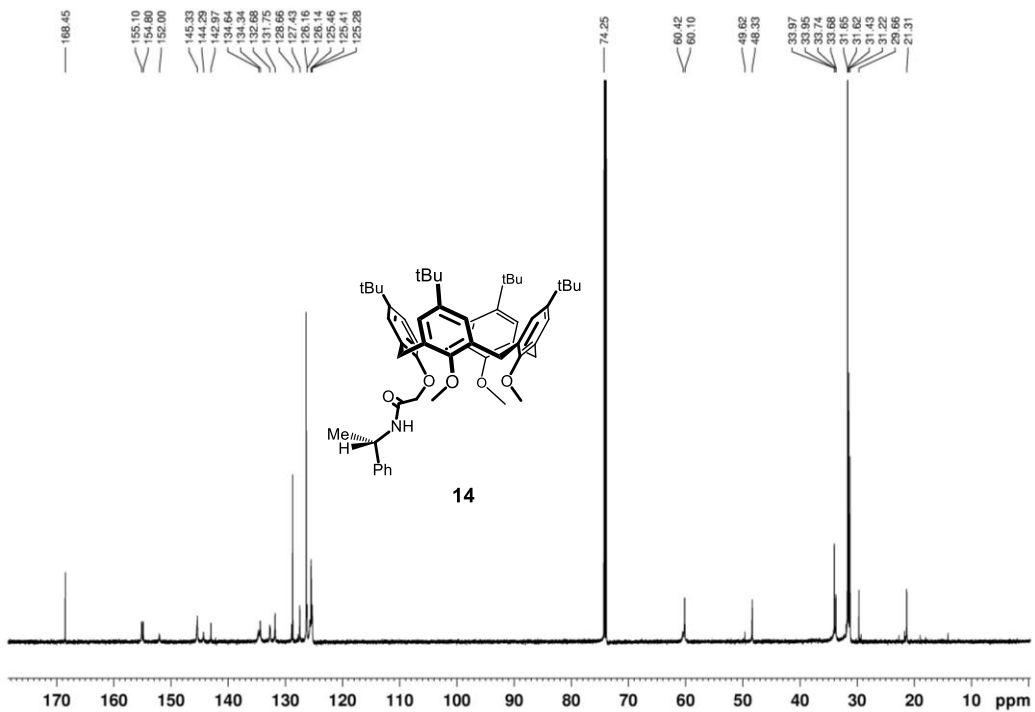


**Figure 56.** <sup>13</sup>C NMR spectrum of derivative **14** (150 MHz, TCDE, 353 K).

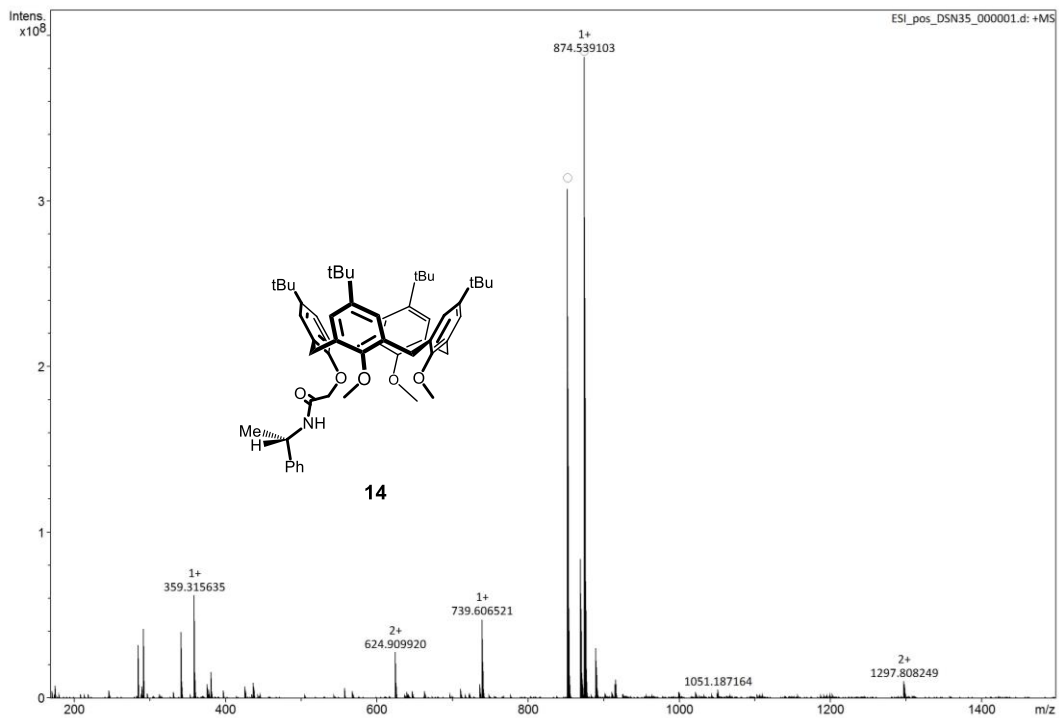


**Figure 57.** HR-ESI (+) MS spectrum of derivative **14**.

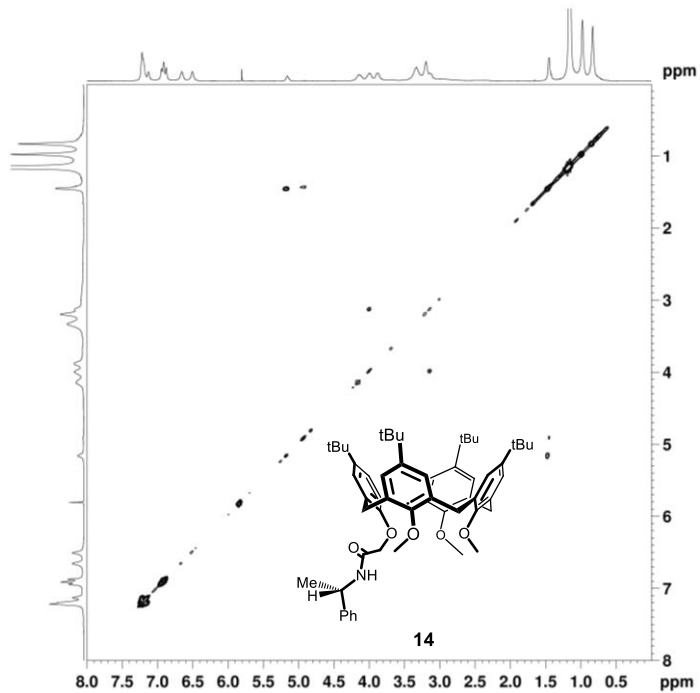


**Figure 58.** 2D COSY-45 spectrum (600 MHz, TCDE, 353 K) of **14**.

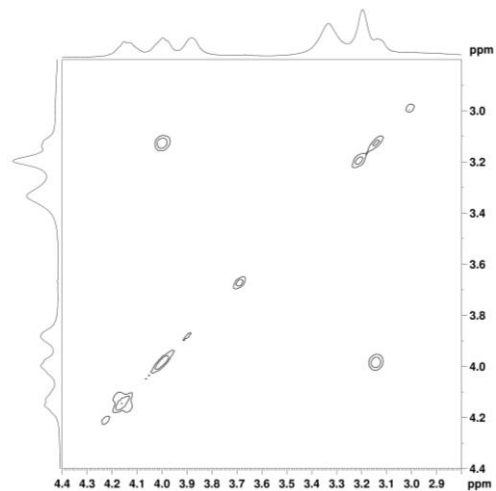


**Figure 59.** Section of 2D COSY-45 spectrum (600 MHz, TCDE, 353 K) of **14**.

### 6.2.5. *Synthesis of Derivative 15.*

Oxalyl chloride (0.78 mL, 9.3 mmol) was slowly added to a stirred solution of **19** (0.20 g, 0.24 mmol) in 10 mL of dry CHCl<sub>3</sub> at 0 °C. The reaction mixture was refluxed under nitrogen atmosphere for 15 h, then was cooled at room temperature and the solvent was removed under reduced pressure to give a white solid. The crude product was dissolved in 7 mL of dry CHCl<sub>3</sub> and added dropwise to a stirred solution of (S)-1-(2-naphthyl)ethylamine (0.22 g, 1.3 mmol) and dry Et<sub>3</sub>N (0.18 mL, 1.3 mmol) in 13 mL of dry CHCl<sub>3</sub> at 0 °C. The reaction mixture was stirred for 63 h at room temperature under nitrogen atmosphere, then was washed a 1N aqueous solution of HCl (2 × 10 mL). The aqueous phase was extracted with CHCl<sub>3</sub> (3 × 10 mL). The collected organic layers were washed with H<sub>2</sub>O (25 mL), dried over Na<sub>2</sub>SO<sub>4</sub> and evaporated. The crude product was purified by column chromatography (SiO<sub>2</sub>, CH<sub>2</sub>Cl<sub>2</sub>/Et<sub>2</sub>O 96/4 (v/v)) to afford compound **15** as white solid (0.24 g, 76 %): mp 138-139 °C;  $[\alpha]_D^{20} = -424 \pm 4$  ( $c = 0.0938$ , CHCl<sub>3</sub>); <sup>1</sup>H NMR (600 MHz, CDCl<sub>3</sub>, 298 K): δ 7.88 (s, ArH, 1H), 7.85 (broad, NH, 1H), 7.83 (broad, NH, 1H), 7.81 (s, ArH, 1H), 7.75 – 7.63 (overlapped, ArH, 7H), 7.58 (s, ArH, 1H), 7.57 (s, ArH, 1H), 7.51 (s, ArH, 1H), 7.50 (s, ArH, 1H), 7.47 (broad, NH, 1H), 7.55

– 7.37 (overlapped, ArH, 6H), 7.13 (d,  $J = 1.8$  Hz, ArH, 1H), 7.12 (d,  $J = 1.8$  Hz, ArH, 1H), 7.09 (s, ArH, 2H), 7.06 (d,  $J = 2.4$  Hz, ArH, 1H), 6.94 (d,  $J = 2.4$  Hz, ArH, 1H), 6.50 (broad, ArH, 1H), 6.47 (broad, ArH, 1H), 6.45 (d,  $J = 2.4$  Hz, ArH, 1H), 6.36 (d,  $J = 1.8$  Hz, ArH, 1H), 5.49–5.43 (overlapped, COCHPhCH<sub>3</sub>, 2H), 5.11–5.08 (*m*, COCHPhCH<sub>3</sub>, 1H), 4.75–4.71 (overlapped, OCH<sub>2</sub>CO, 2H), 4.53 (d,  $J = 13.2$  Hz, ArCH<sub>2</sub>Ar, 1H), 4.34 (d,  $J = 12.6$  Hz, ArCH<sub>2</sub>Ar, 1H), 4.25 (broad, OCH<sub>2</sub>CO, 2H), 4.17–4.12 (overlapped, OCH<sub>2</sub>CO, 2H), 4.10–4.06 (overlapped, ArCH<sub>2</sub>Ar, 2H), 3.73 (*s*, OCH<sub>3</sub>, 3H), 3.23–3.21 (overlapped, ArCH<sub>2</sub>Ar, 2H), 3.17 (*d*,  $J = 13.2$  Hz, ArCH<sub>2</sub>Ar, 1H), 2.87 (*d*,  $J = 12.6$  Hz, ArCH<sub>2</sub>Ar, 1H), 1.74 (*d*,  $J = 7.2$  Hz, CHPhCH<sub>3</sub>, 3H), 1.60 (*d*,  $J = 7.2$  Hz, CHPhCH<sub>3</sub>, 3H), 1.39 (*d*,  $J = 6.6$  Hz, CHPhCH<sub>3</sub>, 3H), 1.31 (*s*, CCH<sub>3</sub>, 9H), 1.30 (*s*, CCH<sub>3</sub>, 9H), 0.87 (*s*, CCH<sub>3</sub>, 9H), 0.84 (*s*, CCH<sub>3</sub>, 9H). <sup>13</sup>C NMR (150 MHz, CDCl<sub>3</sub>, 298 K):  $\delta$  168.6, 155.1, 152.3, 145.4, 145.2, 140.9, 140.6, 140.3, 134.8, 134.6, 133.4, 133.3, 132.8, 132.7, 131.5, 131.1, 128.5, 128.4, 128.3, 128.1, 128.0, 128.0, 127.7, 127.7, 126.2, 126.1, 126.0, 125.9, 125.8, 125.4, 125.2, 125.0, 124.9, 124.8, 74.8, 60.4, 48.8, 48.6, 34.2, 34.2, 33.8, 33.7, 31.7, 31.2, 21.8, 21.4, 21.3. HRMS (ESI+)  $m/z$  [M + Na]<sup>+</sup> calcd for C<sub>87</sub>H<sub>98</sub>N<sub>3</sub>NaO<sub>7</sub>, 1319.7297; found 1319.7256.

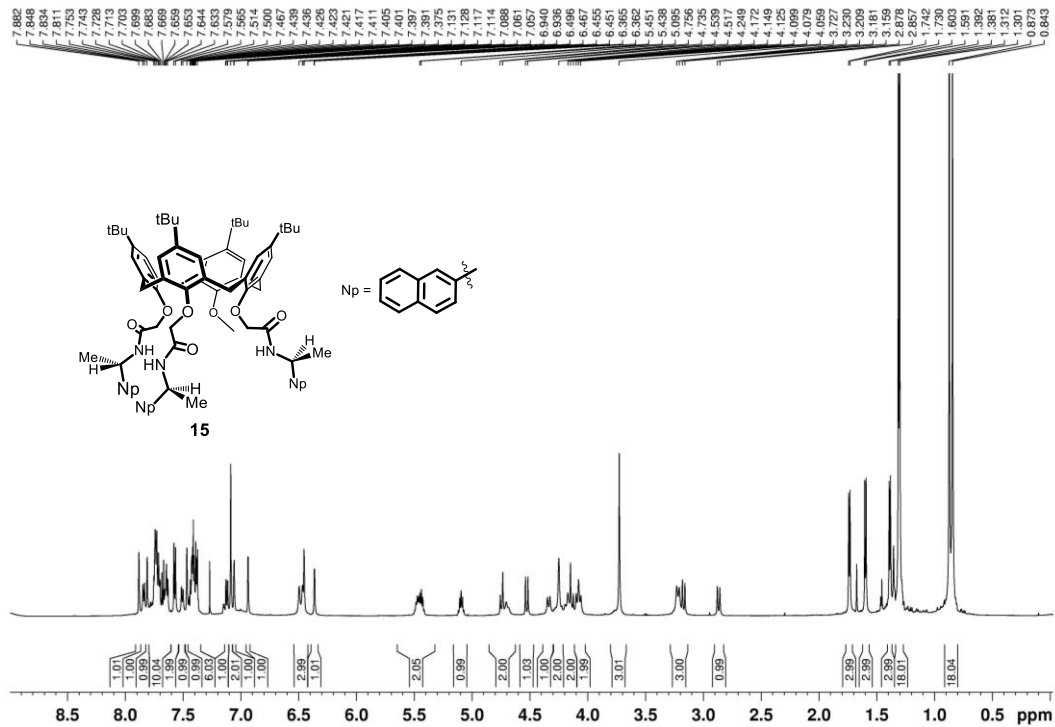


**Figure 60.** <sup>1</sup>H NMR spectrum of derivative **15** (600 MHz, CDCl<sub>3</sub>, 298 K).

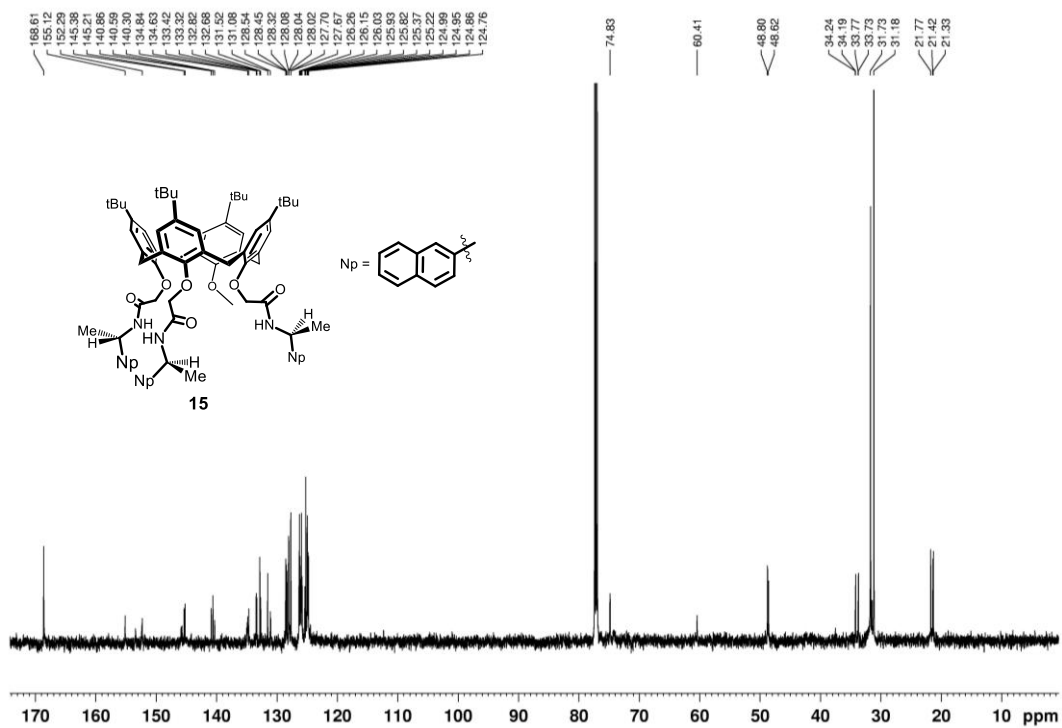


**Figure 61.**  $^{13}\text{C}$  NMR spectrum of derivative **15** (150 MHz,  $\text{CDCl}_3$ , 298 K).

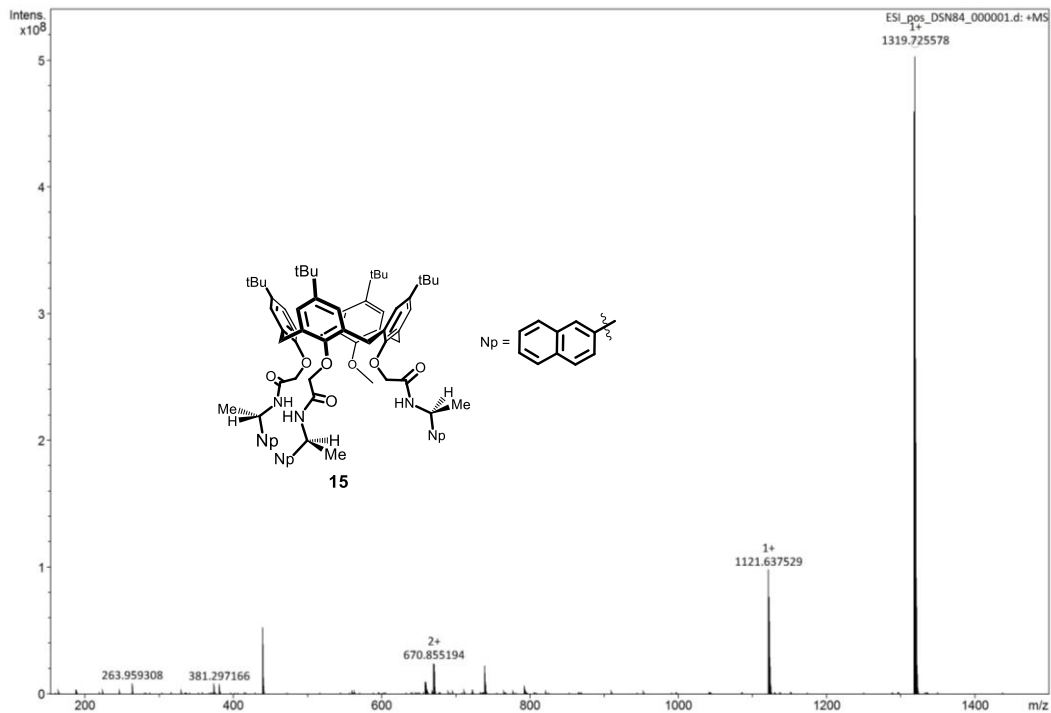


**Figure 62.** HR-ESI (+) MS spectrum of derivative **15**.

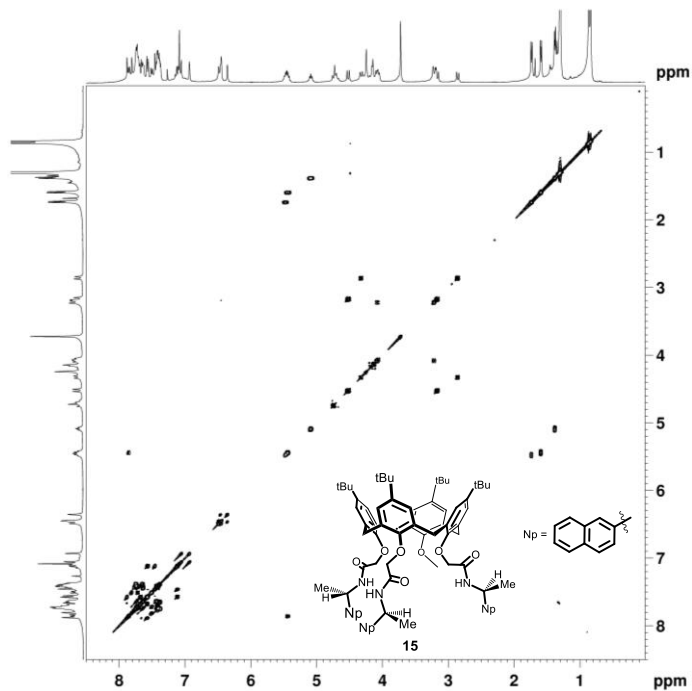


**Figure 63.** 2D COSY-45 spectrum (400 MHz,  $\text{CDCl}_3$ , 298 K) of **15**.

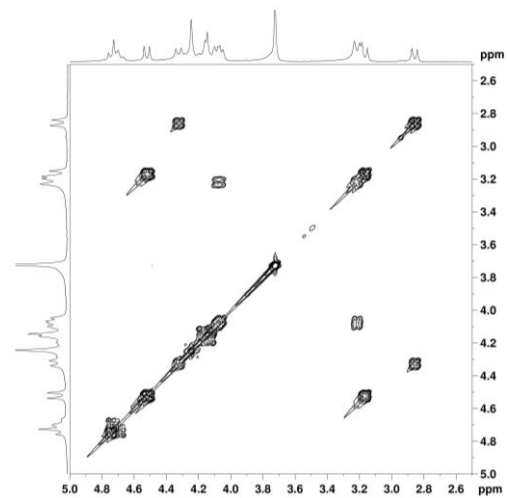


**Figure 64.** Section of the 2D COSY-45 spectrum (400 MHz,  $\text{CDCl}_3$ , 298 K) of **15**.

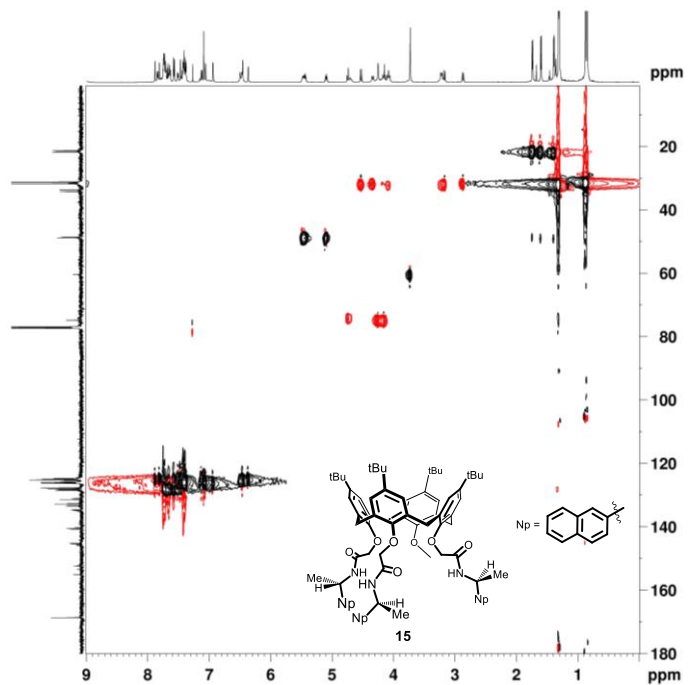


**Figure 65.** HSQC Spectrum (600 MHz, CDCl<sub>3</sub>, 298 K) of **15**.

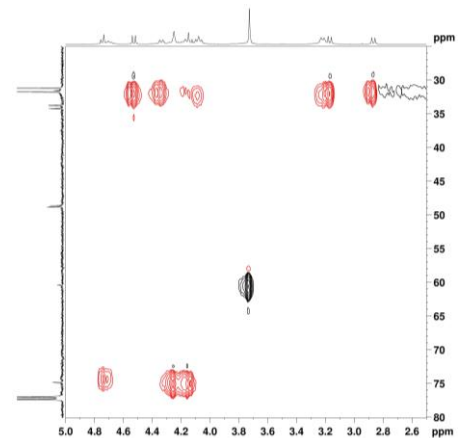


**Figure 66.** Section of the HSQC spectrum (600 MHz, CDCl<sub>3</sub>, 298 K) of **15**.

### 6.2.6. Synthesis of Derivative 18.

CH<sub>3</sub>I (0.38 mL, 6.09 mmol) was added to a suspension of **16** (0.55 g, 0.61 mmol) and K<sub>2</sub>CO<sub>3</sub> (0.34 g, 2.44 mmol) in CH<sub>3</sub>CN (15 mL) at 0 °C. The reaction mixture was refluxed for 15 h. The solvent was evaporated under reduced pressure and the crude product was suspended in CH<sub>2</sub>Cl<sub>2</sub> (30 mL) and washed with a 1N aqueous solution of HCl (2 × 15 mL). The aqueous layer was extracted with CH<sub>2</sub>Cl<sub>2</sub> (3 × 10 mL). The collected organic layers were washed with H<sub>2</sub>O, dried over Na<sub>2</sub>SO<sub>4</sub> and evaporated. The crude product was triturated with methanol, filtered and the solid was washed with cold methanol to give the derivative **18** as a white solid (0.39 g, 70 % yield): mp >250 °C dec; <sup>1</sup>H NMR (600 MHz, TCDE, 353 K): δ 6.96 (s, ArH, 2H), 6.88 (s, ArH, 2H), 6.64 (broad, ArH, 1H), 6.48 (broad, ArH, 1H), 6.43 (s, ArH, 2H), 4.64 – 4.62 (overlapped, OCH<sub>2</sub> + ArCH<sub>2</sub>Ar, 4H), 4.54 (d, *J* = 12.6 Hz, ArCH<sub>2</sub>Ar, 2H), 4.37 (s, OCH<sub>2</sub>CO, 2H), 4.29 (s, OCH<sub>2</sub>CO, 2H), 4.12 (q, *J* = 7.2 Hz, OCH<sub>2</sub>CH<sub>3</sub>, 4H), 4.00 (q, *J* = 7.2 Hz, OCH<sub>2</sub>CH<sub>3</sub>, 2H), 3.65 (s, OCH<sub>3</sub>, 3H), 3.05 (d, *J* = 12.6 Hz, ArCH<sub>2</sub>Ar, 4H), 1.18 – 1.16 (overlapped, C(CH<sub>3</sub>)<sub>3</sub>, + OCH<sub>2</sub>CH<sub>3</sub>, 24H), 1.09 (t, *J* = 6.6 Hz, OCH<sub>2</sub>CH<sub>3</sub>, 3H), 0.81 (s, C(CH<sub>3</sub>)<sub>3</sub>, 18H). <sup>13</sup>C NMR (150 MHz, TCDE, 353 K): δ 171.0, 169.7, 156.2, 156.1, 153.4, 145.5, 145.2, 135.1, 133.7,

132.5, 132.1, 132.0, 126.0, 125.7, 125.5, 125.3, 74.5, 72.3, 71.8, 60.7, 60.2, 51.5, 34.2, 34.1, 33.8, 32.4, 31.8, 31.6, 31.5, 14.4, 14.3, 14.3. (ESI+)  $m/z$   $[M+Na]^+$ : 943.5 Anal. Calcd for  $C_{57}H_{76}O_{10}$ : C, 74.32; H, 8.32. Found: C, 74.30; H, 8.34.

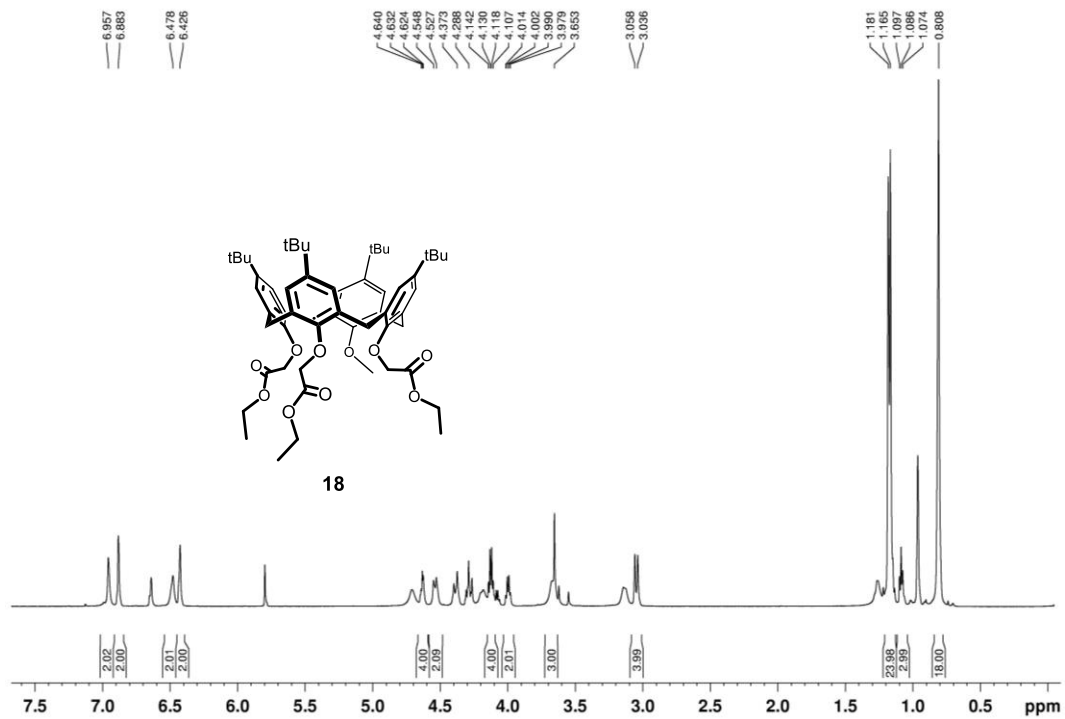


**Figure 67.**  $^1\text{H}$  NMR spectrum of derivative **18** (600 MHz, TCDE, 353 K).

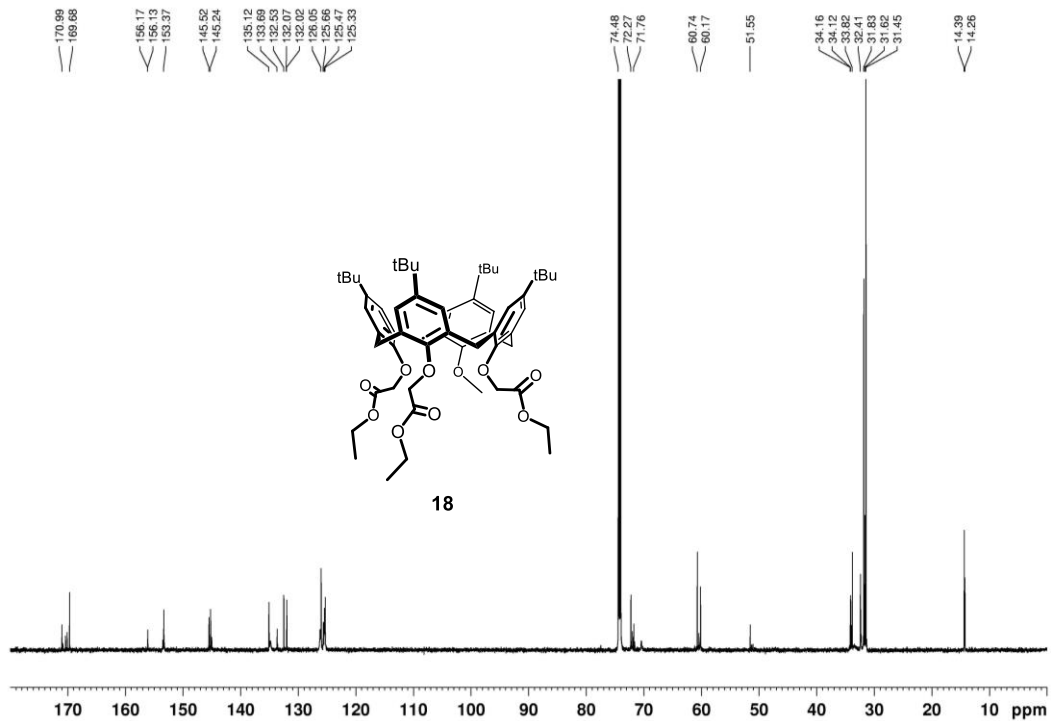


**Figure 68.**  $^{13}\text{C}$  NMR spectrum of derivative **18** (150 MHz, TCDE, 353 K).

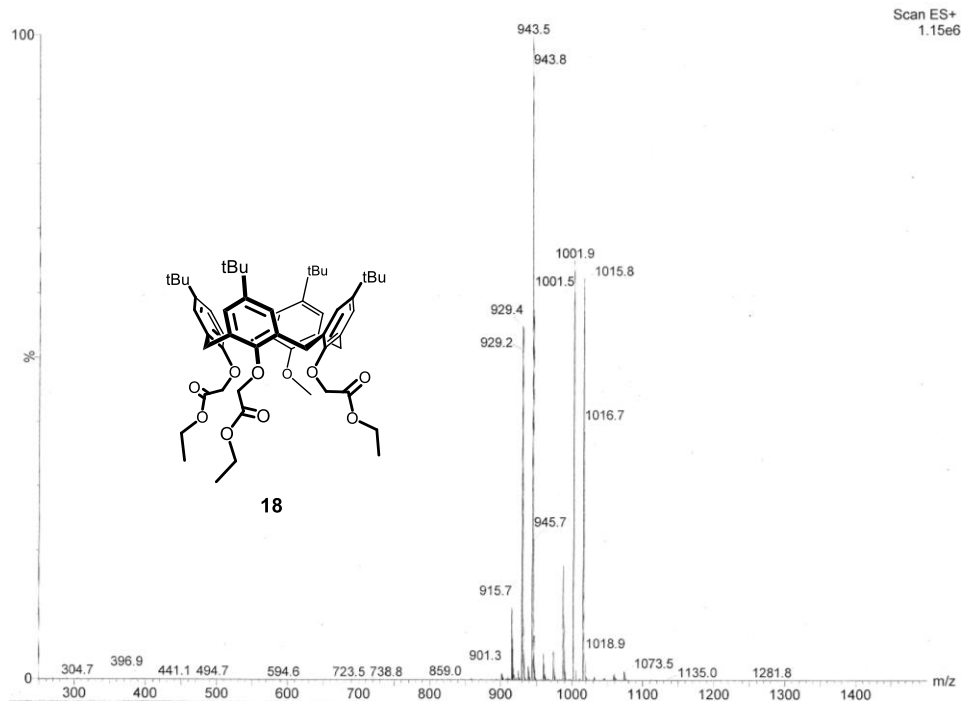


**Figure 69.** ESI (+) MS spectrum of derivative **18**.

### 6.2.7. Synthesis of Derivative 19.

A suspension of NaOH (0.57 g, 14 mmol) in EtOH (4 mL) and H<sub>2</sub>O (3 mL) was added to a solution of **18** (0.44 g, 0.47 mmol) in EtOH (14 mL). The reaction mixture was refluxed for 14 h. Then the solvent was evaporated under reduced pressure and the crude product was triturated with a 1N aqueous solution of HCl, filtered and the solid washed with cold H<sub>2</sub>O and dried in vacuo to give the derivative **19** as a white solid (0.38 g, 96 %): mp 248 –250 °C; <sup>1</sup>H NMR (400 MHz, CDCl<sub>3</sub>, 298 K): δ 9.06 (broad, COOH, 3H), 7.16 (overlapped, ArH, 4H), 6.61 (overlapped, ArH, 4H), 4.86 – 4.75 (overlapped, ArCH<sub>2</sub>Ar + OCH<sub>2</sub>COOH, 6H), 4.56 (broad s, OCH<sub>2</sub>COOH, 2H), 4.28 (d, *J* = 12.8 Hz, ArCH<sub>2</sub>Ar, 2H), 3.79 (s, OCH<sub>3</sub>, 3H), 3.28 – 3.21 (overlapped, ArCH<sub>2</sub>Ar, 4H), 1.32 (s, C(CH<sub>3</sub>)<sub>3</sub>, 18H), 0.85 (s, C(CH<sub>3</sub>)<sub>3</sub>, 18H). <sup>13</sup>C NMR (100 MHz, CDCl<sub>3</sub>, 298 K): δ 173.4, 171.0, 151.0, 149.7, 147.0, 146.3, 145.8, 134.5, 134.1, 132.9, 131.9, 131.7, 125.9, 125.8, 125.4, 125.2, 72.0, 71.7, 63.3, 34.0, 33.6, 31.5, 31.3, 31.2, 30.9, 30.9, 30.5. HRMS (ESI+) *m/z* [M + K]<sup>+</sup> calcd for C<sub>51</sub>H<sub>64</sub>NaO<sub>10</sub>, 859.3818; found 859.4391.

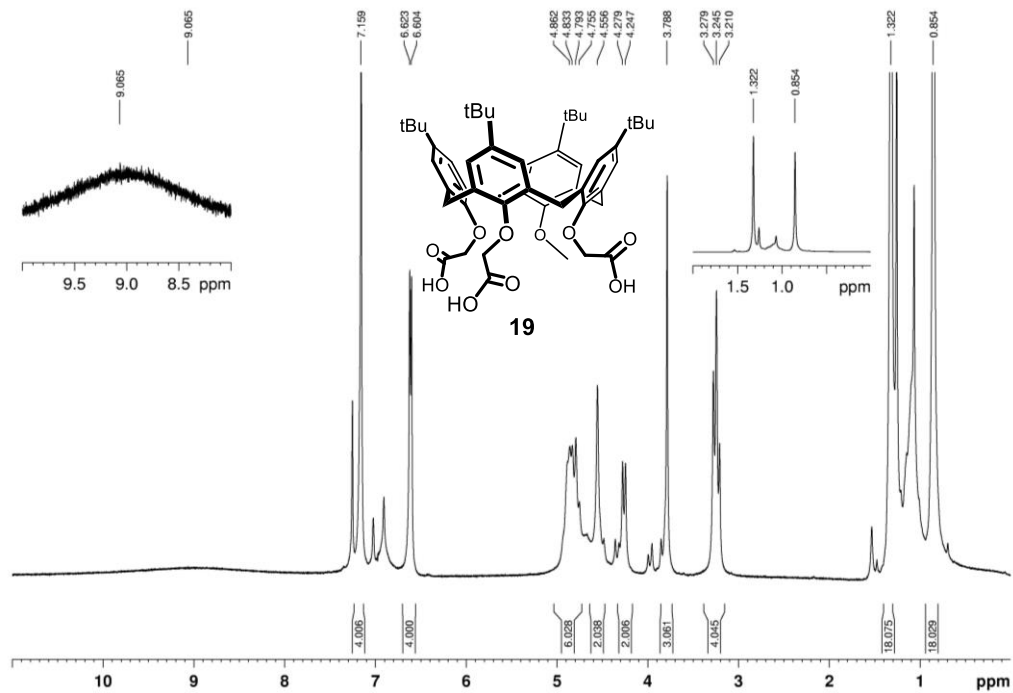


**Figure 70.**  $^1\text{H}$  NMR spectrum of derivative **19** (400 MHz,  $\text{CDCl}_3$ , 298 K).

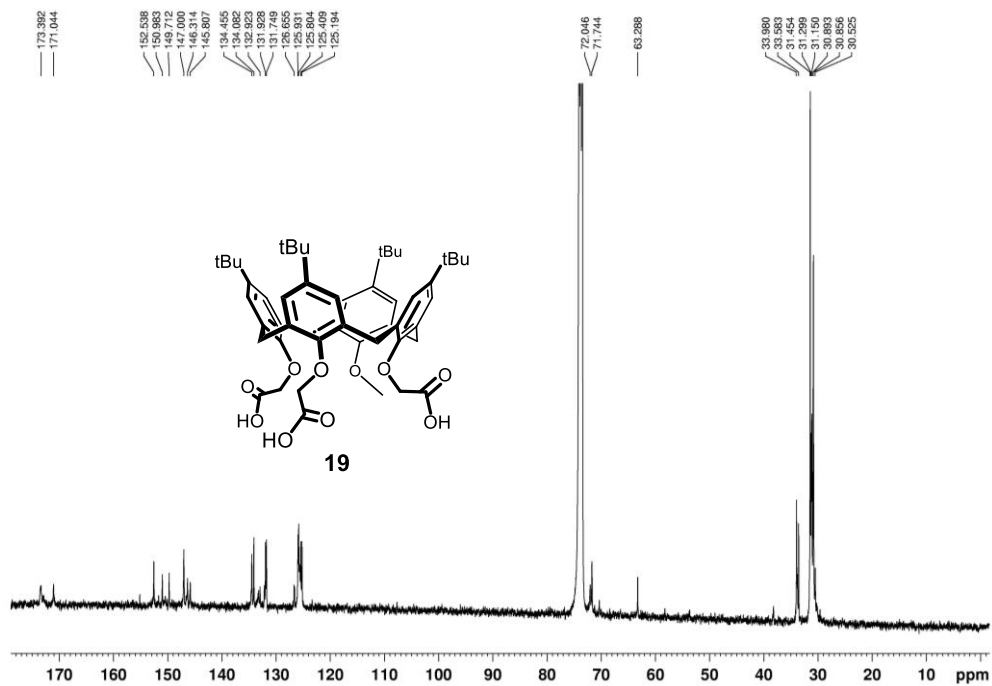


**Figure 71.**  $^{13}\text{C}$  NMR spectrum of derivative **19** (100 MHz,  $\text{CDCl}_3$ , 298 K).

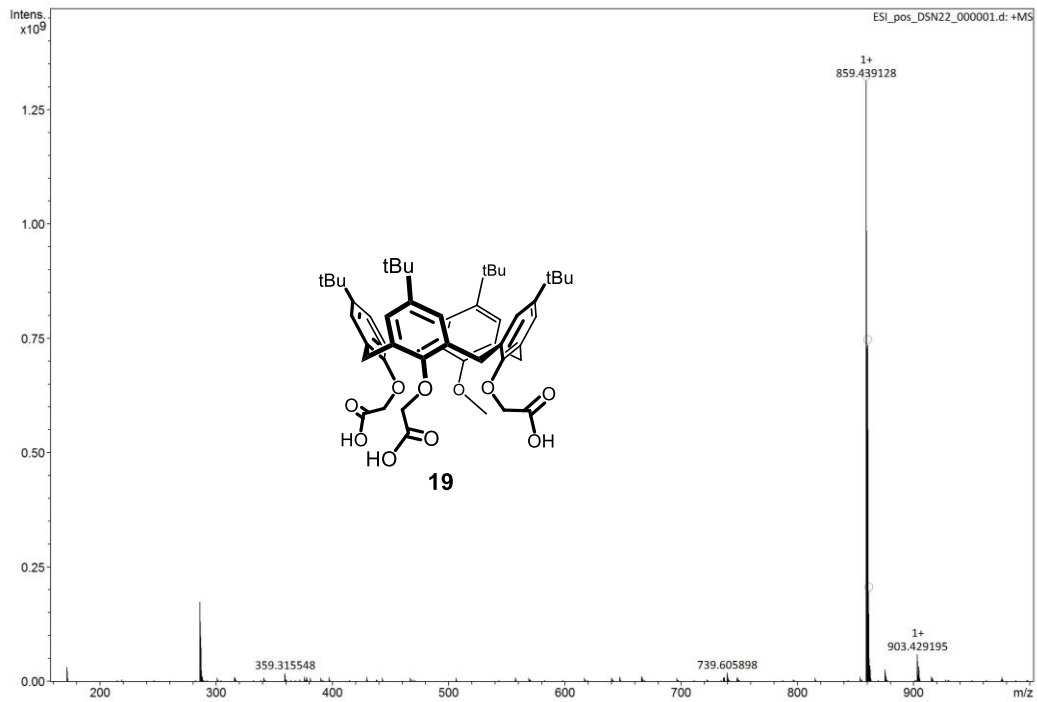


**Figure 72.** HR-ESI (+) MS spectrum of derivative **19**.

### 6.2.8. Synthesis of Derivative 35.

To a stirred solution of amine **34** (198 mg, 0.809 mmol) in CH<sub>2</sub>Cl<sub>2</sub> (3 mL) at 0 °C under nitrogen atmosphere was added dropwise a solution of isothiocyanate **33** (492 mg, 0.809 mmol, 1 eq) in CH<sub>2</sub>Cl<sub>2</sub> (3 mL). The resulting mixture was stirred at RT for 48 h, then the solvent was removed under reduced pressure and the crude product was purified by flash chromatography on silica gel with CH<sub>2</sub>Cl<sub>2</sub>/Et<sub>2</sub>O (1:0 to 99:1) eluent to afford compound **35**. Pale brown solid; 60% yield (431 mg); mp 146–150 °C;  $[\alpha]_D^{20} = -51.79 \pm 0.09$  (c = 1.00, CHCl<sub>3</sub>); <sup>1</sup>H NMR (600 MHz, CDCl<sub>3</sub>, 298 K): δ 7.85 (m, 2H, ArH), 7.74 (m, 2H, ArH), 6.94–6.92 (overlapped, 2H, ArH), 6.87 (d, *J* = 6.2 Hz, 1H, ArH), 6.81 (t, *J* = 7.4 Hz, 1H, ArH), 6.66–6.62 (overlapped, 3H, ArH, NH), 6.35 (t, *J* = 7.4 Hz, 1H, ArH), 6.27 (d, *J* = 7.2 Hz, 1H, ArH), 6.24 (d, *J* = 7.2 Hz, 1H, ArH), 6.03 (s, 1H, ArH), 5.77 (s, 1H, ArH), 5.35 (d, *J* = 9.0 Hz, 1H, NH), 4.97 (m, 1H, CH<sub>2</sub>CH<sub>2</sub>CHN), 4.45–4.39 (overlapped, 4H, ArCH<sub>2</sub>Ar), 3.95–3.80 (overlapped, 7H, OCH<sub>2</sub>CH<sub>2</sub>CH<sub>3</sub>, CH<sub>2</sub>CH<sub>2</sub>CHN), 3.70 (t, *J* = 7.0 Hz, 2H, OCH<sub>2</sub>CH<sub>2</sub>CH<sub>3</sub>), 3.17–3.05 (overlapped, 4H, ArCH<sub>2</sub>Ar), 2.54 (m, 1H, CH<sub>2</sub>CH<sub>2</sub>CHN), 2.25 (m, 1H, CH<sub>2</sub>CH<sub>2</sub>CHN), 1.95–1.84 (overlapped, 9H, OCH<sub>2</sub>CH<sub>2</sub>CH<sub>3</sub>, CH<sub>2</sub>CH<sub>2</sub>CHN), 1.78–1.74 (overlapped, 2H, CH<sub>2</sub>CH<sub>2</sub>CHN,

$CH_2CH_2CHN$ ), 1.49 (m, 1H,  $CH_2CH_2CHN$ ), 1.28 (m, 1H,  $CH_2CH_2CHN$ ), 1.10 (t,  $J = 7.4$  Hz, 3H,  $OCH_2CH_2CH_3$ ), 1.04 (overlapped, 4H,  $OCH_2CH_2CH_3$ ,  $CH_2CH_2CHN$ ) 0.93–0.90, (overlapped, 6H,  $OCH_2CH_2CH_3$ );  $^{13}C$  NMR (150 MHz,  $CDCl_3$ , 298 K):  $\delta$  179.9, 168.5, 157.4, 157.3, 156.8, 156.0, 155.4, 136.6, 136.5, 136.3, 135.6, 135.5, 135.3, 134.1, 134.0, 133.97, 129.1, 128.9, 128.7, 128.5, 128.2, 128.17, 128.0, 127.8, 125.2, 124.7, 123.4, 122.4, 122.2, 121.9, 121.4, 115.5, 76.75, 76.71, 76.69, 55.4, 54.2, 33.1, 31.1, 31.05, 31.0, 28.8, 25.5, 24.5, 23.6, 23.5, 23.2, 10.8, 10.7, 10.1; HRMS (ESI+) calcd for  $C_{55}H_{64}N_3O_6S$  [M + H] $^+$  894.4510, found 894.4533.

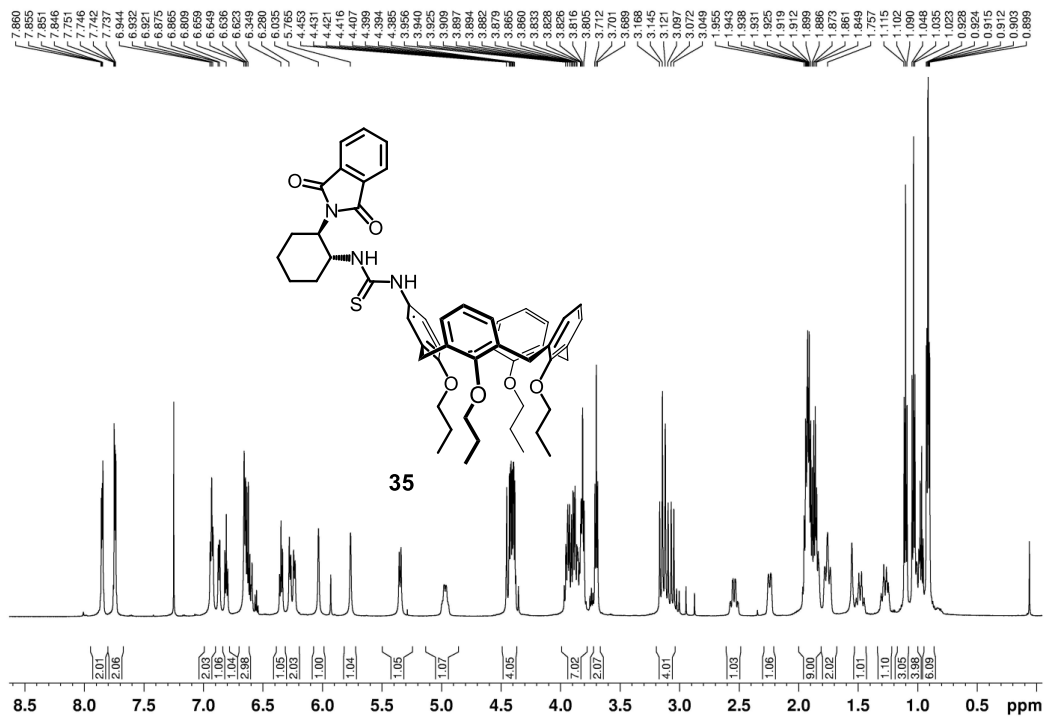


**Figure 73.**  $^1\text{H}$  NMR spectrum of derivative **35** (600 MHz,  $\text{CDCl}_3$ , 298 K).

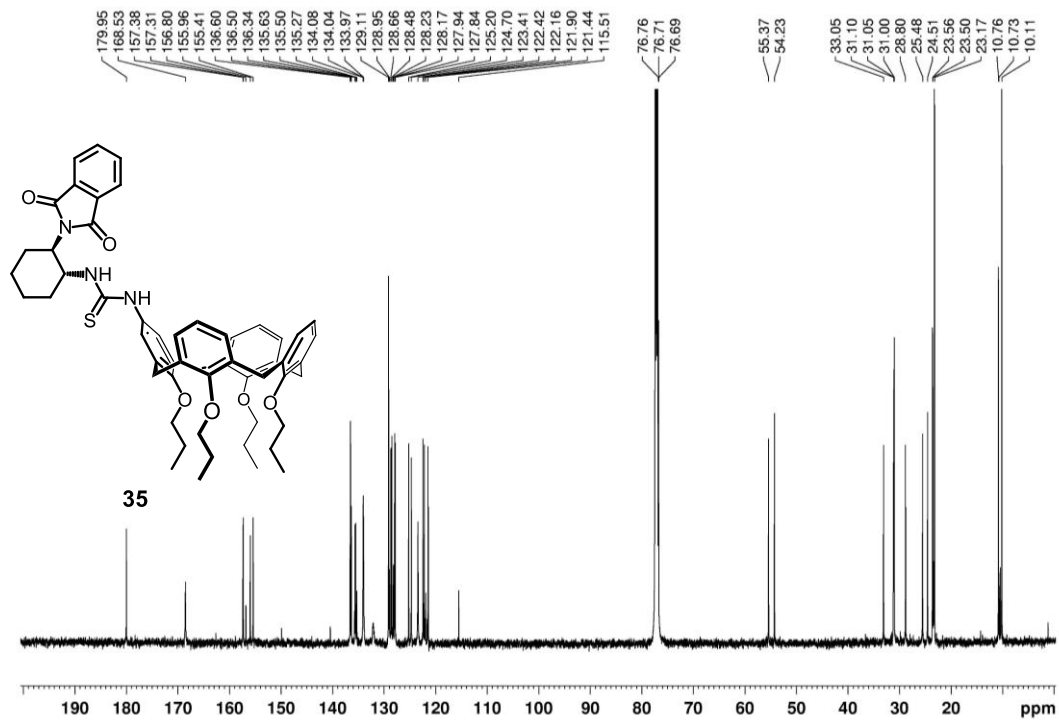


**Figure 74.** <sup>13</sup>C NMR spectrum of derivative **35** (150 MHz, CDCl<sub>3</sub>, 298 K).



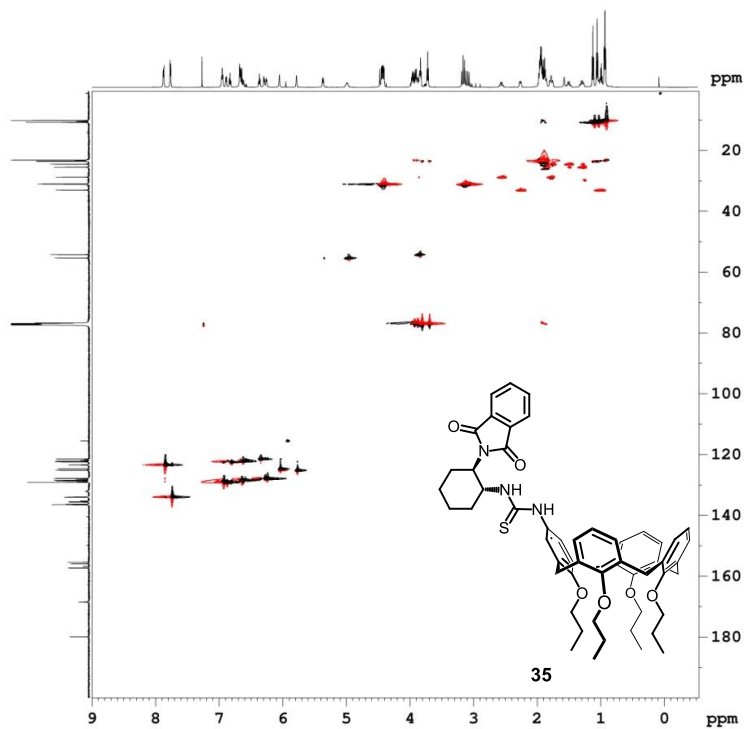


**Figure 76.** HSQC Spectrum (600 MHz,  $\text{CDCl}_3$ , 298 K) of **35**.

### 6.2.9. Synthesis of Derivative 16.

A solution of compound **35** (416 mg, 0.465 mmol), and  $\text{NH}_2\text{NH}_2 \cdot \text{H}_2\text{O}$  (0.6 mL) in ethanol (7 mL) was heated to reflux for 2 h, then the solvent was removed under reduced pressure. The crude product was suspended in  $\text{CH}_2\text{Cl}_2$  (10 mL) and washed with water (2x10 mL). The aqueous layer was extracted with  $\text{CH}_2\text{Cl}_2$  (10 mL). The collected organic layers were dried over  $\text{Na}_2\text{SO}_4$ , filtered and evaporated under reduced pressure. The product **16** was precipitated from  $\text{CH}_3\text{CN}$  and recovered by filtration. White solid; 52% yield (186 mg); mp 95–97 °C;  $[\alpha]_{\text{D}}^{20} = + 2.9 \pm 0.2$  ( $c = 1.00$ ,  $\text{CHCl}_3$ );  $^1\text{H NMR}$  (600 MHz,  $\text{CDCl}_3$ , 298 K):  $\delta$  7.07–6.68 (overlapped, 7H, ArH, NH), 6.45–6.34 (overlapped, 3H, ArH), 6.09 (broad, 2H, ArH), 5.60 (broad, 1H, NH), 4.44–4.42 (overlapped, 4H, ArCH<sub>2</sub>Ar) 4.09 (broad, 1H, CH<sub>2</sub>CH<sub>2</sub>CHN), 3.95–3.88 (overlapped, 4H, OCH<sub>2</sub>CH<sub>2</sub>CH<sub>3</sub>), 3.76–3.71 (overlapped, 4H, OCH<sub>2</sub>CH<sub>2</sub>CH<sub>3</sub>), 3.17–3.09 (overlapped, 4H, ArCH<sub>2</sub>Ar), 2.37 (broad, 1H, CH<sub>2</sub>CH<sub>2</sub>CHN), 2.04–1.99 (overlapped, 2H, CH<sub>2</sub>CH<sub>2</sub>CHN), 1.93–1.86 (overlapped, 8H, OCH<sub>2</sub>CH<sub>2</sub>CH<sub>3</sub>), 1.73–1.69 (overlapped, 2H, CH<sub>2</sub>CH<sub>2</sub>CHN), 1.34–1.19 (overlapped, 4H, CH<sub>2</sub>CH<sub>2</sub>CHN), 1.07–1.03 (overlapped, 6H, OCH<sub>2</sub>CH<sub>2</sub>CH<sub>3</sub>), 0.92–0.90, (overlapped, 6H, OCH<sub>2</sub>CH<sub>2</sub>CH<sub>3</sub>);  $^{13}\text{C NMR}$  (150 MHz,  $\text{CDCl}_3$ ,

298 K):  $\delta$  180.2, 157.4, 156.1, 155.0, 136.6, 136.4, 135.5, 134.2, 129.2, 128.5, 128.4, 127.9, 127.87, 124.1, 123.8, 122.4, 121.6, 76.72, 61.7, 55.9, 34.9, 32.1, 31.2, 31.1, 31.08, 29.8, 25.1, 25.0, 23.5, 23.2, 10.7, 10.68, 10.1; HRMS (ESI+) calcd for  $C_{47}H_{62}N_3O_4S$   $[M + H]^+$  764.4456, found 764.4462.

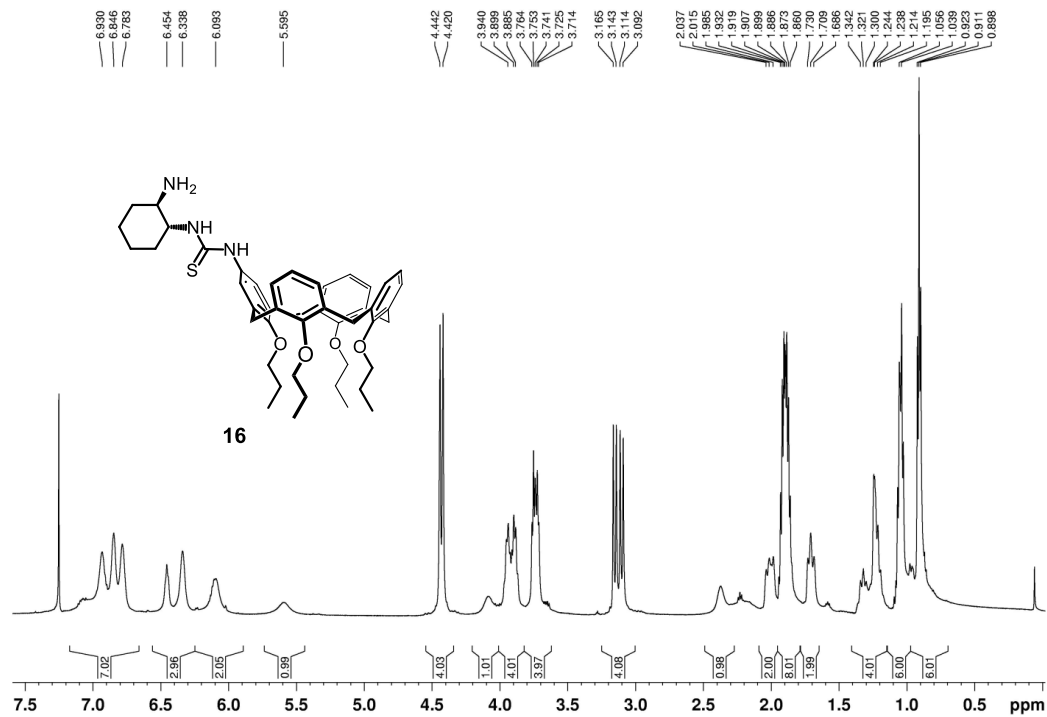


**Figure 77.**  $^1\text{H}$  NMR spectrum of derivative **16** (600 MHz,  $\text{CDCl}_3$ , 298 K).

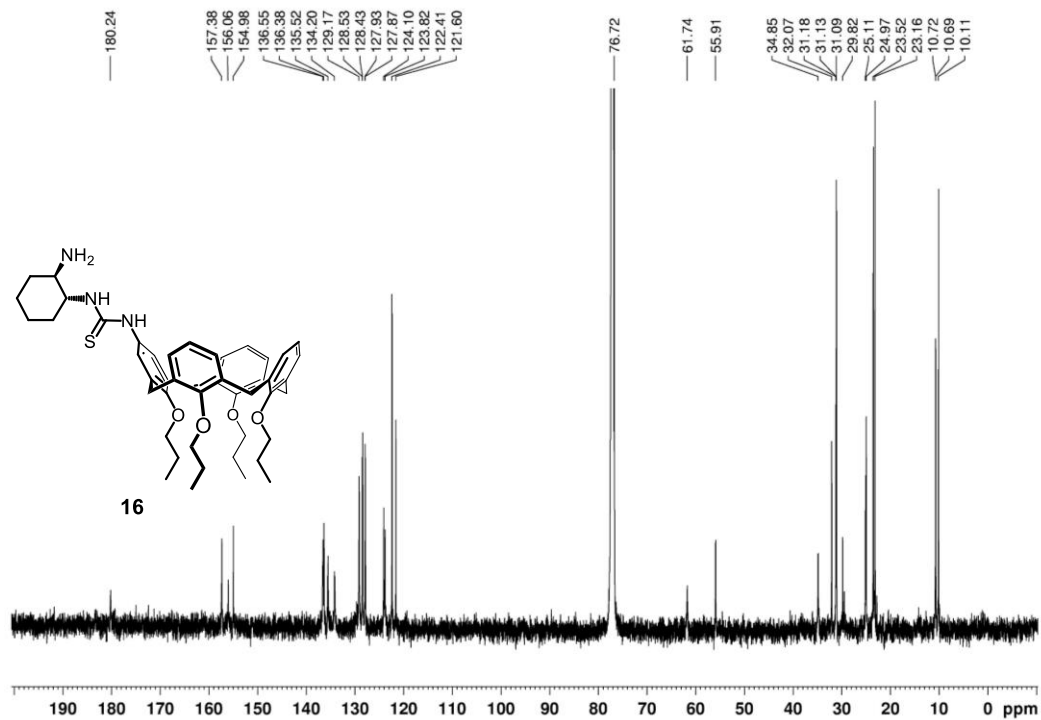


**Figure 78.**  $^{13}\text{C}$  NMR spectrum of derivative **16** (150 MHz,  $\text{CDCl}_3$ , 298 K).

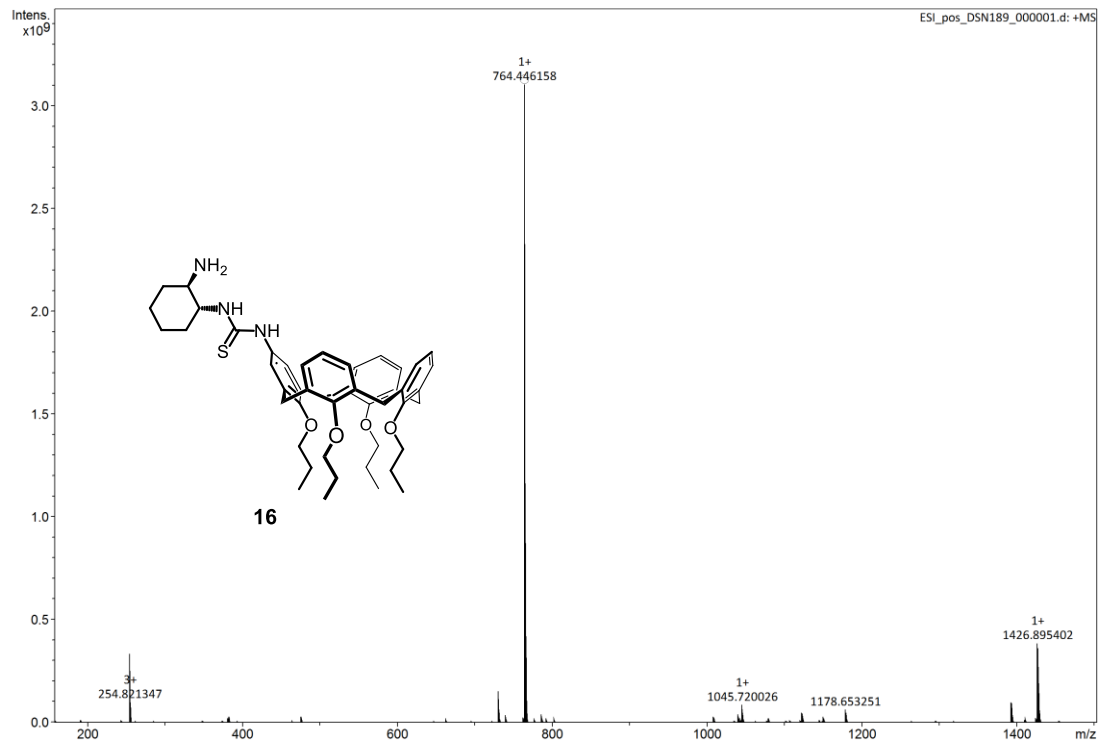


**Figure 79.** HR-ESI (+) MS spectrum of derivative **16**.

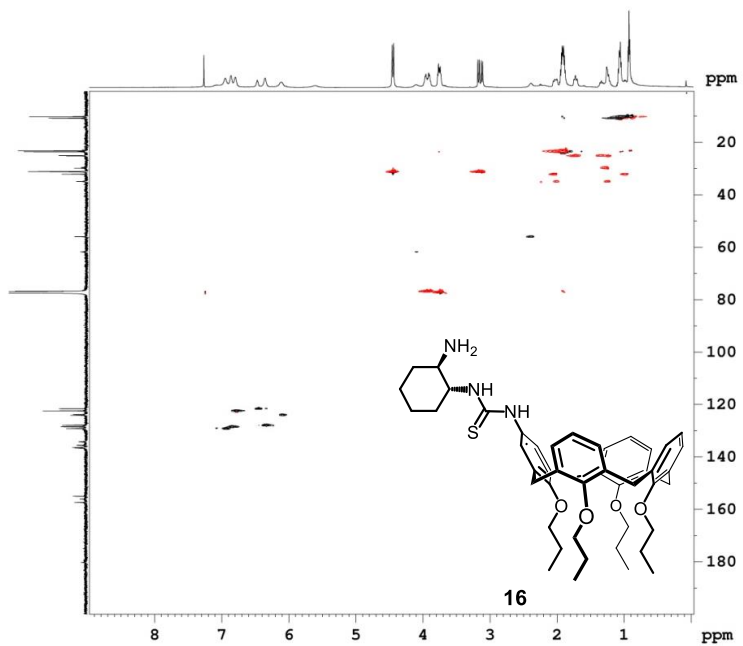


**Figure 80.** HSQC Spectrum (600 MHz, CDCl<sub>3</sub>, 298 K) of **16**.

### 6.2.10. Synthesis of Derivative 31a.

A solution of compound **38** (200 mg, 0.488 mmol), and  $\text{NH}_2\text{NH}_2 \cdot \text{H}_2\text{O}$  (0.63 mL) in ethanol (4 mL) was heated to reflux for 2 h, then the solvent was removed under reduced pressure. The crude product was suspended in  $\text{CH}_2\text{Cl}_2$  (10 mL) and washed with water (2x10 mL). The aqueous layer was extracted with  $\text{CH}_2\text{Cl}_2$  (10 mL). The collected organic layers were dried over  $\text{Na}_2\text{SO}_4$ , filtered and evaporated under reduced pressure. The product **31a** was precipitated from  $\text{CH}_3\text{CN}$  and recovered by filtration. White solid; 76% yield (103 mg); mp 144-145 °C;  $[\alpha]_{\text{D}}^{20} = + 34.9 \pm 0.7$  (c = 1.00,  $\text{CHCl}_3$ );  $^1\text{H NMR}$  (400 MHz,  $\text{CDCl}_3$ , 298 K):  $\delta$  8.04 (br, 1H, *NH*), 7.21–7.19 (overlapped, 2H, *ArH*), 6.93–6.91 (overlapped, 2H, *ArH*), 5.92 (broad, 1H, *NH*), 4.13 (broad, 1H,  $\text{CH}_2\text{CH}_2\text{CHN}$ ), 3.81 (s, 3H,  $\text{OCH}_3$ ), 2.42 (broad, 1H,  $\text{CH}_2\text{CH}_2\text{CHN}$ ), 2.12 (m, 1H,  $\text{CH}_2\text{CH}_2\text{CHN}$ ), 1.93 (m, 1H,  $\text{CH}_2\text{CH}_2\text{CHN}$ ), 1.72–1.70 (overlapped, 2H,  $\text{CH}_2\text{CH}_2\text{CHN}$ ), 1.35–1.21 (overlapped, 4H,  $\text{CH}_2\text{CH}_2\text{CHN}$ );  $^{13}\text{C NMR}$  (100 MHz,  $\text{CDCl}_3$ , 298 K):  $\delta$  181.5, 158.7, 127.4, 115.2, 62.0, 56.0, 55.7, 35.5, 32.2, 25.0, 25.0; HRMS (ESI+) calcd for  $\text{C}_{14}\text{H}_{22}\text{N}_3\text{OS}$   $[\text{M} + \text{H}]^+$  280.1478, found 280.1478.

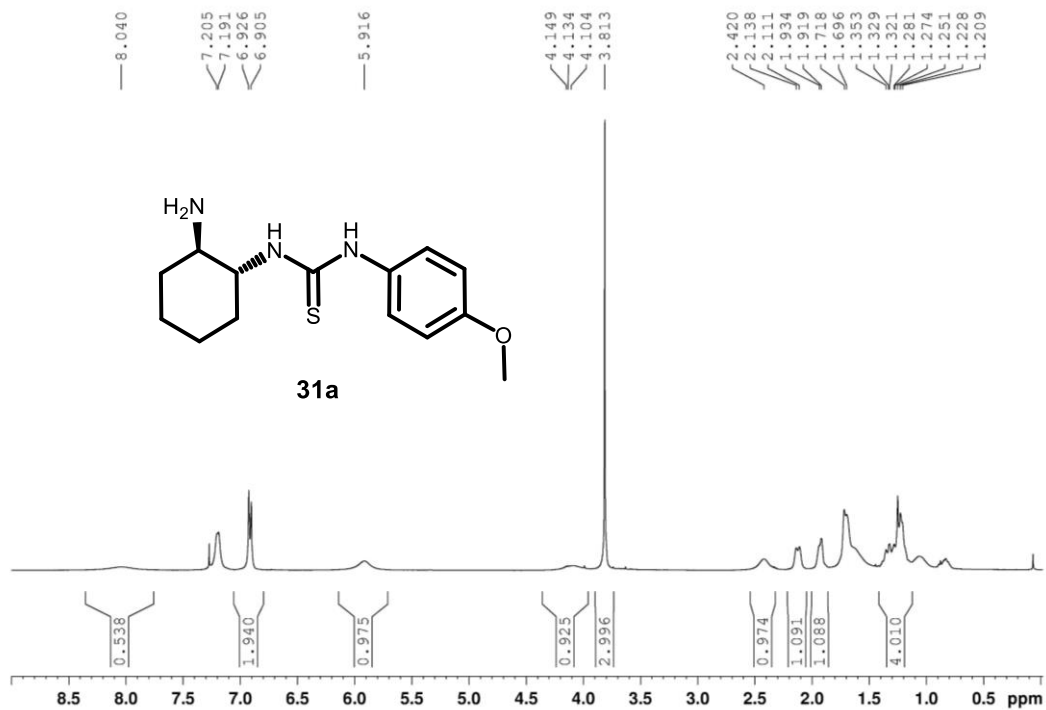


**Figure 81.** <sup>1</sup>H NMR spectrum of derivative **31a** (400 MHz, CDCl<sub>3</sub>, 298 K).

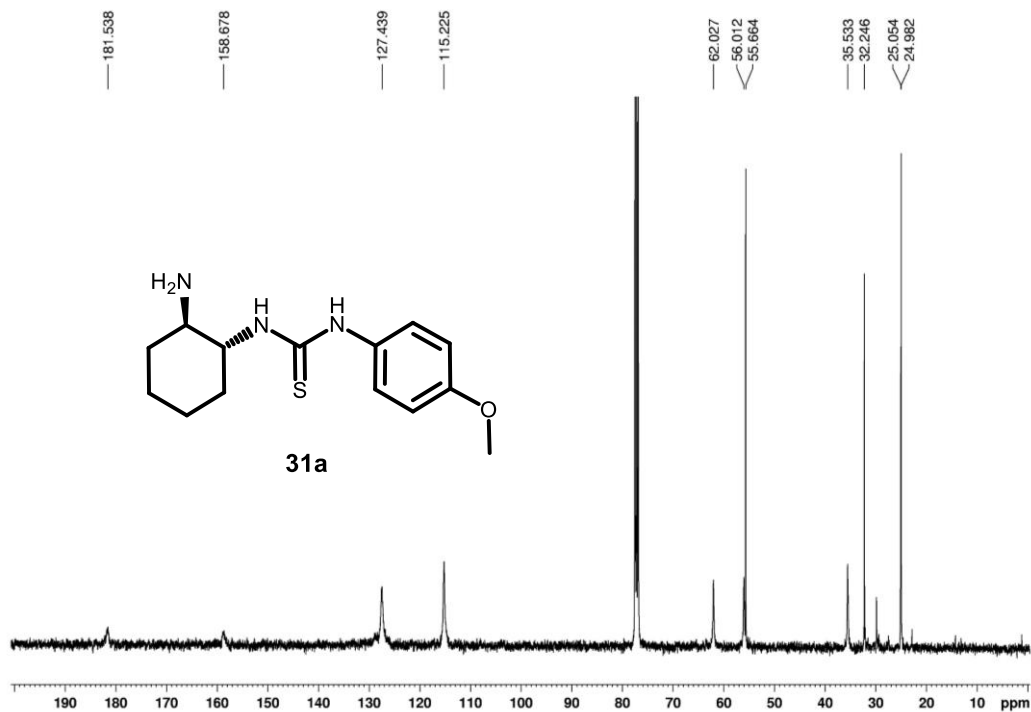


**Figure 82.**  $^{13}\text{C}$  NMR spectrum of derivative **31a** (100 MHz,  $\text{CDCl}_3$ , 298 K).

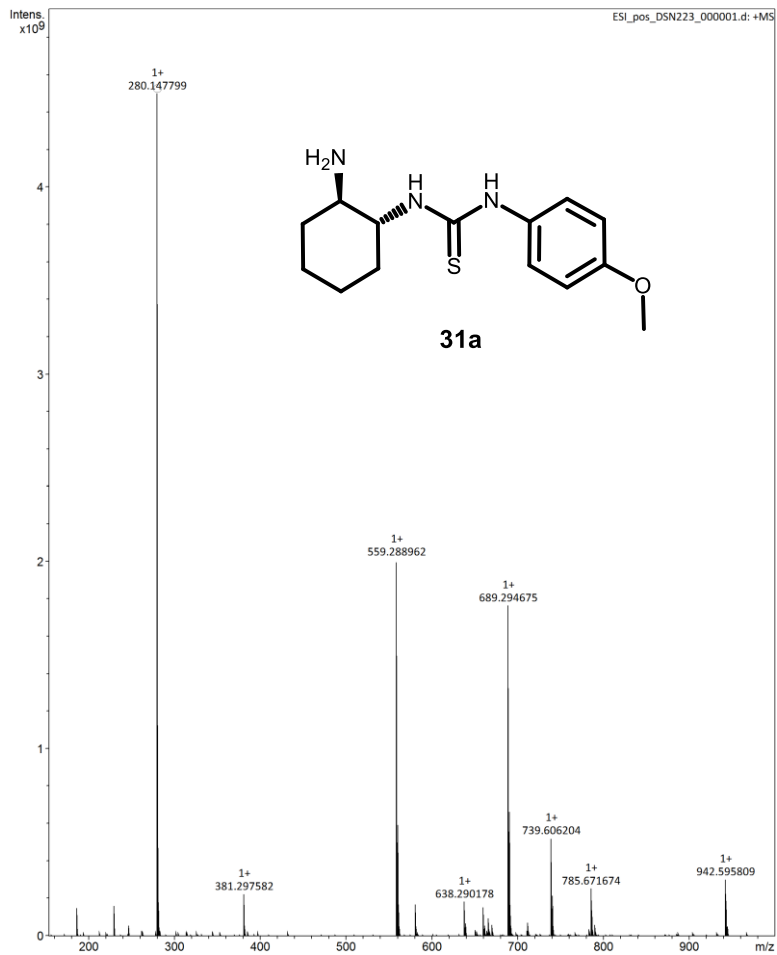


**Figure 83.** HR-ESI (+) MS spectrum of derivative **31a**.

### ***6.3. Preparation of Complexes and $K_a$ Determination***

#### ***6.3.1. General Procedure for the Preparation of $\text{Na}^+\text{C}X$ ( $X = 9, 12, 13$ and $15$ ) Complexes.***

Calixarene-amide derivative (1 mmol) and sodium TFPB salt (1 mmol) were dissolved in  $\text{CDCl}_3$  (0.5 mL). Each solution was sonicated at room temperature for 15 min and then transferred into an NMR tube for 1D and 2D NMR spectra acquisition. The  $K_a$  values were determined by integration of  $^1\text{H}$  NMR signals of free and complexed host.

### 6.3.2. Determination of $\text{Na}^+\text{C}X$ ( $X = 9$ and $15$ ) $K_a$ Value

$$K_a = \frac{[\text{HOST-GUEST}]}{[\text{HOST}][\text{GUEST}]} = \frac{[\text{HG}]}{[\text{H}][\text{G}]}$$

$$[\text{H}] = [\text{G}] \implies K_a = \frac{[\text{HG}]}{[\text{H}]^2}$$

$$[\text{HG}] = \%_{\text{HG}}[\text{H}]_{\text{in}} = \frac{\text{AREA}_{\text{HG}}}{\text{AREA}_{\text{H}} + \text{AREA}_{\text{HG}}} [\text{H}]_{\text{in}} = \frac{A_{\text{HG}}}{A_{\text{H}} + A_{\text{HG}}} [\text{H}]_{\text{in}}$$

$$[\text{H}] = \%_{\text{H}}[\text{H}]_{\text{in}} = \frac{\text{AREA}_{\text{G}}}{\text{AREA}_{\text{H}} + \text{AREA}_{\text{HG}}} [\text{H}]_{\text{in}} = \frac{A_{\text{H}}}{A_{\text{H}} + A_{\text{HG}}} [\text{H}]_{\text{in}}$$

$$\implies K_a = \frac{\frac{A_{\text{HG}}}{A_{\text{H}} + A_{\text{HG}}} [\text{H}]_{\text{in}}}{\left( \frac{A_{\text{H}}}{A_{\text{H}} + A_{\text{HG}}} [\text{H}]_{\text{in}} \right)^2}$$

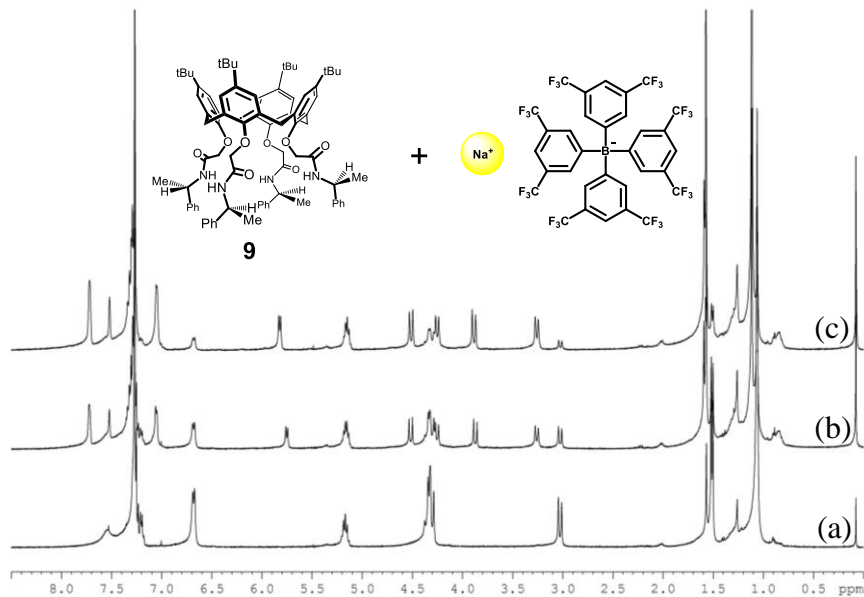
### 6.3.3. Determination of $\text{Na}^+\text{C}12$ $K_a$ Value

$K_a$  value of the  $\text{Na}^+\text{C}12$  complex was determined via  $^1\text{H}$  NMR competition experiments, performed by analysis of a 1:1:1 mixture of  $\text{NaTFPB}$  (1 mmol), **12** (1 mmol) and **15** (1 mmol) in  $\text{CDCl}_3$  (0.5 mL).

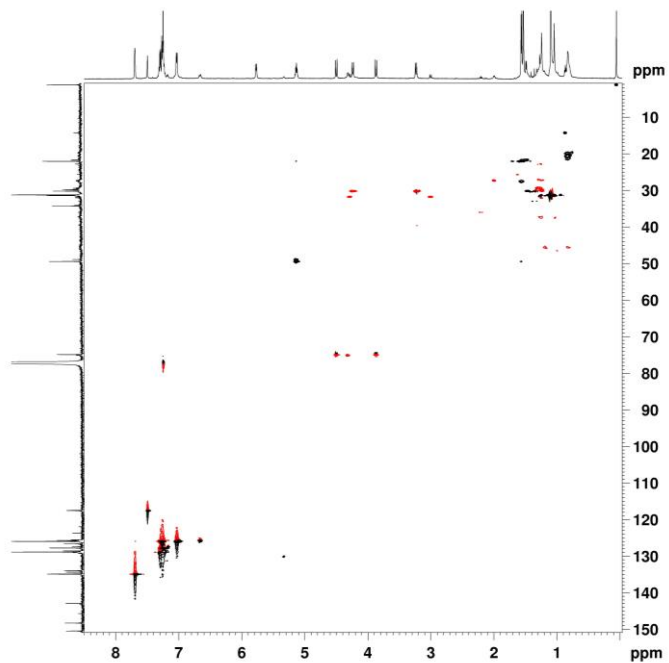
$$K_a(\mathbf{12}) = \frac{[\mathbf{12Na}^+]}{[\mathbf{12}][\text{Na}^+]} \quad \Rightarrow \quad K_{rel} = \frac{K_a(\mathbf{12})}{K_a(\mathbf{15})} = \frac{[\mathbf{12Na}^+][\mathbf{15}][\text{Na}^+]}{[\mathbf{12}][\text{Na}^+][\mathbf{15Na}^+]}$$

$$K_a(\mathbf{15}) = \frac{[\mathbf{15Na}^+]}{[\mathbf{15}][\text{Na}^+]}$$

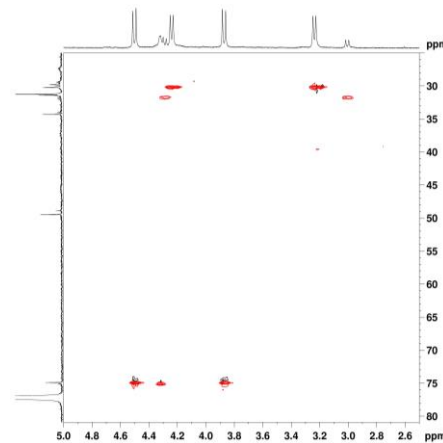
$$\begin{aligned} [\mathbf{12Na}^+] &= [\mathbf{15}] \\ [\mathbf{15Na}^+] &= [\mathbf{12}] \end{aligned} \quad \Rightarrow \quad K_{rel} = \frac{[\mathbf{12Na}^+]^2}{[\mathbf{15Na}^+]^2} = \frac{\text{AREA}(\mathbf{12Na}^+)}{\text{AREA}(\mathbf{15Na}^+)}$$



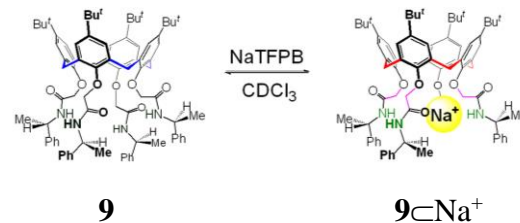
**Figure 84.**  $^1\text{H}$  NMR spectra (400 MHz,  $\text{CDCl}_3$ , 298 K) of: (a) derivative **9**; (b) an equimolar solution (1.9 mM) of **9** and **NaTFPB** after mixing; (c) an equimolar solution (1.9 mM) of **9** and **NaTFPB** after 3 days at 298 K.

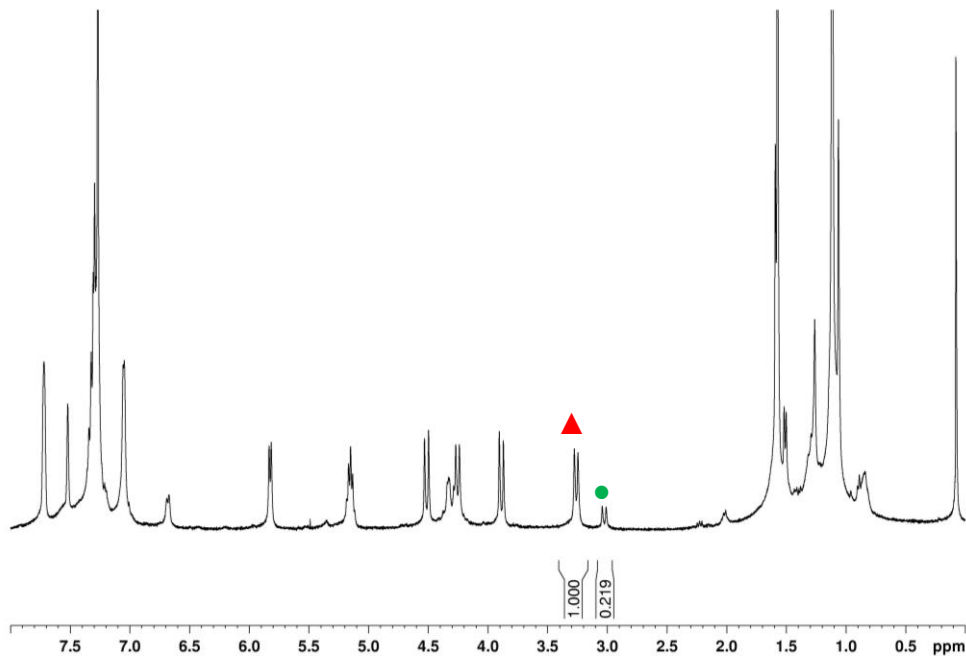


**Figure 85.** HSQC Spectrum (600 MHz,  $\text{CDCl}_3$ , 298 K) of an equimolar solution (1.9 mM) of **9** and **NaTFPB** after equilibration for 3 d at 298 K.

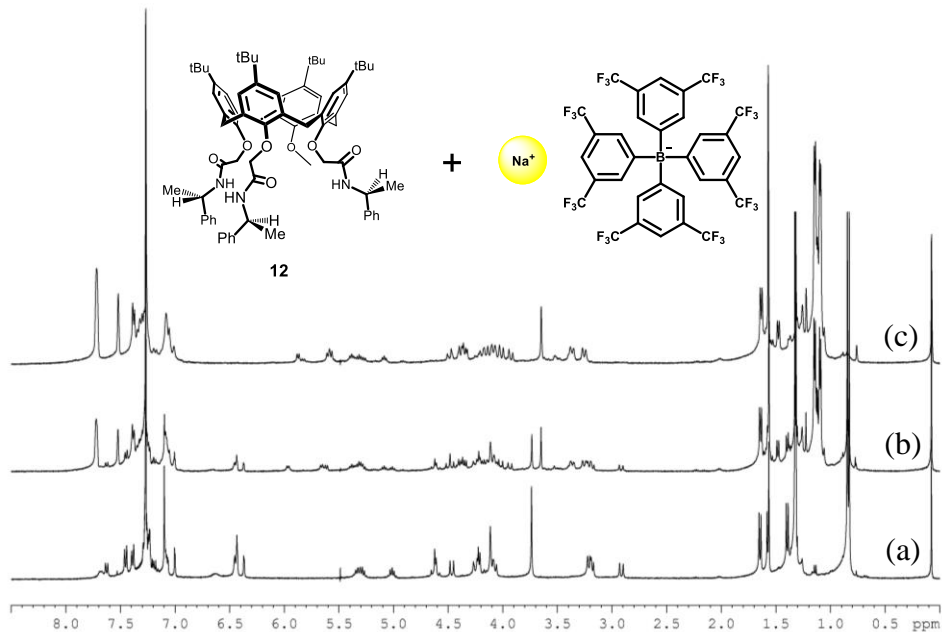


**Figure 86.** Section of the HSQC spectrum (600 MHz,  $\text{CDCl}_3$ , 298 K) in figure 82.

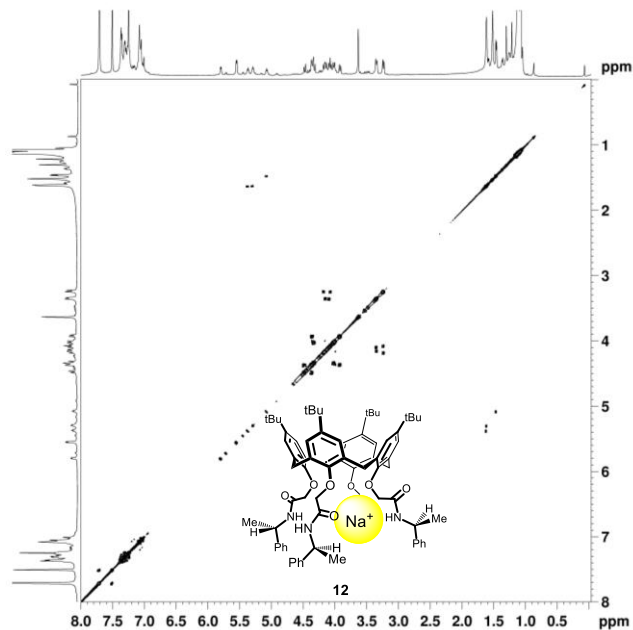




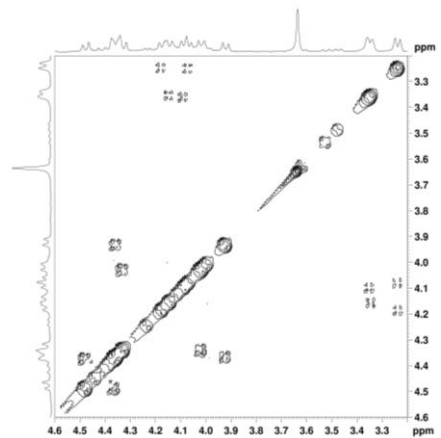
**Figure 87.** <sup>1</sup>H NMR spectrum (400 MHz, CDCl<sub>3</sub>, 298 K) of a 1:1 mixture of **9** ( $1.9 \times 10^{-3}$  M) and NaTFPB ( $1.9 \times 10^{-3}$  M). The association constant  $K_a$  value was calculated by integration of complexed ArCH<sub>2</sub>Ar (▲) and free ArCH<sub>2</sub>Ar (●) signals of host **9**.  $K_a = (1/1.22 \times 1.9 \times 10^{-3}) / (0.22/1.22 \times 1.9 \times 10^{-3})^2 = 1.22 \pm 0.04 \times 10^4$  M



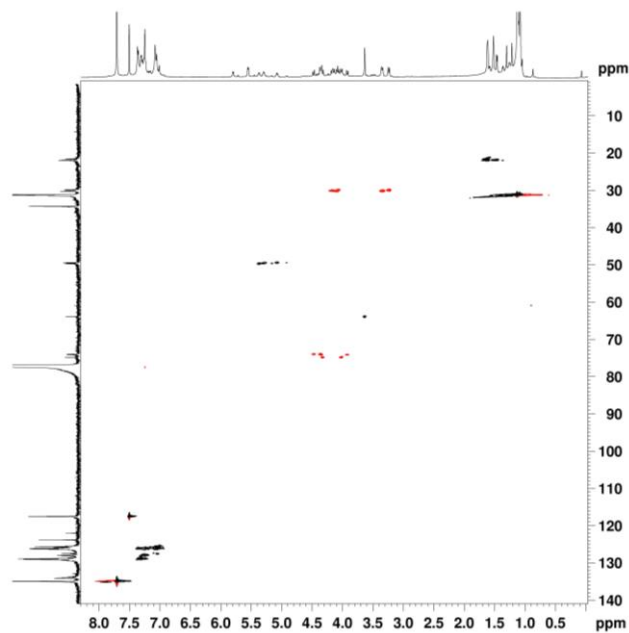
**Figure 88.**  $^1\text{H}$  NMR spectra (400 MHz,  $\text{CDCl}_3$ , 298 K) of: (a) derivative **12**; (b) an equimolar solution (1.9 mM) of **12** and **NaTFPB** after mixing; (c) an equimolar solution (1.9 mM) of **12** and **NaTFPB** after 3 days at 298 K.



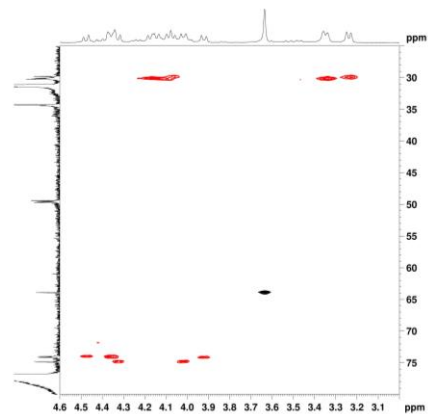
**Figure 89.** 2D COSY-45 spectrum (600 MHz,  $\text{CDCl}_3$ , 298 K) of an equimolar solution (1.9 mM) of **12** and **NaTFPB** after equilibration for 3 d (72 h) at 298 K.



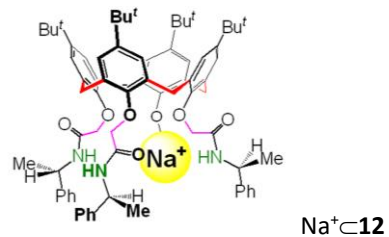
**Figure 90.** Section of the 2D COSY-45 spectrum in Figure 86.

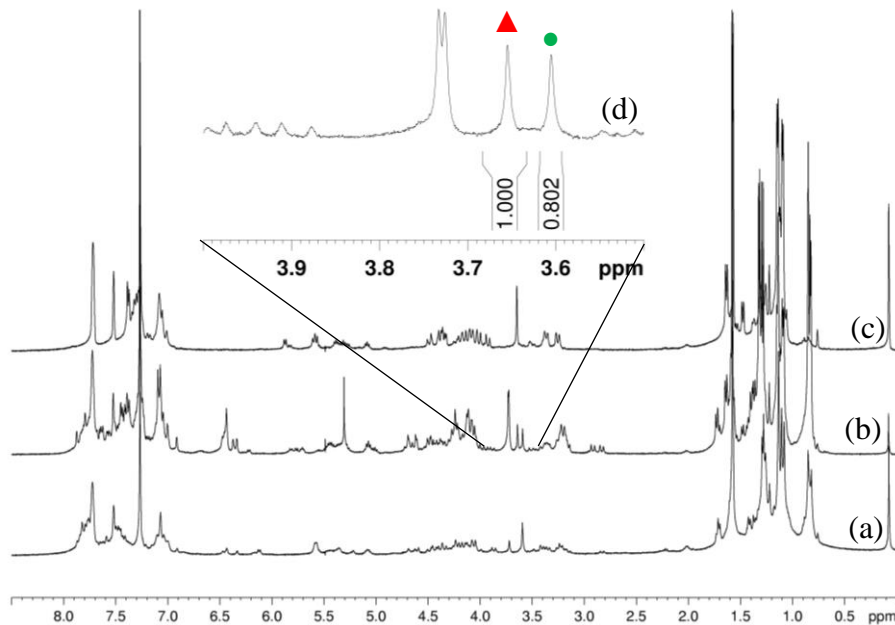


**Figure 91.** HSQC Spectrum (600 MHz,  $\text{CDCl}_3$ , 298 K) of an equimolar solution (1.9 mM) of **12** and **NaTFPB** after equilibration for 3 d (72 h) at 298 K.

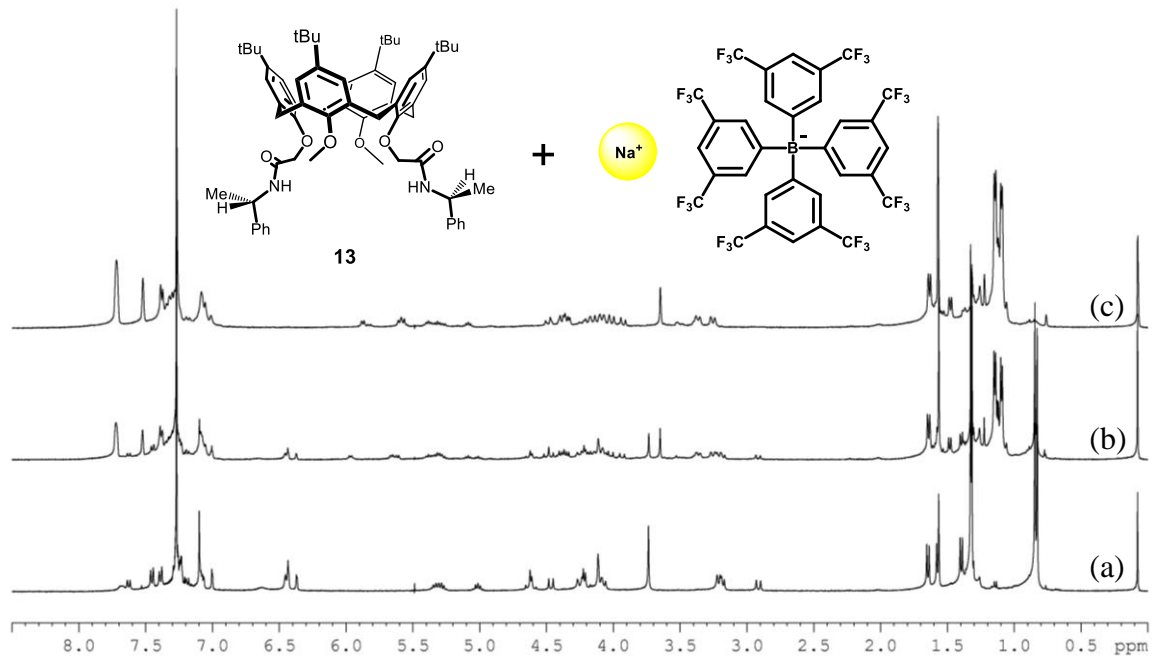


**Figure 92.** Section of the HSQC spectrum in Figure 88.

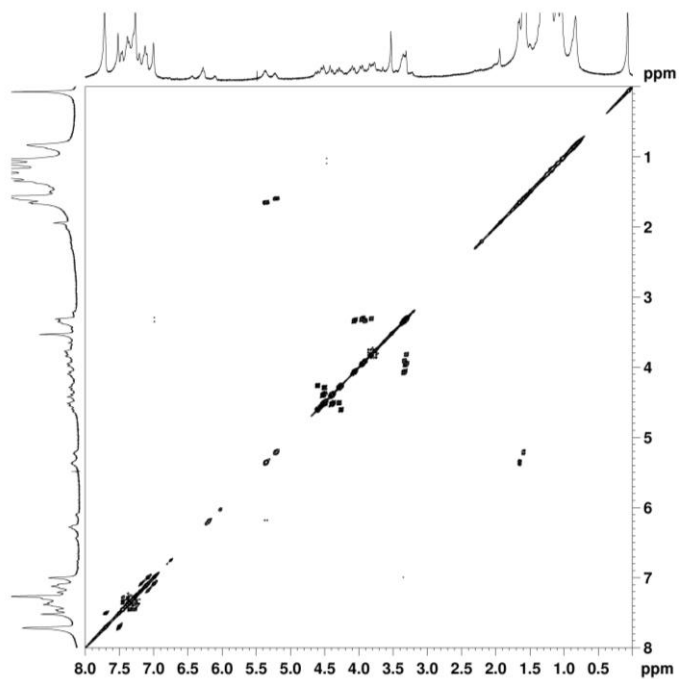




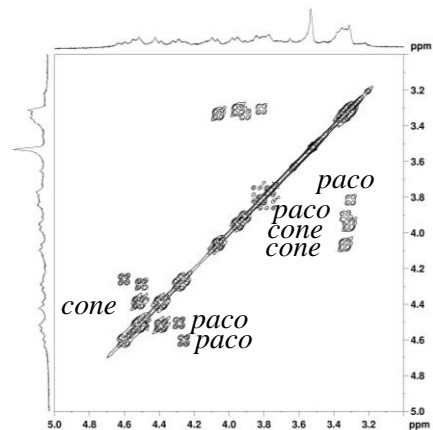
**Figure 93.**  $^1\text{H}$  NMR spectra (400 MHz,  $\text{CDCl}_3$ , 298 K) of: (a) an equimolar solution (1.9 mM) of **15** and **NaTFPB** after equilibration for 3 days at 298 K; (b) an equimolar solution (1.9 mM) of **NaTFPB**, **15** and **12** after equilibration for 3 days; (c) an equimolar solution (1.9 mM) of **12** and **NaTFPB** after equilibration for 3 days at 298 K; (d) section of the  $^1\text{H}$  NMR spectrum of an equimolar solution (1.9 mM) of **NaTFPB**, **15** and **12** after equilibration for 3 days. The association constant  $K_a$  value was calculated by integration of complexed  $\text{OCH}_3$  signals of hosts **12** ( $\blacktriangle$ ) and **15** ( $\bullet$ ).  $K_a = [(1/1.80 \times 1.9 \times 10^{-3})^2 / (0.79/1.80 \times 1.9 \times 10^{-3})^2] \times 8.59 \times 10^3 \text{ M}^{-1} = 1.30 \pm 0.06 \times 10^4 \text{ M}^{-1}$



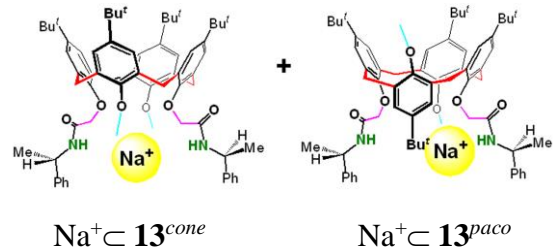
**Figure 94.**  $^1\text{H}$  NMR spectra (400 MHz,  $\text{CDCl}_3$ , 298 K) of: (a) derivative **13**; (b) an equimolar solution (1.9 mM) of **13** and  $\text{NaTFPB}$  after mixing; (c) an equimolar solution (1.9 mM) of **13** and  $\text{NaTFPB}$  after 3 days at 298 K

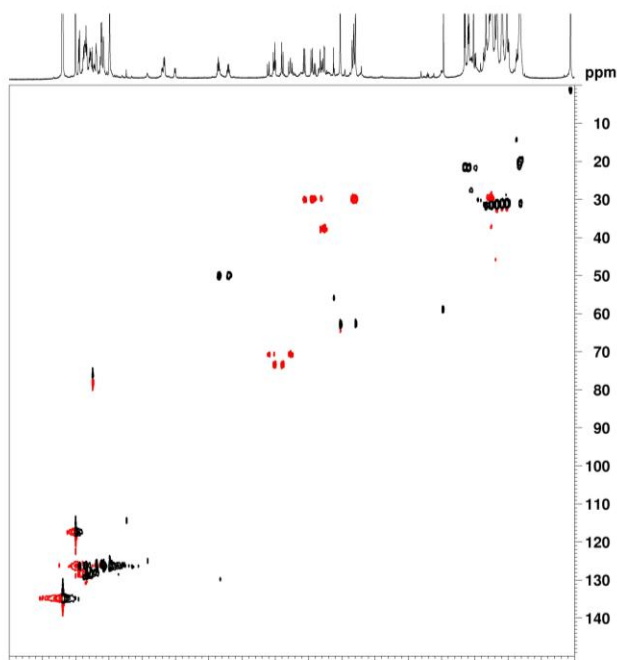


**Figure 95.** 2D COSY-45 spectrum (400 MHz,  $\text{CDCl}_3$ , 298 K) of the  $\text{Na}^+ \subset \mathbf{13}^{\text{cone}}$  and  $\text{Na}^+ \subset \mathbf{13}^{\text{paco}}$  complexes.

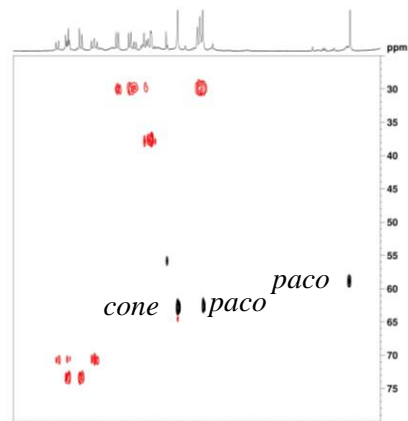


**Figure 96.** Section of the 2D COSY-45 spectrum in figure 92.

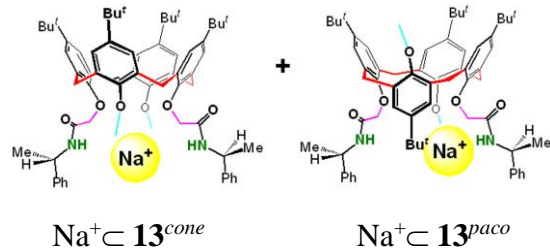




**Figure 97.** HSQC Spectrum (600 MHz,  $\text{CDCl}_3$ , 298 K) of the  $\text{Na}^+ \subset \mathbf{13}^{\text{cone}}$  and  $\text{Na}^+ \subset \mathbf{13}^{\text{paco}}$  complexes.



**Figure 98.** Section of the HSQC spectrum in figure 94.



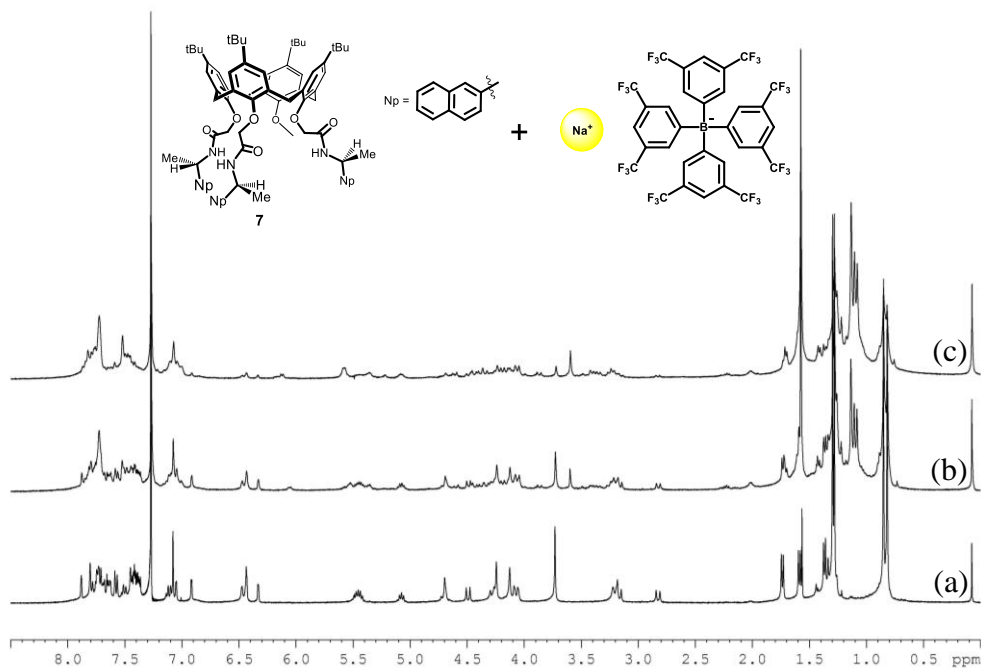


**Figure 99.**  $^1\text{H}$  NMR spectra (400 MHz,  $\text{CDCl}_3$ , 298 K) of: (a) derivative **15**; (b) an equimolar solution (1.9 mM) of **15** and **NaTFPB** after mixing; (c) an equimolar solution (1.9 mM) of **15** and **NaTFPB** after 3 days at 298 K.

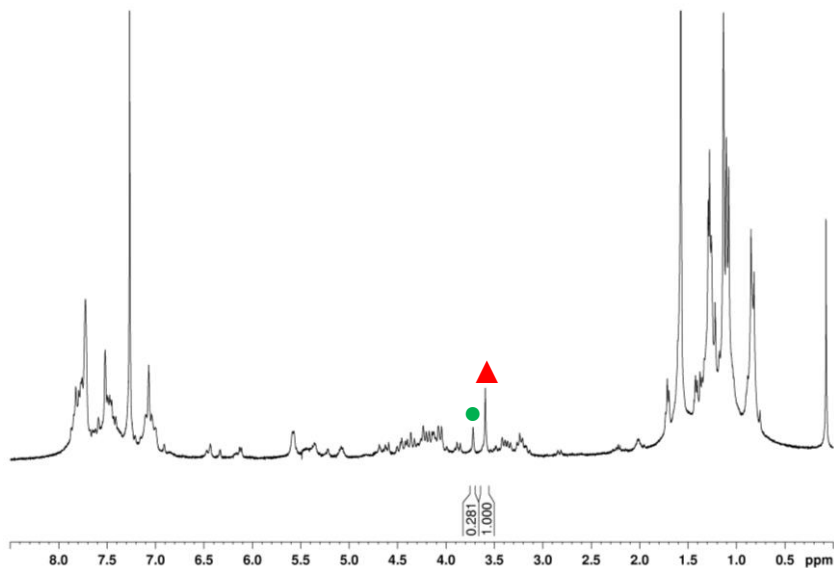


**Figure 100.** <sup>1</sup>H NMR spectrum (400 MHz, CDCl<sub>3</sub>, 298 K) of a 1:1 mixture of **15** ( $1.9 \times 10^{-3}$  M) and **NaTFPB** ( $1.9 \times 10^{-3}$  M). The association constant  $K_a$  value was calculated by integration of complexed OCH<sub>3</sub> (▲) and free OCH<sub>3</sub> (●) signals of host **15**.  $K_a = (1/1.28 \times 1.9 \times 10^{-3}) / (0.28/1.28 \times 1.9 \times 10^{-3})^2 = 9.16 \pm 0.04 \times 10^3 \text{ M}^{-1}$

#### ***6.3.4. Synthesis of the complex $17(\text{Zr-O-}t\text{Bu})_2$***

A solution of  $\text{Zr}(\text{O}^i\text{Bu})_4$  (0.27 g, 0.71 mmol) in THF (3 mL) was added to a stirred solution of proligand **17H<sub>6</sub>** (0.50 g, 0.36 mmol) in THF (5 mL) at room temperature. The resulting yellow solution was stirred for 30 minutes after which the volatiles were removed in vacuum. The residue was washed with pentane (2x10 mL) to give **17**(Zr-O-*t*Bu)<sub>2</sub> as a pale-green solid (60% yield).

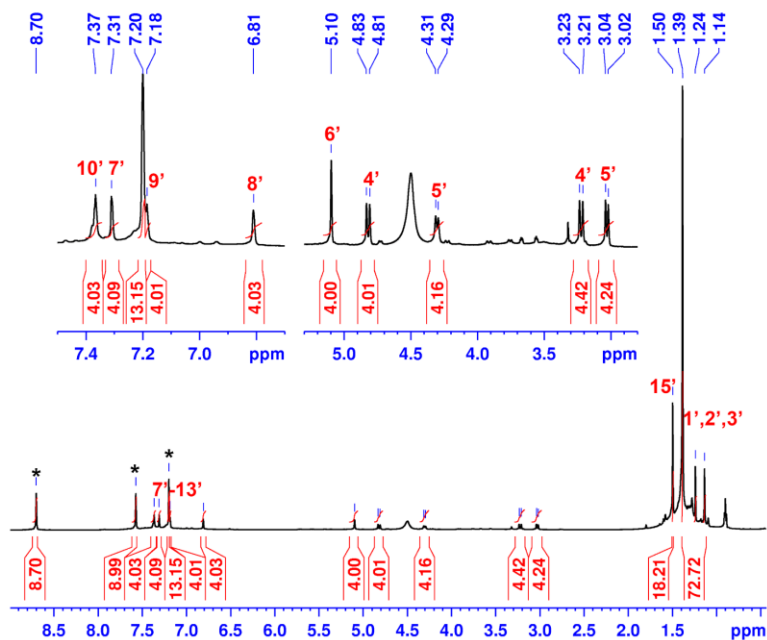


**Figure 101.**  $^1\text{H}$  NMR spectrum of  $17(\text{Zr-O-}^t\text{Bu})_2$  at  $25\text{ }^\circ\text{C}$  (600 MHz,  $\text{pyridine-}d_5$ ).

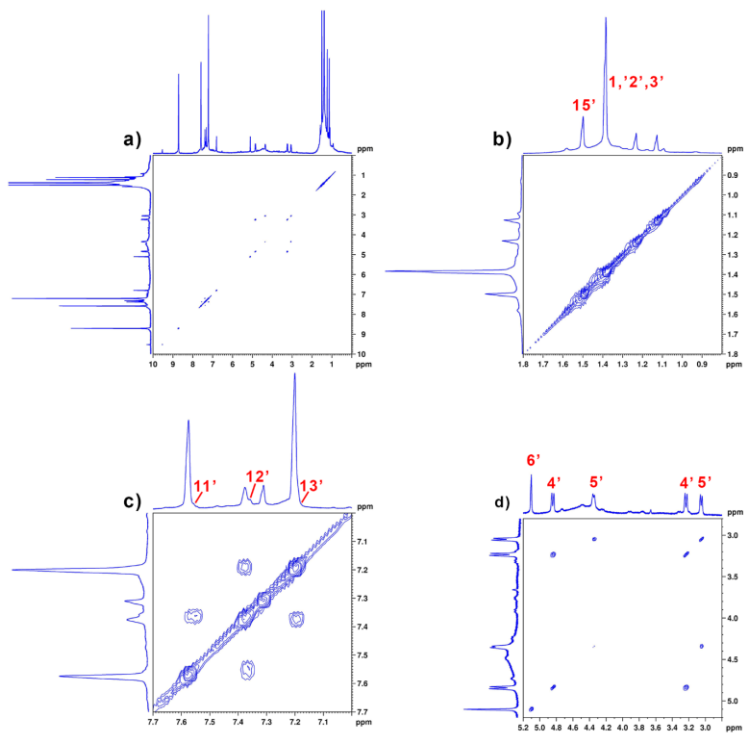


**Figure 102.**  $^1\text{H}$ - $^1\text{H}$  COSY spectrum (600 MHz, pyridine- $d_5$ ,  $90^\circ\text{C}$ ) of  $17(\text{Zr-O-}^t\text{Bu})_2$  (a) with magnifications of the diagnostic regions (b-d).

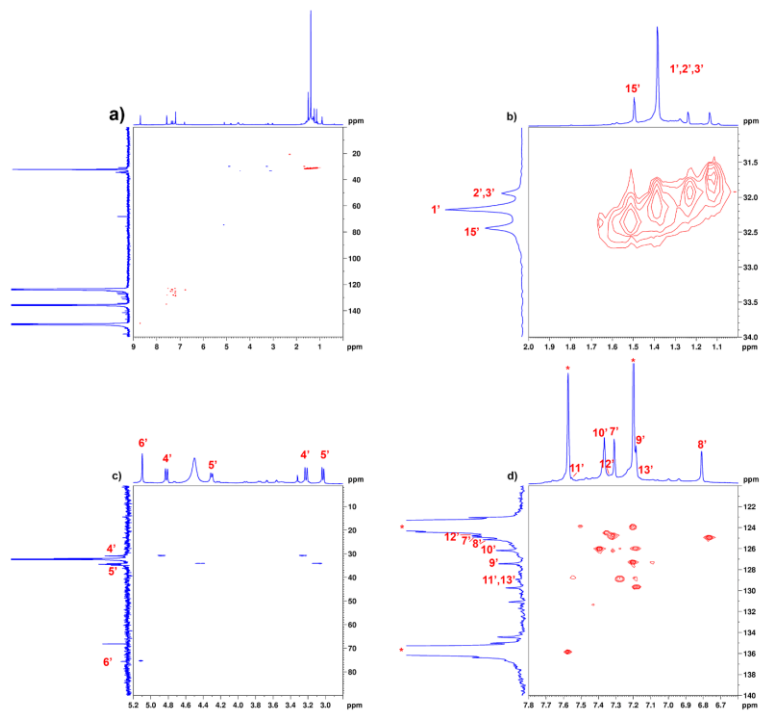


**Figure 103.**  $^1\text{H}$ - $^{13}\text{C}$  HSQC spectrum (600 MHz, pyridine- $d_5$ , 25°C) of the complex **17**(Zr-O-*t*Bu) $_2$  (a) with magnifications of the diagnostic regions (b-d).

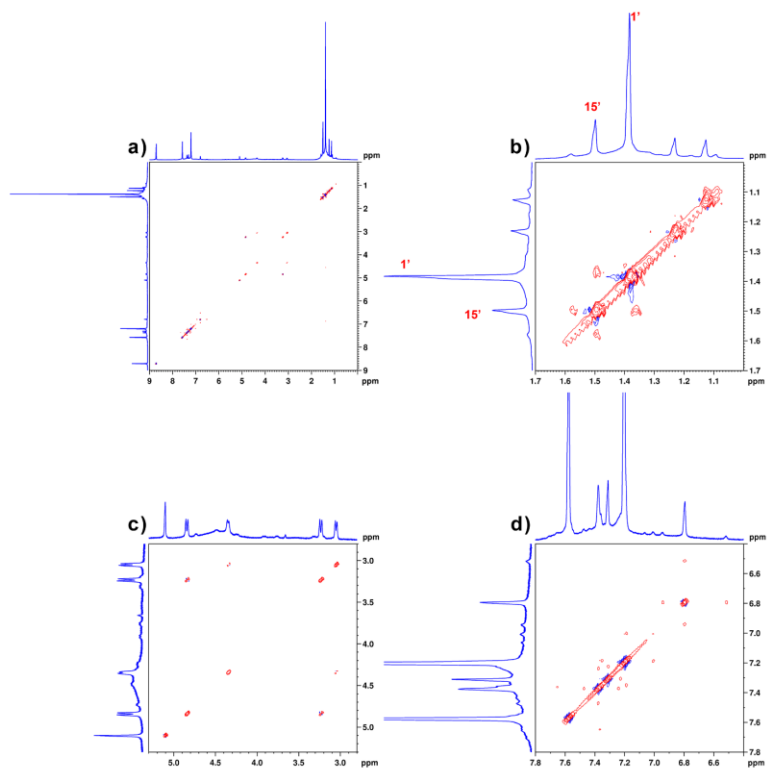


**Figure 104.**  $^1\text{H}$ - $^1\text{H}$  NOESY spectrum (600 MHz, pyridine- $d_5$ ,  $90^\circ\text{C}$ ) of the complex  $17(\text{Zr-O}^t\text{Bu})_2$  (a) with magnifications of the diagnostic regions (b-d).

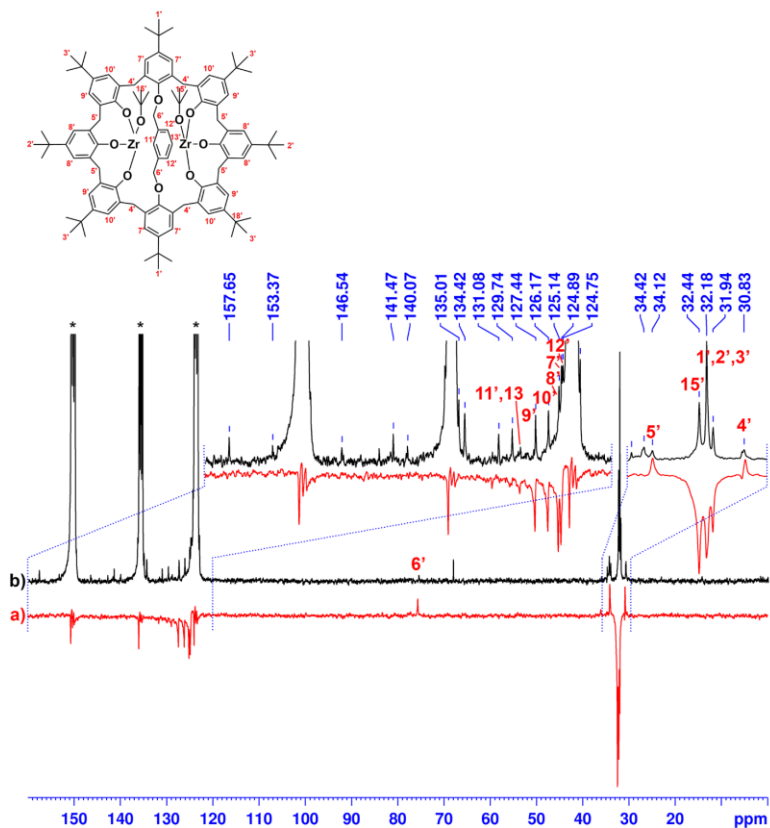


**Figure 105.** DEPT135 (a) and <sup>13</sup>C NMR (b) spectra (600 MHz, pyridine-*d*<sub>5</sub>, 90°C) of the complex **17**(Zr-O-*t*Bu)<sub>2</sub>.

## 6.4. Catalytic conditions

### 6.4.1. General Procedure for the Phase-Transfer Alkylation of *N*-(Diphenylmethylene)glycine *tert*-Butyl Ester (**14**) Catalyzed by Chiral Calixarene-Amide **12**.

To a solution of *N*-(diphenylmethylene)glycine *tert*-butyl ester **22** (148 mg, 0.50 mmol) and chiral catalyst **12** (28.8 mg, 0.025 mmol) in mesitylene (5.0 mL) under an inert gas, alkyl bromide (1.2–1.5 equiv.) was added. The mixture was degassed and then cooled to 0 °C. Degassed aqueous NaOH (50 %, 0.5 mL) was then added. The reaction mixture was stirred at 0 °C until TLC disappearance of the starting material. Then the suspension was diluted with CH<sub>2</sub>Cl<sub>2</sub> (25 mL) and water (15 mL), and the organic layer was taken. The aqueous layer was extracted with CH<sub>2</sub>Cl<sub>2</sub> (2 × 25 mL), and the combined organic phases were dried with Na<sub>2</sub>SO<sub>4</sub>, filtered, and concentrated in vacuo. Purification of the residue by flash column chromatography with silica gel (petroleum ether/ethyl acetate, 98:2 to 90:10) afforded the pure alkylated products.

***6.4.2. General Procedure for Catalytic Enantioselective Michael Reaction of Isobutyraldehyde with Maleimide in Water.***

To a suspension of N-phenylmaleimide (17.3 mg, 0.1 mmol) and catalyst **16** (11.5 mg, 0.015 mmol) in water (200  $\mu$ L) isobutyraldehyde (36  $\mu$ L, 0.4 mmol) was added and the suspension was stirred vigorously at room temperature for 40 minutes. The crude compound **39** was purified by flash chromatography (eluting from PE/ ethyl acetate 9:1 to 7:3).

***6.4.3. General Procedure for Solvent-free Catalytic Enantioselective Michael Reaction of Isobutyraldehyde with Maleimide.***

A sample vial was charged with N-phenylmaleimide (17.3 mg, 0.1 mmol), catalyst **16** (11.5 mg, 0.015 mmol) and finally the isobutyraldehyde (36  $\mu$ L, 0.4 mmol). The reaction mixture was stirred at room temperature until completion, monitored by TLC (eluent PE/ ethyl acetate 7:3). The crude compound **39** was purified by flash chromatography (eluting from PE/ ethyl acetate 9:1 to 7:3).

#### ***6.4.4. Catalytic Asymmetric Solvent-free Michael Addition of Isobutyraldehyde to Nitroolefins.***

The nitroolefin (0.1 mmol), catalyst **16** (11.5 mg, 0.015 mmol) and finally the isobutyraldehyde (36  $\mu$ L, 0.4 mmol) were loaded in capped vial. The reaction mixture was stirred at room temperature until completion, monitored by TLC (eluent PE/ ethyl acetate 9:1, visualized by UV light and by p-anisaldehyde staining solution). The residue was purified by flash chromatography (eluting from PE/ ethyl acetate 100:1 to 9:1).

#### ***6.4.5. Catalytic Enantioselective Solvent-free Addition of Dimethyl Malonate to Benzylideneacetone.***

A sample vial was charged with benzylideneacetone (14.6 mg, 0.1 mmol), catalyst **16** (11.5 mg, 0.015 mmol) and benzoic acid (0.9 mg, 0.0075 mmol). At the end dimethyl malonate (46  $\mu$ L, 0.4 mmol) was added and the reaction mixture was stirred at room temperature until completion, monitored by TLC (eluent PE/ ethyl acetate 8:2, visualized by UV light and by p-anisaldehyde staining solution). The crude compound **53** was purified by flash chromatography (eluting from PE/ ethyl acetate 9:1 to 7:3).

## REFERENCES

---

1. a) P. Ballestrer, A. Vidal-Ferran, P. W. N. M. Van Leeuwen, *Adv. Catal.* **2011**, *54*, 63–126; b) J. Liu, L. Chen, H. Cui, J. Zhang, L. Zhang, C.-Y. Su, *Chem. Soc. Rev.* **2014**, *43*, 6011–6061; c) J. J. Roach, R. A. Shenvi, *Nat. Chem.* **2015**, *7*, 187–189; d) C. J. Brown, F. D. Toste, R. G. Bergman, K. N. Raymond, *Chem. Rev.* **2015**, *115*, 3012–3035; e) A.-L. Lee, *Nat. Chem.* **2016**, *8*, 8–9; e) A. Chołuj, A. Zieliński, K. Grela, M. J. Chmielewski, *ACS Catal.* **2016**, *6*, 6343–6349.
2. a) P. W. N. M. van Leeuwen, *Supramolecular Catalysis*, Wiley-VCH, Weinheim, **2008**; b) J. Meeuwissen, J. N. H. Reek, *Nat. Chem.* **2010**, *2*, 615–621; c) M. Raynal, P. Ballestrer, A. Vidal-Ferran, P. W. N. M. van Leeuwen, *Chem. Soc. Rev.* **2014**, *43*, 1660–1733.
3. a) D. Ringe, G. A. Petsko, *Science* **2009**, *320*, 1428–1429; b) Z. Dong, Q. Luo, J. Liu, *Chem. Soc. Rev.* **2012**, *41*, 7890–7908; c) M. Raynal, P. Ballestrer, A. Vidal-Ferran, P. W. N. M. van Leeuwen, *Chem. Soc. Rev.* **2014**, *43*, 1734–1787.
4. a) A. J. Kirby, F. Hollfelder, *From Enzyme Models to Model Enzymes*, RSC Publishing, Cambridge, **2009**; b) L. Marchetti, M. Levine, *ACS Catal.* **2011**, *1*, 1090–1118; c) P. A. Gale, J. W. Steed, *Supramolecular Chemistry: From Molecules to Nanomaterials*, Wiley-VCH, Weinheim, **2012**.
5. a) R. Breslow, L. E. Overman, *J. Am. Chem. Soc.* **1970**, *92*, 1075–1077; b) I. Tabushi, N. Shimizu, T. Sugimoto, M. Shiozuka, K. Yamamura, *J. Am. Chem. Soc.* **1977**, *99*, 7100–7102; c) I. Tabushi, *Acc. Chem. Res.* **1982**, *15*, 66–72; d) I. Tabushi, *Tetrahedron* **1984**, *40*, 269–292; e) R. Breslow, *Acc. Chem. Res.* **1995**, *28*, 146–153.

- 
6. a) E. Iglesias A. Fernández, *J. Chem. Soc., Perkin Trans. 2* **1998**, 1691–1699; b) E. Iglesias, *J. Am. Chem. Soc.* **1998**, *120*, 13057–13069; c) D. T. H. Chou, J. Zhu, X. Huang A. J. Bennet, *J. Chem. Soc., Perkin Trans. 2* **2001**, 83–89; d) J. Báscuas, L. García-Río J. R. Leis, *Org. Biomol. Chem.* **2004**, *2*, 1186–1193; e) N. Basilio, L. García-Río, J. A. Moreira and M. Pessego, *J. Org. Chem.* **2010**, *75*, 848–855.
7. a) J. W. Lee, S. Samal, N. Selvapalam, H.-J. Kim, K. Kim, *Acc. Chem. Res.* **2003**, *36*, 621–630; b) J. Lagona, P. Mukhopadhyay, S. Chakrabarti L. Isaacs, *Angew. Chem., Int. Ed.* **2005**, *44*, 4844–4870; c) W. M. Nau, M. Florea, K. I. Assaf, *Isr. J. Chem.* **2011**, *51*, 559–577; d) G. Parvari, O. Reany, E. Keinan, *Isr. J. Chem.* **2011**, *51*, 646–663; e) E. Masson, X. X. Ling, R. Joseph, L. Kyeremeh-Mensah, X. Y. Lu, *RSC Adv.* **2012**, *2*, 1213–1247; f) B. C. Pemberton, R. Raghunathan, S. Volla J. Sivaguru, *Chem.–Eur. J.* **2012**, *18*, 12178–12190; g) J. Lu, J. X. Lin, M. N. Cao, R. Cao, *Coord. Chem. Rev.* **2013**, *257*, 1334–1356.
8. a) Y. Chao, D. J. Cram, *J. Am. Chem. Soc.* **1976**, *98*, 1015–1017; b) J.-P. Behr, J.-M. Lehn, *J. Chem. Soc., Chem. Commun.* **1978**, 143–146; c) T. Matsui, K. Koga, *Tetrahedron Lett.* **1978**, *19*, 1115–1118; d) D. J. Cram, G. D. Y. Sogah, *J. Chem. Soc., Chem. Commun.* **1981**, 625–628; e) M. W. Hosseini, J. M. Lehn, K. C. Jones, K. E. Plute, K. B. Mertes, M. P. Mertes, *J. Am. Chem. Soc.* **1989**, *111*, 6330–6335.
9. a) A. Gissot J. Rebek Jr., *J. Am. Chem. Soc.* **2004**, *126*, 7424–7425; b) R. J. Hooley, J. Rebek Jr., *J. Am. Chem. Soc.* **2005**, *127*, 11904–11905; c) R. J. Hooley, J. Rebek Jr., *Org. Biomol. Chem.* **2007**, *5*, 3631–3636; d) R. J. Hooley, T. Iwasawa, J.

- 
- Rebek Jr., *J. Am. Chem. Soc.* **2007**, *129*, 15330–15339; e) R. J. Hooley, J. Rebek Jr., *Chem. Biol.* **2009**, *16*, 255–264; f) K. E. Djernes, O. Moshe, M. Mettry, D. D. Richards, R. J. Hooley, *Org. Lett.* **2012**, *14*, 788–791.
10. a) P. Molenveld, J. F. J. Engbersen, D. N. Reinhoudt, *Chem. Soc. Rev.* **2000**, *29*, 75–86; b) D. T. Schühle, J. A. Peters, J. Schatz, *Coord. Chem. Rev.* **2011**, *255*, 2727–2745.
11. a) Z. Asfari, V. Böhmer, J. Harrowfield, J. Vicens, Eds., *Calixarenes 2001*, Kluwer, Dordrecht, **2001**; b) J. Vicens, J. Harrowfield, Eds., *Calixarenes in the Nanoworld*, Springer, Dordrecht, **2007**; c) C. D. Gutsche, *Calixarenes, An Introduction*, Royal Society of Chemistry, Cambridge, UK, **2008**; d) P. Neri, J. L. Sessler, M.-X. Wang B., Eds., *Calixarenes and Beyond*, Springer, Dordrecht, **2016**.
12. a) C. D. Gutsche, P. F. Pagoria, *J. Org. Chem.* **1985**, *50*, 5795–5802; b) C. D. Gutsche, L.-G. Lin, *Tetrahedron* **1986**, *42*, 1633–1640; c) S. Shinkai, H. Koreishi, K. Ueda, T. Arimura, O. Manabe, *J. Am. Chem. Soc.* **1987**, *109*, 6371–6376; d) W. Verboom, A. Durie, R. J. M. Egberink, Z. Asfari, D. N. Reinhoudt, *J. Org. Chem.* **1992**, *57*, 1313–1316; e) A. Casnati, Y. Ting, D. Berti, M. Fabbi, A. Pochini, R. Ungaro, D. Sciotto, G. G. Lombardo, *Tetrahedron* **1993**, *49*, 9815–9822; f) A. Arduini, S. Fanni, G. Manfredi, A. Pochini, R. Ungaro, A. R. Sicuri, F. Ugozzoli, *J. Org. Chem.* **1995**, *60*, 1448–1453; g) M. De Rosa, A. Soriente, G. Concilio, C. Talotta, C. Gaeta, P. Neri, *J. Org. Chem.* **2015**, *80*, 7295–7300.
13. a) F. Troisi, L. Mogavero, C. Gaeta, E. Gavuzzo, P. Neri, *Org. Lett.* **2007**, *9*, 915–918; b) C. Gaeta, C. Talotta, F. Farina, M. Camalli, G. Campi, P. Neri, *Chem. Eur. J.* **2012**, *18*, 1219–

- 
- 1230; c) N. Dozova, R. Kumar, T. Pradhan, F. Lacomat, B. Valeur, J. S. Kim, P. Plaza, *Chem. Commun.* **2015**, *51*, 14859–14861; d) E. Brunetti, S. Moerkerke, J. Wouters, K. Bartik, I. Jabin, *Org. Biomol. Chem.* **2016**, *14*, 10201–10207; e) G. De Leener, F. Evoung-Evoung, A. Lascaux, J. Mertens, A. G. Porras-Gutierrez, N. Le Poul, C. Lagrost, D. Over, Y. R. Leroux, F. Reniers, P. Hapiot, Y. Le Mest, I. Jabin, O. Reinaud, *J. Am. Chem. Soc.* **2016**, *138*, 12841–12853.
14. a) C. Talotta, C. Gaeta, T. Pierro, P. Neri, *Org. Lett.* **2011**, *13*, 3104–3107; b) A. Arduini, R. Bussolati, A. Credi, A. Secchi, S. Silvi, M. Semeraro, M. Venturi, *J. Am. Chem. Soc.* **2013**, *135*, 9924–9930; c) C. Gaeta, C. Talotta, L. Margarucci, A. Casapullo, P. Neri, *J. Org. Chem.* **2013**, *78*, 7627–7638.
15. a) M. Giuliani, I. Morbioli, F. Sansone, A. Casnati, *Chem. Commun.* **2015**, *51*, 14140–14159; b) S. Tommasone, C. Talotta, C. Gaeta, L. Margarucci, M. C. Monti, A. Casapullo, B. Macchi, S. P. Prete, A. L. De Araujo, P. Neri, *Angew. Chem. Int. Ed.* **2015**, *54*, 15405–15409.
16. a) A. Soriente, M. De Rosa, M. Fruilo, L. Lepore, C. Gaeta, P. Neri, *Adv. Synth. Catal.* **2005**, *347*, 816–824; b) D. H. Homden, C. Redshaw, *Chem. Rev.* **2008**, *108*, 5086–5130; c) M. Yilmaz, S. Sayin in *Calixarenes and Beyond* (Eds: P. Neri, J. L. Sessler, M.–X. Wang), Springer, Dordrecht, **2016**, pp. 719–741; d) M. Durmaz, A. Tataroglu, H. Yilmaz, A. Sirit, *Tetrahedron: Asymmetry* **2016**, *27*, 148–156; e) M. De Rosa, P. La Manna, A. Soriente, C. Gaeta, C. Talotta, P. Neri, *RSC Adv.* **2016**, *6*, 91846–91851.
17. a) J. O. Magrans, A. R. Ortiz, A. Molins, P. H. P. Lebouille, J. Sánchez-Quesada, P. Prados, M. Pons, F. Gago, J. de Mendoza,

- 
- Angew. Chem., Int. Ed. Engl.* **1996**, *35*, 1712–1715; b) J. de Mendoza, V. Alcázar, E. Botana, A. Galán, G. Lu, J. O. Magrans, M. Martín-Portugués, P. Prados, A. Salmerón, J. Sánchez-Quesada, C. Seel, M. Segura, *Pure Appl. Chem.* **1997**, *69*, 577–582; c) F. Cuevas, S. Di Stefano, J. O. Magrans, P. Prados, L. Mandolini, J. de Mendoza, *Chem.–Eur. J.* **2000**, *6*, 3228–3234.
18. a) P. Molenveld, J. F. J. Engbersen, D. N. Reinhoudt, *Eur. J. Org. Chem.* **1999**, 3269–3275; b) P. Molenveld, W. M. G. Stikvoort, H. Kooijman, A. L. Spek, J. F. J. Engbersen, D. N. Reinhoudt, *J. Org. Chem.* **1999**, *64*, 3896–3906.
19. a) T. Heinz, D. M. Rudkevich, J. Rebek, Jr. *Nature* **1998**, *394*, 764–766; b) F. C. Tucci, D. M. Rudkevich, J. Rebek, Jr. *J. Am. Chem. Soc.* **1999**, *121*, 4928–4929; c) S. K. Körner, F. C. Tucci, D. M. Rudkevich, T. Heinz, J. Rebek, Jr. *Chem.–Eur. J.* **1999**, *6*, 187–195; d) J. Chen, J. Rebek, Jr., *Org. Lett.*, **2002**, *4*, 327–329.
20. a) M. Fujita, D. Oguro, M. Miyazawa, H. Oka, K. Yamaguchi, K. Ogura, *Nature*, **1995**, *378*, 469–471; b) S.-Y. Yu, T. Kusukawa, K. Biradha, M. Fujita, *J. Am. Chem. Soc.* **2000**, *122*, 2665–2666; c) M. Yoshizawa, M. Tamura, M. Fujita, *Science* **2006**, *312*, 251–254.
21. a) D. H. Leung, D. Fiedler, R. G. Bergman, K. N. Raymond, *Angew. Chem.* **2004**, *116*, 981–984; b) D. Fiedler, R. G. Bergman, K. N. Raymond, *Angew. Chem.* **2004**, *116*, 6916–6919; c) D. H. Leung, R. G. Bergman, K. N. Raymond, *J. Am. Chem. Soc.* **2006**, *128*, 9781–9797; d) D. Fiedler, H. van Halbeek, R. G. Bergman, K. N. Raymond, *J. Am. Chem. Soc.*

- 
- 2006**, 128, 10240–10252; e) M. D. Pluth, R. G. Bergman, K. N. Raymond, *Science*, **2007**, 316, 85–88.
22. a) F.-R. Dai, Z. Wang, *J. Am. Chem. Soc.* **2012**, 134, 8002–8005; b) F.-R. Dai, U. Sambasivam, A. J. Hammerstrom, Z. Wang, *J. Am. Chem. Soc.* **2014**, 136, 7480–7491; c) N. L. Netzer, F.-R. Dai, Z. Wang, C. Jiang, *Angew. Chem. Int. Ed.* **2014**, 53, 10965–10969; d) F.-R. Dai, D. C. Becht, Z. Wang, *Chem. Commun.* **2014**, 50, 5385–5387; e) F.-R. Dai, Y. Qiao, Z. Wang, *Inorg. Chem. Front.* **2016**, 3, 243–249; f) Y. Qiao, L. Zhang, J. Li, W. Lin, Z. Wang, *Angew. Chem. Int. Ed.* **2016**, 55, 12778–12782.
23. N. A. De Simone, R. Schettini, C. Talotta, C. Gaeta, I. Izzo, G. Della Sala, P. Neri, *Eur. J. Org. Chem.* **2017**, 5649–5659.
24. N. De Simone, S. Meninno, C. Talotta, C. Gaeta, L. Lattanzi, P. Neri, manuscript in preparation.
25. R. Lapenta, N. A. De Simone, A. Buonerba, C. Talotta, C. Gaeta, P. Neri, A. Grassi, S. Milione, paper submitted.
26. a) C. M. Starks, C. L. Liotta, M. Halpern, *Phase-Transfer Catalysis*, Chapman & Hall, New York, **1994**; b) M. Małosza, *Pure Appl. Chem.* **2000**, 72, 1399–1403; c) M. Małosza, M. Fedoryński, *Curr. Catal.* **2012**, 1, 79–87.
27. a) S. Shimizu, K. Kito, Y. Sasaki, C. Hirai, *Chem. Commun.* **1997**, 1629–1630; b) S. Shimizu, S. Shirakawa, T. Suzuki, Y. Sasaki, *Tetrahedron* **2001**, 57, 6169–6173; c) S. Shimizu, S. Shirakawa, Y. Sasaki, C. Hirai, *Adv. Synth. Catal.* **2002**, 344, 370–378; d) S. Shimizu, N. Shimada, Y. Sasaki, *Green Chem.* **2006**, 8, 608–614; e) P. Srivastava, R. Srivastava, *Tetrahedron*

- 
- Lett.* **2007**, *48*, 4489–4493; f) E. Akceylan, M. Yilmaz, *Tetrahedron* **2011**, *67*, 6240–6245; g) F. Yang, H. Guo, Z. Jiao, C. Li, J. Ye, *J. Iran. Chem. Soc.* **2012**, *9*, 327–332; h) Y. Xie, L. Mao, L. Li, *J. Chem. Res.* **2013**, 476–479; i) S. Sayin, M. Yilmaz, *RSC Adv.* **2014**, *4*, 2219–2225.
28. a) F. Arnaud-Neu, G. Barrett, S. Fanni, D. Marrs, W. McGregor, A. M. McKerverey, M.-J. Schwing-Weill, V. Vetrogon, S. Wechsler, *J. Chem. Soc., Perkin Trans. 2* **1995**, 453–461; b) F. Arnaud-Neu, S. Barbosa, F. Berny, A. Casnati, N. Muzet, A. Pinalli, R. Ungaro, M.-J. Schwing-Weill, G. Wipff, *J. Chem. Soc., Perkin Trans. 2* **1999**, 1727–1738; c) F. Arnaud-Neu, S. Barbosa, S. Fanni, M.-J. Schwing-Weill, *Ind. Eng. Chem. Res.* **2000**, *39*, 3489–3492.
29. a) P. L. H. M. Cobben, R. J. M. Egberink, J. G. Bommer, P. Bergveld, W. Verboom, D. N. Reinhoudt, *J. Am. Chem. Soc.* **1992**, *114*, 10573–10582; b) F. Arnaud-Neu, M. A. McKerverey, J. Schwing-Weill in *Calixarenes 2001* (Eds.: Z. Asfari, V. Böhmer, J. Harrowfield, J. Vicens), Kluwer, Dordrecht, **2001**, pp. 385–406; c) F. Cadogan, K. Nolan, D. Diamond in *Calixarenes 2001* (Eds.: Z. Asfari, V. Böhmer, J. Harrowfield, J. Vicens), Kluwer, Dordrecht, **2001**, pp. 627–641; d) P. J. Greenawalt, S. Amemiya, *Anal. Chem.* **2016**, *88*, 5827–5835; e) S. Amemiya, *Anal. Chem.* **2016**, *88*, 8893–8901.
30. K. Araki, A. Yanagi, S. Shinkai, *Tetrahedron* **1993**, *49*, 6763–6772.
31. a) H. Taniguchi, E. Nomura, *Chem. Lett.* **1988**, *20*, 1773–1776; b) E. Nomura, H. Taniguchi, K. Kawaguchi, Y. Otsuji, *Chem. Lett.* **1991**, *20*, 2167–2170; c) E. Nomura, H. Taniguchi, K. Kawaguchi, Y. Otsuji, *J. Org. Chem.* **1993**, *58*, 4709–4715.

- 
32. F. Yang, Y. Wang, H. Guo, J. Xie, Z. Liu, *Can. J. Chem.* **2010**, *88*, 622–627.
33. a) T. Ooi, K. Maruoka, *Angew. Chem. Int. Ed.* **2007**, *46*, 4222–4266; b) S.-s. Jew, H.-g. Park, *Chem. Commun.* **2009**, 7090–7103; c) S. Shirakawa, K. Maruoka, *Angew. Chem. Int. Ed.* **2013**, *52*, 4312–4348; d) J. Tan, N. Yasuda, *Org. Process Res. Dev.* **2015**, *19*, 1731–1746; e) S. Kaneko, Y. Kumatabara, S. Shirakawa, *Org. Biomol. Chem.* **2016**, *14*, 5367–5376.
34. S. Bozkurt, M. Durmaz, M. Yilmaz, A. Sirit, *Tetrahedron: Asymmetry* **2008**, *19*, 618–623.
35. W. Su, C. Jin, L. Huang, *J. Chem. Res.* **2012**, *36*, 532–535.
36. b) S. Shimizu, S. Shirakawa, *Eur. J. Org. Chem.* **2009**, 1916–1924; c) S. Shirakawa, S. Shimizu, *New J. Chem.* **2010**, *34*, 1217–1222.
37. I. Stibor, M. Růžičková, R. Krátký, M. Vindiš, J. Havlíček, E. Pinkhassik, P. Lhoták, A. R. Mustafina, Y. E. Morozova, E. K. Kazakova, V. P. Gubskaya, *Collect. Czech. Chem. Commun.* **2001**, *66*, 641–662.
38. a) K. Iwamoto, S. Shinkai, *J. Org. Chem.* **1992**, *57*, 7066–7073; b) J. Kulesza, M. Guzinski, M. Bochenska, V. Hubscher-Bruder, F. Arnaud-Neu, *Polyedron*, **2014**, *77*, 89–95.
39. A. Arduini, A. Casnati, M. Fabbi, P. Minari, A. Pochini, A. R. Sicuri, R. Ungaro, *Supramol. Chem.* **1992**, *1*, 235–246.

- 
40. N. Sabbatini, A. Casnati, C. Fischer, R. Girardini, I. Guardigli, I. Manet, G. Sarti, R. Ungaro, *Inorg. Chim. Acta* **1996**, *252*, 19–24.
41. V. S. Talanov, H.-S. Hwang, R. A. Bartsch, *J. Chem. Soc., Perkin Trans. 2*, **2001**, 1103–1108.
42. a) M. J. O'Donnell, W. D. Bennett, S. Wu, *J. Am. Chem. Soc.* **1989**, *111*, 2353–2355; b) T. Ooi, Y. Uematsu, K. Maruoka, *Tetrahedron Lett.* **2004**, *45*, 1675–1678.
43. a) S.-s. Jew, Y.-J. Lee, J. Lee, M. J. Kang, B.-S. Jeong, J.-H. Lee, M.-S. Yoo, M.-J. Kim, S.-h. Choi, J.-M. Ku, H.-g. Park, *Angew. Chem. Int. Ed.* **2004**, *43*, 2382–2385; b) M. Kitamura, S. Shirakawa, Y. Arimura, X. Wang, K. Maruoka, *Chem. Asian J.* **2008**, *3*, 1702–1714; c) M. Waser, K. Gratzler, R. Herchl, N. Müller, *Org. Biomol. Chem.* **2012**, *10*, 251–254.
44. a) T. B. Poulsen, L. Bernardi, M. Bell, K. A. Jørgensen, *Angew. Chem. Int. Ed.* **2006**, *45*, 6551–6554; b) F. Fini, G. Micheletti, L. Bernardi, D. Pettersen, M. Fochi, A. Ricci, *Chem. Commun.* **2008**, 4345–4347.
45. a) S. Braun, H.-O. Kalinowsky, S. Berger, Eds., *150 and More Basic NMR experiments: A Practical Course*, Wiley-VCH, Weinheim, **1996**, pp. 232–233 ; b) K. Hirose, *J. Inclusion Phenom. Macrocyclic Chem.* **2001**, *39*, 193–209 ; c) K. Hirose in *Analytical Methods in Supramolecular Chemistry* (Ed.: C. A. Schalley), Wiley-VCH, Weinheim, **2007**, Chapter 2, pp. 17–54.
46. a) H. Hou, K. C.-F. Leung, D. Lanari, A. Nelson, J. F. Stoddart, R. H. Grubbs, *J. Am. Chem. Soc.* **2006**, *128*, 13358–13359; b) B. A. Blight, A. Camara-Campos, S. Djurdjevic, M. Kaller, D.

- 
- A. Leigh, F. M. McMillan, H. Mc Nab, A. M. Slawin, *J. Am. Chem. Soc.* **2009**, *131*, 14116–14122; c) C. Li, X. Shu, J. Li, J. Fan, Z. Chen, L. Weng, X. Jia, *Org. Lett.* **2012**, *14*, 4126–4129.
47. S. H. Strauss, *Chem Rev.* **1993**, *93*, 927–942.
48. H. Nishida, N. Takada, M. Yoshimura, T. Sonoda, H. Kobayashi, *Bull. Chem. Soc. Jpn.* **1984**, *57*, 2600–2604.
49. a) C. Jaime, J. de Mendoza, P. Prados, P. M. Nieto, C. Sanchez, *J. Org. Chem.* **1991**, *56*, 3372–3376; b) J. O. Magrans, J. de Mendoza, M. Pons, P. Prados, *J. Org. Chem.* **1997**, *62*, 4518–4520; c) G. Bifulco, L. Gomez-Paloma, R. Riccio, C. Gaeta, F. Troisi, P. Neri, *Org. Lett.* **2005**, *7*, 5757–5760; d) G. Bifulco, R. Riccio, C. Gaeta, P. Neri, *Chem. Eur. J.* **2007**, *13*, 7185–7194.
50. B. List, R. A. Lerner, C. F. Barbas III, *J. Am. Chem. Soc.* **2000**, *122*, 2395–2396.
51. K. A. Ahrendt, C. J. Borths, D. W. C. MacMillan, *J. Am. Chem. Soc.* **2000**, *122*, 4243–4244.
52. a) P. I. Dalko, L. Moisan, *Angew. Chem., Int. Ed.* **2004**, *43*, 5138–5175; b) M. J. Gaunt, C. C. C. Johansson, A. McNally, N. T. Vo, *Drug Discovery Today* **2007**, *12*, 8–27; c) A. Erkkilä, I. Majander, P. M. Pihko, *Chem. Rev.* **2007**, *107*, 5416–5470; d) A. Dondoni, A. Massi, *Angew. Chem., Int. Ed.* **2008**, *47*, 4638–4660; e) P. Melchiorre, M. Marigo, A. Carlone, G. Bartoli, *Angew. Chem., Int. Ed.* **2008**, *47*, 6138–6171.
53. a) T. Okino, Y. Hoashi, Y. Takemoto, *J. Am. Chem. Soc.* **2003**, *125*, 12672–12673; b) T. Okino, S. Nakamura, T. Furukawa, Y.

- 
- Takemoto, *Org. Lett.* **2004**, *6*, 625–627; c) Y. Takemoto, *Org. Biomol. Chem.*, **2005**, *3*, 4299–4306.
54. a) S. B. Tsogoeva, D. A. Yalalov, M. J. Hateley, C. Weckbecker, K. Huthmacher, *Eur. J. Org. Chem.* **2005**, 4995–5000; b) D. A. Yalalov, S. B. Tsogoeva, S. Schmatz, *Adv. Synth. Catal.* **2006**, *348*, 826–832; c) F. Xue, L. Liu, S. Zhang, W. Duan, W. Wang, *Chem. Eur. J.* **2010**, *16*, 7979–7982.
55. a) M. Durmaz, A. Sirit, *Tetrahedron Asymm.* **2013**, *24*, 1443–1448; b) M. Durmaz, A. Sirit, *Supramol. Chem.* **2013**, *25*, 292–301.
56. N. Hayama, T. Azuma, Y. Kobayashi, Y. Takemoto, *Chem. Pharm. Bull.* **2016**, *64*, 704–717.
57. A. M. A. van Wageningen, E. Snip, W. Verboom, D. N. Reinhoudt, H. Boerrigter, *Liebigs Ann./Recueil* **1997**, 2235–2245.
58. M. Kaik J. Gawroński, *Tetrahedron Asymm.* **2003**, *14*, 1559–1563.
59. K. Nakashima, M. Kawada, S. Hirashima, M. Kato, Y. Koseki, T. Miura *Synlett* **2015**, *26*, 1248–1252.
60. a) R. Breslow, K. Groves, M. U. Mayer, *Pure Appl. Chem.* **1998**, *70*, 1933–1938; b) S. Narayan, J. Muldoon, M. J. Finn, V. V. Fokin, H. Kolb, K. B. Sharpless, *Angew. Chem. Int. Ed.* **2005**, *44*, 3275–3279; c) A. Chanda, V. V. Fokin, *Chem. Rev.* **2009**, *109*, 725–748; d) R. N. Butler, A. G. Coyne, *Chem. Rev.* **2010**, *110*, 6302–6337; e) F. Biedermann, W. N. Nau, H.-J. Schneider, *Angew. Chem. Int. Ed.* **2014**, *53*, 11158–11171.

- 
61. a) M. De Rosa, P. La Manna, A. Soriente, C. Gaeta, C. Talotta, P. Neri, *RSC Adv.* **2016**, *6*, 91846–91851; b) M. De Rosa, P. La Manna, A. Soriente, C. Gaeta, C. Talotta, N. Hickey, S. Geremia, P. Neri, *Chem. Eur. J.* **2017**, *23*, 7142–7151.
62. a) T. He, Q. Gu, X.-Y. Wu *Tetrahedron* **2010**, *66*, 3195–3198; b) I. Sagamanova, C. Rodríguez-Esrich, I. G. Molnár, S. Sayalero, R. Gilmour, M. A. Pericas *ACS Catal.* **2015**, *5*, 6241–6248.
63. K. Dudziński, A. M. Pakulska, P. Kwiatkowski, *Org. Lett.*, **2012**, *14*, 4222–4225.
64. a) S. Mecking, *Angew. Chem., Int. Ed.* **2004**, *43*, 1078–1085; b) A. J. Ragauskas, C. K. Williams, B. H. Davison, G. Britovsek, J. Cairney, C. A. Eckert, W. J. Frederick, J. P. Hallett, D. J. Leak, C. L. Liotta, J. R. Mielenz, R. Murphy, R. Templer, T. Tschaplinski, *Science* **2006**, *311*, 484–489; c) M. J.-L. Tschan, E. Brulé, P. Haquette, C. M. Thomas, *Polym. Chem.* **2012**, *3*, 836–851; d) R. Mülhaupt, *Macromol. Chem. Phys.* **2013**, *214*, 159–174; e) S. A. Miller, *ACS Macro Lett.* **2013**, *2*, 550–554.
65. a) E. Chiellini, R. Solaro, *Adv. Mater.* **1996**, *8*, 305–313; b) Y. Ikada, H. Tsuji, *Macromol. Rapid Commun.* **2000**, *21*, 117–132; c) A.-C. Albertsson, I. K. Varma, *Biomacromolecules* **2003**, *4*, 1466–1486; d) R. Auras, B. Harte, S. Selke, *Macromol. Biosci.* **2004**, *4*, 835–864.
66. a) J. Roovers, in *Cyclic Polymers* (Ed.: J. A. Semlyen), Springer Netherlands, Dordrecht, **2002**, pp. 347–384; b) J. N. Hoskins, S. M. Grayson, *Polym. Chem.* **2011**, *2*, 289–299.

- 
67. J. N. Hoskins, S. M. Grayson, *Macromolecules* **2009**, *42*, 6406–6413.
68. N. Nasongkla, B. Chen, N. Macaraeg, M. E. Fox, J. M. J. Fréchet, F. C. Szoka, *J. Am. Chem. Soc.* **2009**, *131*, 3842–3843.
69. B. Chen, K. Jerger, J. M. J. Fréchet, F. C. Szoka, *J. Controlled Release* **2009**, *140*, 203–209.
- 70 a) Y. Zhu, N. S. Hosmane, *ChemistryOpen* **2015**, *4*, 408–417; b) X.-Y. Tu, M.-Z. Liu, H. Wei, *J. Polym. Sci., Part A: Polym. Chem.* **2016**, *54*, 1447–1458; c) Y. A. Chang, R. M. Waymouth, *J. Polym. Sci., Part A: Polym. Chem.* **2017**, *55*, 2892–2902.
71. M. H. Chisholm, J. C. Gallucci, H. Yin, *Proc. Natl. Acad. Sci.* **2006**, *103*, 15315–15320.
72. a) S. Roelens, A. Dalla Cort, L. Mandolini, *J. Org. Chem.* **1992**, *57*, 1472–1476; b) H. R. Kricheldorf, S.-R. Lee, *Macromolecules* **1995**, *28*, 6718–6725; c) M. Ryner, A. Finne, A.-C. Albertsson, H. R. Kricheldorf, *Macromolecules* **2001**, *34*, 7281–7287; d) H. R. Kricheldorf, G. Schwarz, *Macromol. Rapid Commun.* **2003**, *24*, 359–381; e) H. Li, A. Debuigne, R. Jérôme, P. Lecomte, *Angew. Chem. Int. Ed.* **2006**, *45*, 2264–2267.
73. D. A. Culkin, W. Jeong, S. Csihony, E. D. Gomez, N. P. Balsara, J. L. Hedrick, R. M. Waymouth, *Angew. Chem. Int. Ed.* **2007**, *46*, 2627–2630.
74. a) B. J. O’Keefe, M. A. Hillmyer, W. B. Tolman, *J. Chem. Soc., Dalton Trans.* **2001**, 2215–2224; b) O. Dechy-Cabaret, B. Martin-Vaca, D. Bourissou, *Chem. Rev.* **2004**, *104*, 6147–6176;

- 
- c) M. J. Stanford, A. P. Dove, *Chem. Soc. Rev.* **2010**, *39*, 486–494; d) C. M. Thomas, *Chem. Soc. Rev.* **2010**, *39*, 165–173; e) P. J. Dijkstra, H. Du, J. Feijen, *Polym. Chem.* **2011**, *2*, 520–527; f) J. C. Buffet, J. Okuda, *Polym. Chem.* **2011**, *2*, 2758–2763.
75. a) E. Bukhaltsev, L. Frish, Y. Cohen, A. Vigalok, *Org. Lett.* **2005**, *7*, 5123–5126; b) Y. Sarazin, R. H. Howard, D. L. Hughes, S. M. Humphrey, M. Bochmann, *Dalton Trans.* **2006**, 340–350; c) H.-Y. Chen, M.-Y. Liu, A. K. Sutar, C.-C. Lin, *Inorg. Chem.* **2010**, *49*, 665–674; d) M. Normand, T. Roisnel, J. F. Carpentier, E. Kirillov, *Chem. Commun.* **2013**, *49*, 11692–11694; e) L. Chen, W. Li, D. Yuan, Y. Zhang, Q. Shen, Y. Yao, *Inorg. Chem.* **2015**, *54*, 4699–4708; f) H.-C. Tseng, H.-Y. Chen, Y.-T. Huang, W.-Y. Lu, Y.-L. Chang, M. Y. Chiang, Y.-C. Lai, H.-Y. Chen, *Inorg. Chem.* **2016**, *55*, 1642–1650.
76. C. K. Williams, N. R. Brooks, M. A. Hillmyer, W. B. Tolman, *Chem. Commun.* **2002**, 2132–2133.
77. A. Sauer, A. Kapelski, C. Fliedel, S. Dagorne, M. Kol, J. Okuda, *Dalton Trans.* **2013**, *42*, 9007–9023.
78. a) A. L. Zelikoff, J. Kopilov, I. Goldberg, G. W. Coates, M. Kol, *Chem. Commun.* **2009**, 6804–6806; b) M. G. Hu, M. Wang, H. J. Zhu, L. Zhang, H. Zhang, L. C. Sun, *Dalton Trans.* **2010**, *39*, 4440–4446; c) T. K. Saha, V. Ramkumar, D. Chakraborty, *Inorg. Chem.* **2011**, *50*, 2720–2722; d) S. K. Roymuhury, D. Chakraborty, V. Ramkumar, *Dalton Trans.* **2015**, *44*, 10352–10367.
79. C. Redshaw, *Dalton Trans.* **2016**, *45*, 9018–9030.

- 
80. J. D. Ryan, K. J. Gagnon, S. J. Teat, R. D. McIntosh, *Chem. Commun.* **2016**, *52*, 9071–9073.
81. G. E. Hofmeister, F. E. Hann, S. F. Pedersen, *J. Am. Chem. Soc.* **1989**, *111*, 2318–2319.
82. C. Gaeta, L. Gregoli, M. Martino, P. Neri, *Tetrahedron Lett.* **2002**, *43*, 8875–8878.
83. T. Nakamura, K. Tateishi, S. Tsukagoshi, S. Hashimoto, S. Watanabe, V. A. Soloshonok, J. L. Acena, O. Kitagawa, *Tetrahedron* **2012**, *68*, 4013–4017.
84. B. König, T. Fricke, K. Gloe, C. Chartroux, *Eur. J. Inorg. Chem.* **1999**, 1557–1562.

---

## ACKNOWLEDGEMENTS

*I wish to thank my Supervisor, Prof. Placido Neri and his research group: Prof. Carmine Gaeta, Dr. Carmen Talotta, Dr. Paolo Della Sala and former members Dr. Stefano Tommasone and Dr. Gerardo Concilio.*

*I would also like to give special thanks to the people I've collaborated with. Prof. Irene Izzo, Dr. Giorgio Della Sala and Dr. Rosaria Schettini for the phase transfer catalysis project. Prof. Alessandra Lattanzi and Dr. Sara Meninno for the bifunctional organocatalysts study. Prof. Alfonso Grassi, Dr. Stefano Milione, Dr. Antonio Buonerba and Dr. Rosita Lapenta for the ring opening polymerization project.*

*My greatest gratitude goes to my amazing family, my friends and most of all to Chiara.*